Investigation of parameters governing the corrosion protection efficacy of fusion bonded epoxy coatings

By
Andrei Ramniceanu

Dissertation submitted to the faculty of the

Department of Civil and Environmental Engineering

Virginia Polytechnic Institute and State University

in partial fulfillment of the requirements for the degree of

Doctor of Philosophy

In

Civil and Environmental Engineering

Committee Members

Richard E. Weyers, Chair

Carin L. Roberts – Wollmann

Michael C. Brown

John J. Lesko

Judy S. Riffle

May 18th, 2007

Blacksburg, Virginia

Keywords: corrosion; ECR; concrete durability; epoxy coating; FBE

Investigation of parameters governing the corrosion protection efficacy of fusion bonded epoxy coatings

Andrei Ramniceanu

ABSTRACT

The primary cause of corrosion in transportation structures is due to chlorides which are applied to bridge decks as deicing salts. The direct cost of corrosion damage to the country's infrastructure is approximately $8.3 billion per year. ECR is one of the most common corrosion abatement methods in the United.

The purpose of this study was to investigate various coating and exposure parameters to determine their effects on the corrosion of reinforcing steel. The parameters investigated were: chloride content at the bar depth, coated bar corroded area, corrosion product color under the coating, epoxy coating adhesion, coating color, coating damage (holidays and holes), coating thickness, coating moisture, glass transition and EDS analysis and SEM coating cracking investigation. This was accomplished by testing new coated bar specimens as well as specimens extracted from 27 bridge decks located in Virginia.

This study demonstrated the following: The extracted ECR coating samples presented extensive cracking compared to the new ECR samples in which the coating cracking was limited to only one sample. The DSC results showed that both the extracted samples as well as new samples are not fully cured during the manufacturing process. The coating degree of curing data also showed that the bars are insufficiently and unevenly heated prior to the application of the powder coating. Additionally, the samples investigated presented significant permanent adhesion loss with little or no epoxy coating residue present on the bar surface, while the EDS analysis showed that once adhesion is lost, corrosion will proceed unimpeded under the coating even in the absence of chlorides.

The parameters that presented a direct correlation with the observed corrosion activity were the number of holidays and the number of damaged areas per unit length of bar. This indicates that the passivation of the bare steel exposed to the concrete pore solution at the breaches in the epoxy coating is not the same as a bare bar under similar exposure conditions allowing it instead to corrode at lower concrete chloride concentration levels than bare bars.

The results also show a distinct loss of quality control in the handling and possibly storage of new coated bars. The new ECR samples had significantly higher damage density than the samples extracted from concrete even though the coating is damaged during the placement of the concrete, while there was no change in the number of holidays and cure condition.

Finally, the data presented further evidence that while limited, the non-destructive corrosion assessment methods available for bare steel reinforced structures may also be used on ECR reinforced structures. In particular, the corrosion rate measurements correlated reasonably well with the chloride concentrations at bar level. This indicates that while the chlorides may not influence the corrosion activity under the coating, they do influence the corrosion activity at breaches in the coating.

ACKNOWLEDGEMENTS

During my time as a graduate student at Virginia Tech I have had the pleasure of meeting numerous people whose knowledge, mentorship, encouragement, dedication and friendship made the last four years truly unforgettable and helped me complete this endeavor successfully.

First and foremost I would like say that I owe a perpetual dept of gratitude and my most heartfelt thanks to Dr. Richard Weyers, my principal advisor and committee chairman. His patient guidance, support, mentorship, dedication and friendship made the last four years possible.

The members of my advisory committee warrant special mention. I am particularly indebted to Dr. Judy Riffle who in addition to giving her time and expertise also inspired me to continue my pursuit of knowledge in polymer chemistry. In no small measure, thanks also go to Dr. Michael Brown of Virginia Transportation Research Council with whom I worked shoulder to shoulder collecting field data and whose work ethic never ceased to inspire me. I am equally indebted to Drs. Carin Roberts-Wollmann and Jack J. Lesko. Their obvious commitment and enthusiasm for learning are part of what inspired and motivated me to pursue an academic career.

I would also like to acknowledge the generous financial contributions of the National Science Foundation IGERT Program, Virginia Transportation Research Council and Virginia Tech.

Thanks also go to Brett Farmer, Dennis Huffman, Clark Brown and Steve McCartney for their assistance, insights and technical knowledge they were never too busy to share.

I would also like to thank Vicky Mouras, Vicky Graham, Val Dymond, Lindy Cranwell, Sheila Collins, Bonnie Franklin, Mary Hunter, Ann Crate and Beverly Williams who were always there to lend a helping hand, who always had a kind word and who made my time at Virginia Tech infinitely easier.

I would especially like to thank Ozma Lane who spent countless hours teaching me how to interpret NMR and FT-IR spectra. Thanks also go to my close friends Jennifer Lin, Mike Sawchuk and Sarah Hameline, Greg Williamson, Devin Harris and Sarah Ragsdale who were there to inspire, motivate, or provide much needed emotional support during difficult times.

In no small measure, thanks also go Claire and Tom Clasen, who have generously helped both Katie and I in our education endeavors during the last 11 years.

I would also like to thank my mom, Adriana Ramniceanu. She gave up her life in Romania so that her children could have a better one here. Without her sacrifice I would not be here writing this.

I would indeed be remiss if I did not acknowledge the unfailing support and love that my wife, Katie, has given me over the course of my education. Her patience in encouraging me to continue, while pursuing her own doctoral work, particularly when my research did not go as planned, seemingly knew no bounds. She is my ultimate source of inspiration.

Finally, I dedicate this dissertation to my grandfather, Mişa “Bunelu” Stratienco, a humble but proud mariner and World War II veteran. He told me often when I was a young boy how important it was that I get a good education. I have never forgotten his wise words.

И наконец, я хочу посвятить эту работу моему дедушке, Мише "Бунелу" Стратиенко, скромному но гордому моряку и ветерану Второй Мировой Войны. Когда я был ещё маленьким мальчиком, он мне часто говорил что очень важно получить хорошее образование. Я никогда не забывал его мудрых слов.

TABLE OF CONTENTS

ACKNOWLEDGEMENTS……iii
TABLE OF CONTENTS.....v
LIST OF TABLES……...viii
LIST OF FIGURES.....ix
1.0 INTRODUCTION……...……1
2.0 PURPOSE……....3
3.0 SCOPE……....4
4.0 BACKGROUND……. ……..……..5
4.1 Steel Corrosion in Concrete…….6
4.1.1 Chloride induced corrosion……..7
4.1.2 Carbonation induced corrosion……8
4.1.3 Mechanisms of corrosion…….9
4.2 Corrosion Prevention Methods……..11
4.2.1 Epoxy coated reinforcement (ECR)……..11
4.2.1.1 Background……12
4.2.1.2 Application……...……..13
4.2.1.3 Specifications…….14
4.2.1.4 Performance……...15
4.2.1.5 Failure Mechanisms…….……..19
4.2.2 Water/cement ratio…..……....22
4.2.3 Pozzolans……...22
4.2.4 Slag……23
4.2.5 Corrosion inhibitors……...23
4.2.6 Clear cover depth…….....24
4.3 Corrosion Detection Methods……24
4.3.1 Concrete resistivity……26
4.3.2 Half-cell potentials…….28
4.3.3 Linear polarization…….29
4.4 Summary……32

5.0 METHODS AND MATERIALS……...33
5.1 Sampling of Epoxy Powder and New ECR…….....35
5.1.1 Epoxy powder……35
5.1.2 New ECR……...35
5.2 Bridge Deck Samples…….....36
5.3 Deck Survey……...36
5.3.1 Visual inspection……37
5.3.2 Cover depths……..37
5.3.3 Half-cell potentials…….38
5.3.4 Linear polarization…….38
5.3.5 Concrete resistivity……....38
5.3.6 Core samples……..38
5.4 Concrete Testing…….....39
5.5 Reinforcing Steel Testing……..39
5.6 Epoxy Testing……40
5.6.1 Coating thickness……...40
5.6.2 Coating adhesion……....40
5.6.3 Coating damage assessment……..41
5.6.4 Holidays…….43
5.6.5 Differential scanning calorimetry……..44
5.6.6 Thermo-gravimetric analysis…….44
5.6.7 Scanning electron microscopy……...45
5.6.8 Energy dispersive spectrometry…….45
5.6.9 FT-IR……..45
5.7 Data Analysis…….46
6.0 RESULTS……..47
6.1 Epoxy Powders……..47
6.2 ECR Rebar Samples……..…….48
6.3 Extracted ECR Rebar Samples…...……...52
7.0 ANALYSIS AND DISCUSSION…….79
7.1 Coating Cracking……..79

7.2 Degree of Coating Curing…….82
7.3 Residual Adhesion…….88
7.4 Corrosion Activity…….93
7.5 Corrosion Activity Assessment……100
8.0 CONCLUSIONS…….105
9.0 RECOMMENDATIONS…….107
9.1 Industry Practice……..107
9.2 Future Reseach……107
10.0 REFERENCES……108
VITA
APPENDICES

LIST OF TABLES

Table 4.1 Potentials Interpretation Guidelines……...……29
Table 4.2 3LP Corrosion Rates……..……31
Table 5.1 Bridges Selected for Study……...……..34
Table 5.2 Chloride Exposure by Environmental Zone……..35
Table 5.3 Adhesion Rating…….40
Table 5.4 Corrosion Product Interpretation……..…….42
Table 5.5 Rebar Surface Chemical Composition……...43
Table 5.6 Coating Color…….43
Table 5.7 DSC Process……..44
Table 6.1 Epoxy Powder T_g Values……..…….47
Table 6.2 New ECR Coating T_g and Moisture Content…….……48
Table 6.3 New ECR Sample Measurements……..……50
Table 6.4 Extracted ECR Coating T_g and Moisture Content……..…...53
Table 6.5 Extracted ECR Test Data……..…….57
Table 6.6 Corrosion Measurements and Chloride Concentration……..……70
Table 7.1 Structure 1133-1 C-6 EDS Chemical Composition……...……91
Table 7.2 Structure 1133-1 C-6 EDS Chemical Composition……...……93
Table 7.3 Structure 1007-4 C-3 EDS Chemical Composition……...…97
Table 7.4 Structure 1133-1 C-3 EDS Chemical Composition……...…99
Table 7.5 Summary of relevant correlations……104

LIST OF FIGURES

Figure 4.1 Corrosion Process Diagram……....6
Figure 4.2 The Dissolution of the Passive Layer……..8
Figure 4.3 Phenol, Acetone and Bisphenol-A Structures…….…...12
Figure 4.4 DGEBA Structure……...……...12
Figure 4.5 Bar Coating Process…….……14
Figure 4.6 Quenching Process…….14
Figure 4.7 Coating Disbonding Mechanism……19
Figure 4.8 Cathodic Disbondment……..…….21
Figure 4.9 4 – point Wenner Resistivity Apparatus……...…….26
Figure 4.10 Half-Cell Potential Apparatus……...…….28
Figure 4.11 3LP Test Apparatus……...…….30
Figure 5.1 Bridge Locations…….....……33
Figure 5.2 SEM Micrographs at 2k Magnification……..……...41
Figure 5.3 Structure 1019-8 C-4 5Kx SEM Micrograph and Binary……..…42
Figure 6.1 Fusion Bonded Epoxy Powder FT-IR Spectra…….….47
Figure 6.2 Sample LNE S2 DSC Plot……...……..48
Figure 6.3 ECR Epoxy Coat Thickness Measurements Distribution…….…….51
Figure 6.4 New ECR Coating Thickness……....52
Figure 6.5 1017-3 C1 DSC Plot…….….55
Figure 6.6 6058-9 C6 TGA Plot……..55
Figure 6.7 EECR Epoxy Coat Thickness Measurements Distribution…..…….59
Figure 6.8 EECR Coating Thickness……..60
Figure 6.9 Coating Color Distribution……61
Figure 6.10 EECR Coating Color……..61
Figure 6.11 Residual Adhesion Distribution…….62
Figure 6.12 EECR Residual Adhesion……..63
Figure 6.13 EECR Holidays……..64
Figure 6.14 EECR Holiday CDF Plot…….……..64
Figure 6.15 EECR Number of Damaged Areas CDF Plot……65

Figure 6.16 EECR Number of Damaged Areas ……...66
Figure 6.17 Percent Corroded Area CDF Plot……..……67
Figure 6.18 EECR Percent Corroded Area ……...…67
Figure 6.19 EECR Coating Cracking……...…….68
Figure 6.20 EECR Percent Cracking and Porosity……69
Figure 6.21 Percent Cracking and Porosity Probability Plot…….……69
Figure 6.22 EECR Structures Concrete Resistivity……...……72
Figure 6.23 EECR Structures Corrosion Potentials……..……73
Figure 6.24 Corrosion Rate Measurements……..……74
Figure 6.25 Concrete Chloride Concentration at Bar Level……..75
Figure 6.26 Structure 1020-2 C6 SEM Micrograph…….…76
Figure 6.27 EDS Spectra 1020-2 C-6-1……77
Figure 6.28 EDS Spectra 1020-2 C-6-2……77
Figure 6.29 EDS Spectra 1020-2 C-6-3……78
Figure 7.1 WWBVT – S4 Cracking (SEM Micrograph)……80
Figure 7.2 Scatter Plot of %Moisture vs. Coating cracking……81
Figure 7.3 Scatter Plot of % Moisture vs. ΔT_g……83
Figure 7.4 1017–3 C–2 5x SEM Coating Micrograph……84
Figure 7.5 2820–1 C–4 1x SEM Coating Micrograph……84
Figure 7.6 ΔT_g vs. Thickness……..86
Figure 7.7 ΔT_g vs. Steel Surface Color……...87
Figure 7.8 % Moisture v. Steel Surface Color……87
Figure 7.9 ΔT_g vs. Residual Adhesion……88
Figure 7.10 % Moisture vs. Residual Adhesion……89
Figure 7.11 Structure 1133-1 C-6 SEM Micrograph……90
Figure 7.12 Structure 1133-1 C-6 EDS Coating Spectrum……...90
Figure 7.13 Structure 1133-1 C-6 EDS Metal Spectrum……..90
Figure 7.14 Residual Adhesion vs. Steel Surface Color……...92
Figure 7.15 Structure 1133-1 C-6 EDS Coating Spectrum……...93
Figure 7.16 Structure 1133-1 C-6 EDS Coating Spectrum……...93
Figure 7.17 % Corroded Area vs. Holidays/308 mm……94

Figure 7.18 % Corroded Area vs. Number of Damaged Areas/308 mm……..95
Figure 7.19 Structure 1007-4 C-3 SEM Micrograph……96
Figure 7.20 Structure 1007-4 C-3 EDS Coating Spectrum…….……..96
Figure 7.21 Structure 1007-4 C-3 EDS Coating Spectrum…….……..96
Figure 7.22 Structure 1133-1 C-3 SEM Micrograph……...…….98
Figure 7.23 Structure 1133-1 C-3 EDS Coating Spectrum…….……..98
Figure 7.24 Structure 1133-1 C-3 EDS Coating Spectrum……...98
Figure 7.25 Half-cell Potentials vs. Resistivity……...101
Figure 7.26 Corrosion Current Density vs. Cl^- at Bar Level…….....102
Figure 7.27 Corrosion Current Density vs. % Moisture……..103

1.0 INTRODUCTION

By the early 1970s it became clear that the increase in deicing salt application lead to premature deterioration of transportation structures, primarily reinforced concrete bridge decks. The premature deterioration exhibited through delaminations and spalling of the riding surface was caused by the corrosion of the reinforcing steel. Therefore, to combat this problem, one of the corrosion prevention methods investigated was the barrier protection method implemented through the application of an organic coating, specifically fusion-bonded epoxy. By 1981, barely five years from the first test application of epoxy coated reinforcing steel (ECR), fusion-bonded epoxy coatings became the prevalent corrosion protection method in the United States (Manning, D.G., 1996, Weyers, R.E., 1995).

Since then, some studies have shown that epoxy coating will debond from the steel reinforcement in as little as 4 years (Weyers, R.E. et al, 1998) allowing instead a much more insidious form of corrosion to proceed unimpeded under the coating. More recently, studies conducted at Virginia Tech on samples collected from eight Virginia bridge decks have shown that the epoxy coating develops microscopic cracks (Wheeler, M.C., 2003). These cracks may allow the chloride-laden water to pass through leading to the initiation of the corrosion process. Exposure to the concrete pore solution as well as chlorides and seasonal temperature differences are thought to play a role in coating crack formation; however, the mechanism is not understood at this time.

Although some studies have shown that fusion-bonded epoxy coatings are an effective corrosion protection method (Poon, S.W. and Tasker, I.F., 1998), ECR remains highly controversial. Adding to the controversy is the fact that even after almost 30 years of field use, questions are constantly raised regarding its corrosion protection efficacy. Although some state transportation agencies have started to implement other corrosion protection methods such as using corrosion inhibitors as well as stainless steel, galvanized steel and to a lesser extent micro-composite multi-structural formable steel (MMFX-2), the fact remains that at the time of this study, fusion bonded epoxy coatings

are still the prevalent corrosion protection method. Furthermore, structures built with epoxy coated reinforcing steel (ECR) during the last 20 years are and will be in service for many years to come. Thus, it is important that the influence coating parameters – that may be manipulated during production such as thickness and the degree of curing – have on coating performance and therefore corrosion activity are thoroughly understood. In addition, the non-destructive testing methods currently used to assess the corrosion activity in bare steel reinforced concrete should be further studied with respect to ECR reinforced concrete. Being able to collect concrete parameters and corrosion activity information quickly and accurately will be invaluable to bridge engineers searching for means of assessing and increasing the service life of reinforced concrete bridges.

2.0 PURPOSE

The purpose of this study is to investigate the relationship between epoxy coating parameters such as thickness, curing level, holidays and adhesion, and corrosion parameters such as corrosion current density, corrosion potential, percent corroded area and corrosion product color. Should a relationship exist, the coating parameters that can be manipulated during the manufacturing process will be optimized to increase corrosion protection afforded by the epoxy coating.

In addition, the relationships between the field corrosion related measurements for bare steel and ECR will also be assessed. The ability of measured parameters to determine the condition of the bar underneath the coating will be investigated. The study will encompass extending the use of these testing methods to parameters currently only available through destructive testing, as well as investigating the effect the epoxy coating has on the corrosion test results. Furthermore, having verified in a previous study the fact that the non-destructive corrosion activity measurements obtained from bridge decks reinforced with ECR bars are indeed valid, the objective of this investigation will also be to determine the degree to which the epoxy coating influences those non-destructive measurements.

3.0 **SCOPE**

The scope of this study includes a representative sample of Virginia's bridge decks consisting of 27 ECR reinforced structures located in the state's six environmental zones. This sample was further divided into two groups: one group consisting of 16 structures cast using concrete with a specified water/cement ratio (w/c) of 0.45, and another group consisting of 11 structures cast using concrete with a specified water/cementatious materials ratio (w/cm) of 0.45. Furthermore, for the purpose of laboratory testing approximately 12 core samples, containing a section of a top mat reinforcing bar, were obtained from each bridge deck. A more detailed description of the samples and sample preparation may be found in the experimental section of this work.

In addition to the field samples discussed above, new epoxy coated reinforcing steel samples were collected from five, currently ongoing, bridge projects and one rebar supplier in the Commonwealth of Virginia.

Finally, three epoxy coating powder samples were provided for analysis by 3M, DuPont and Valspar.

The data will be analyzed using commercially available statistical analysis software packages.

4.0 BACKGROUND

Exposed steel will corrode in moist atmospheres due to differences in the electrical potential on the steel surface forming anodic and cathodic sites. These potential differences exist because the metal is not entirely homogeneous and the surface is irregular. Impurities, phase boundaries and stresses will influence the oxidation process in specific locations (McMurray, J. and Fay, R.C. 1998). For corrosion to take place, four essential elements are necessary as illustrated by iron in an acid or base solution:

1. An anode – the corrosion site which is the electron donor.

$$Fe \rightarrow 2e^- + Fe^{2+} \qquad \text{Equation 4.1}$$

$$Fe^{2+} + 2OH^- \rightarrow Fe(OH)_2 \qquad \text{Equation 4.2}$$

$$4Fe(OH)_2 + O_2 \rightarrow 2Fe_2O_3 \cdot H_2O + 2H_2O \qquad \text{Equation 4.3}$$

Or

$$6Fe(OH)_2 + O_2 \rightarrow 2Fe_3O_4 \cdot H_2O + 4H_2O \qquad \text{Equation 4.4}$$

$$Fe_3O_4 \cdot H_2O \rightarrow Fe_3O_4 + H_2O \qquad \text{Equation 4.5}$$

2. A cathode – reduction occurs at cathodic sites, typical cathodic processes being:

$$\tfrac{1}{2}O_2 + H_20 + 2e^-(metal) \rightarrow 2OH^-(aq.) \qquad \text{Equation 4.6}$$

$$2H + (aq.) + 2e^- (metal) \rightarrow H_2 (gas) \qquad \text{Equation 4.7}$$

3. Electronic conduction – electron movement through a conductor, in this case the steel reinforcing bars.

4. Ionic conduction – the movement of ions through a solution, the concrete pore water.

The process is illustrated in Figure 4.1 (Brown, M.C. 2002).

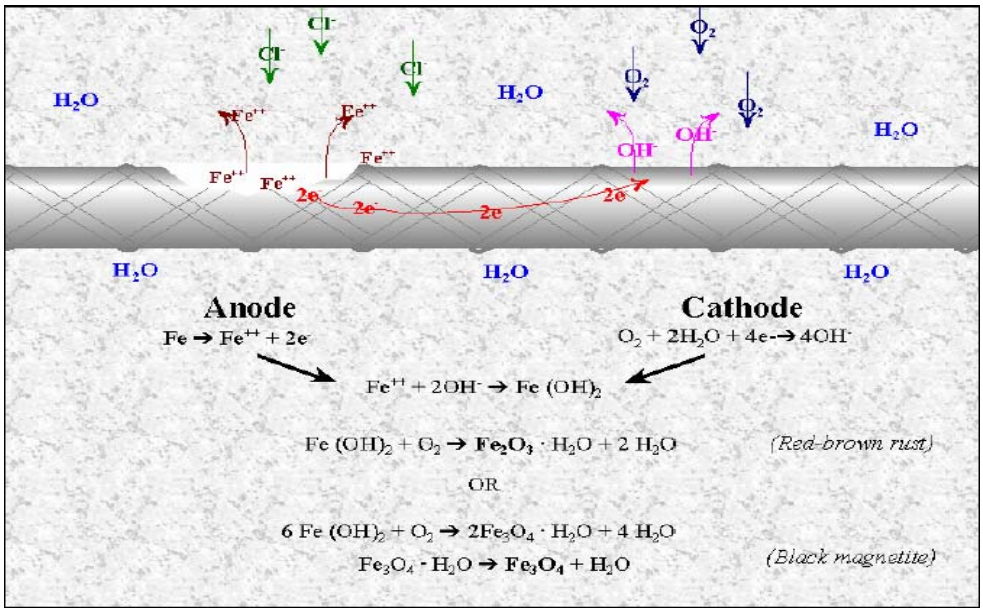

Figure 4.1 Corrosion Process Diagram (Brown, MC 2003)

The corrosion rate depends on the availability of oxygen for the cathodic reaction and on the electrical resistance of concrete, which controls the movement of ions through the concrete between the anodic and cathodic sites (Malhotra, V.M. and Carino, N.J. 2004)

4.1 Steel Corrosion in Concrete

The environment provided by concrete to the steel reinforcement is one of high alkalinity – pH greater than 12 – due to the presence of the hydroxides of sodium, potassium and calcium produced during the hydration reactions. Quality concrete also acts as a physical barrier to many of the steel's aggressors. In such an environment, the steel develops a thin (~ 10 nm), insoluble, tightly adhered oxide layer commonly referred to as a "passive layer" (Bentur, A. et al 1997). If, however, the alkalinity of its surroundings is reduced by neutralization with atmospheric carbon dioxide, or depassivating anions such as chloride, then severe corrosion of the reinforcement will occur. This in turn can result in staining of the concrete by rust and spalling of the cover concrete due to the increase in volume associated with the conversion of iron to iron oxide (Lambert P., 1998). There are three generally accepted and distinct stages when discussing the corrosion of steel embedded in concrete:

· Stage 1: Initiation – Concentration of aggressive species is insufficient to initiate any electrochemical reactions or the electrochemical reaction is occurring very slowly. No physical damage has occurred. The duration of this stage may vary from a few minutes to the design life of the structure.

· Stage 2: Propagation – Electrochemical reactions begin or are continuing, some physical damage such as cracking and/or spalling of the concrete cover may occur due to stresses induced by corrosion products but is insufficient to cause distress. Acceleration of the deterioration process usually occurs during this stage due to increased accessibility of aggressive ions or modification of the concrete environment.

· Stage 3: Deterioration – Rapid breakdown of the fabric of the structure. The combined effects of the physical and electrochemical processes are of sufficient severity that the structure is no longer serviceable (failure occurs) and major remedial work or, in extreme cases, demolition is required.

4.1.1 Chloride induced corrosion

Chlorides can enter concrete in two ways: 1) they may be added during mixing either deliberately as an admixture or as a contaminant in the original constituents, particularly if salt water is used as the mixing water. 2) They may also enter the hardened concrete from an external source as sea water or deicing salts.

Once chlorides have reached the reinforcement in sufficient quantities they will depassivate the embedded steel by breaking down the protective oxide layer normally maintained by the alkaline environment. Although insoluble in the chloride free environment, in the presence of chlorides, the ferrous oxide layer will form a soluble complex that dissolves in the concrete pore water solution as illustrated in equation 4.8 (Bentur, A. et al 1997) and Figure 4.2.

$$Fe(OH)_2 + Cl^- \rightarrow [FeCl]_x \qquad \text{Equation 4.8}$$

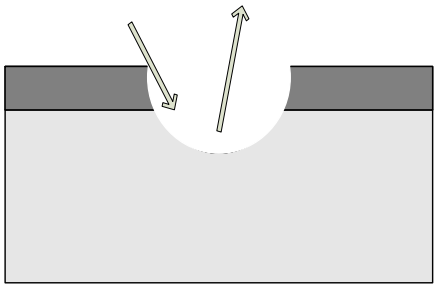

Figure 4.2 The Dissolution of the Passive Layer

The iron in the soluble complex then reacts with the hydroxyls present in the pore water solution freeing the chlorides, which are now available to repeat the reaction leading to the complete dissolution of the passive layer. Additionally, in the absence of the passive layer, the reinforcing bar is now free to continue the oxidation process unimpeded. The concentration of chlorides required to initiate and maintain corrosion is dependent upon the alkalinity of the concrete pore solution. It has been shown that there is an almost linear relationship between hydroxyl ion concentration and the respective threshold level of chloride (Lambert P., 1998). The generally accepted critical chloride threshold level in concrete at the reinforcing steel depth, at which corrosion initiates, is approximately 0.71 kg/m^3 of concrete. This value translates to a Cl^-/OH^- ratio of approximately 0.6 (Broomfield, J. P. 1997).

4.1.2 Carbonation induced corrosion

Carbon dioxide present in the atmosphere combines with moisture in the concrete to form carbonic acid. This reacts with the calcium hydroxide, other alkaline hydroxides and calcium silicate hydrates (CSH) resulting in a reduction in the alkalinity of the concrete. The reactions are illustrated in equations 4.9 and 4.10 (Broomfield, J. P. 1997).

$$CO_2 + H_2O \rightarrow H_2CO_3 \qquad \text{Equation 4.9}$$

$$H_2CO_3 + Ca(OH)_2 \rightarrow CaCO_3 + 2H_2O \qquad \text{Equation 4.10}$$

The rate at which this neutralization occurs is influenced by factors such as moisture levels and concrete quality. The depth of carbonation in a structure can be easily established by the use of phenolphthalein indicator on freshly exposed material. The distinctive color change, from deep pink in unaffected concrete to clear in the carbonated region, is sufficiently accurate for most practical purposes provided a number of measurements are obtained to allow for local variations.

It is important to note here that the contribution to the corrosion of reinforcing steel of carbonation compared to that of chlorides, particularly when discussing bridge decks, is miniscule. Tuutti K. showed in 1982 that for a structure built using concrete with w/c = .45, it would take approximately 100 years for the carbonation front to penetrate 10mm.

4.1.3 Mechanisms of corrosion

There are several corrosion mechanisms of interest associated with the corrosion of reinforcing steel. Of particular interest are uniform corrosion, crevice corrosion and pitting corrosion. Galvanic corrosion, stress induced corrosion and hydrogen embrittlement are also of interest when discussing steel reinforced concrete structures. The principles of galvanic corrosion are of interest, particularly as corrosion protection methods such as galvanized steel. Stress induced corrosion and hydrogen embrittlement are specific to pre- and post-tensioned structures which use high strength steels and therefore are outside the scope of this project.

General or uniform corrosion is probably the most common form of corrosion. It is a process characterized by a uniform attack of the entire metal surface or a very large area. Unlike other more destructive corrosion mechanisms, general corrosion is desirable in some cases. Weathering steel relies on the uniform oxide layer on the surface to protect it from further oxidation. The passivation layer that forms on uncoated reinforcing steel provides near immunity to corrosion in the highly basic concrete environment in the absence of chlorides.

Crevice corrosion is an intense form of localized corrosion that occurs within crevices or shielded areas on the metal surface and is characterized by small pools of stagnant water (Fontana, M. G. and Greene, N. D. 1978). Unlike galvanic corrosion, which may be caused by contact of two dissimilar metals, crevice corrosion can occur due to contact of a metallic and a non-metallic surface. Critical to this type of corrosion is the crevice size. It has to be large enough to permit liquid entry, but small enough to prevent moisture loss and maintain a stagnant pool. Fontana and Greene state that it usually occurs in openings a few thousands of an inch or less and that it rarely occurs in openings larger than 3 mm (Fontana, M. G. and Greene, N. D. 1978). Oxygen depletion is particular to this type of corrosion. Although no further oxygen reduction occurs, the dissolution of metal continues leading to an excess of positive metal ions. The developed positive charge is balanced by the migration of chloride and hydroxide ions into the crevice. The metal and the chloride form a metal-chloride complex that hydrolyzes in water forming an insoluble hydroxide and a free acid (Fontana, M. G. and Greene, N. D. 1978). This reaction is illustrated in Equation 4.11.

$$M^{+}Cl^{-} + H_2O \rightarrow MOH\downarrow + H^{+}Cl^{-} \qquad \text{Equation 4.11}$$

Fontana and Greene state that the fluid within the crevice may contain 3 to 10 times as much chloride as the surrounding bulk solution as a well as having a pH of 2 to 3. The typical concrete pore solution is highly basic with a pH of 12 to 14. Crevice corrosion may take place under the coating of ECR in concrete.

Pitting corrosion is an extreme form of localized attack. The corrosion mechanism is similar to that of crevice corrosion. Lack of oxygen coupled with high metal dissolution leads to a highly acidic local environment. Unlike crevice corrosion however, pitting corrosion takes place on the metal surface without metal-metal or metal-nonmetal contact. A corrosion pit may initiate at a scratch, dislocation or variation in solution composition (Fontana, M. G. and Greene, N. D. 1978). Corrosion of uncoated steel begins as pitting corrosion and may appear as uniform corrosion at later stages.

4.2 Corrosion Prevention Methods

The permeability of the concrete is important in determining the extent to which aggressive external substances can attack the steel. A thick concrete cover of low permeability will significantly delay the time for chlorides from an external source from reaching the steel and causing depassivation. Where an adequate clear cover depth is difficult to achieve due to design considerations or where aggressive environments are expected such as in marine structures or bridge decks, additional protection may be required for the embedded steel. Protection methods take many and varied forms and commercial interest in this field is strong. Some of these methods include lowering the specified water/cement ratio, cementing and non-cementing additives, as well as corrosion inhibitors. The steel reinforcement itself may also be made more able to resist corrosion by providing it with a protective coating such as zinc, epoxy resin or stainless steel cladding. Currently, the most commonly used protection method in the United States is the fusion bonded epoxy coating (Seymour, R.B. et al 1990).

4.2.1 Epoxy coated reinforcement (ECR)

` To combat the corrosion problem exacerbated by the increase in deicing salts application, epoxy coatings were introduced in the late 1970s and became the prevalent protection methods by the mid 1980s. This was carried out without any significant research into the protection mechanism associated with epoxy coatings as applicable to mild steel embedded in concrete (Zemajtis, J. et al 1996). Epoxy coatings were chosen because of their superior chemical resistance, durability, low porosity and high bond strength. This situation may have arisen from the assumption that the environment to which the reinforcing steel, and therefore the protective epoxy coating, were exposed to was similar to previously encountered environments, particularly in the pipeline industry. Other protective coatings are now available but are not as common as fusion bonded epoxies.

4.2.1.1 Background

The most common epoxy coating in the United States is a bisphenol-amine epoxy (Brown, M.C. 2002). This type of epoxy, which is a condensation of bisphenol-A and epichlorohydrin, can be cured at ambient temperatures or elevated temperatures with an amino acid (Seymour, R.B. et al 1990). Bisphenol-A is the product of combining one acetone unit with two phenol groups. Structurally it contains a benzene ring with an attached hydroxyl (C_6H_5OH). Acetone is an organic ketone. Structurally it contains a carbonyl C=O group attached to two organic methyl groups (CH_3COCH_3), and it is primarily used as a solvent (Carey, F. A. 1996). Figures 4.3 illustrates the structures of phenol, acetone and bisphenol-A respectively.

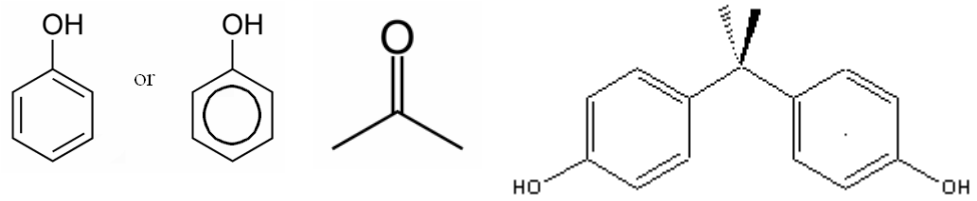

Figure 4.3 Phenol, Acetone and Bisphenol-A Structures

The reaction between bisphenol-A and epichlorohydrin removes unreacted phenol and acetone and attaches two glycidyl groups to the ends of the bisphenol-A, creating a diglycidyl ether of bisphenol A or DGEBA, which is standard epoxy resin. The glycidyl group on both ends of the bisphenol-A are also referred to as an oxirane or ‘epoxy group'. The size of the resulting molecule (and hence its molecular weight) depends upon the ratio of epichlorohydrin to bisphenol A (Odian, G. 1981). The DGEBA structure is presented in Figure 4.4.

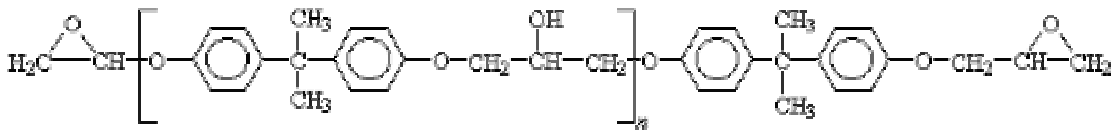

Figure 4.4 DGEBA Structure

The ‘amine' curing agent will react with the oxirane (epoxy group) ring unit on

the ends of the epoxy resin. The result is a new carbon-hydrogen bond, this time using the hydrogen from the curing agent and freeing the epoxy group's hydrogen to combine with the group's oxygen to form a hydroxyl pendant. This hydroxyl group contributes to the epoxy's adhesion to many substrates. The adhesion of epoxies is due to the strong polar bonds it forms with the surfaces it comes in contact with (Odian, G. 1981).

4.2.1.2 Application

The organic epoxy can be applied in two ways: two-part liquid or powder (Brown, M.C. 2002). The liquid can be applied through brushing, spraying or immersing the bar to be coated, which lends it well to field applications. The powder application process consists of three distinct stages:

1. Surface cleaning.

At this stage shot-blast cleaning is the most commonly used method for preparation of reinforcing steel surfaces. The method removes rust and mill scale from the metal surface in an effective manner and produces an industrial grade cleaning and a "rough" surface finish. The resulting profile increases the effective surface area of the steel. It is also believed that the rougher surface topography contributes to the coating adhesion by providing mechanical interlocking.

2. Heating.

Heating can be achieved by using several methods, but the most commonly used ones are ''induction heating'' or ''oven heating''. The steel part is passed through a high frequency alternating current magnetic field, which heats the metal part to the required FBE coating application temperature. The manufacturer recommended temperature range for FBE products commonly used to coat reinforcing steel is 350°F - 450°F (177°C - 232°C).

3. Application and curing.

The epoxy powder is placed on a “fluidization bed”. In a fluidization bed, the powder particles are suspended in a stream of air, in which the powder will “behave” like a fluid. Once the air supply is turned off, the powder will remain in its original form. The fluidized powder is sprayed onto the hot substrate using suitable spray guns. An electrostatic spray gun incorporates an ionizer electrode on it, which gives the powder particles a positive electric charge. The charged powder particles uniform wraps around the substrate, and melts into a liquid form. The specified coating thickness range of stand-alone epoxy coatings is between 175 to 300 µm. The molten powder ‘flows’ into the profile and bonds with the steel. Time to quench varies depending on the substrate temperature from 21 seconds (at 450°F) to 60 seconds (at 350°F). Figure 4.5 illustrates the production process (Brown, M.C. 2003) while Figure 4.6 shows freshly coated bars undergoing quenching under a spray of water.

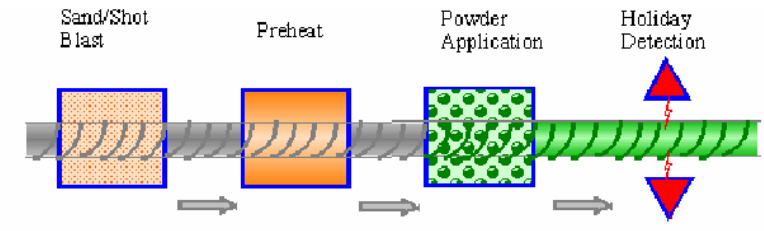

Figure 4.5. Bar Coating Process

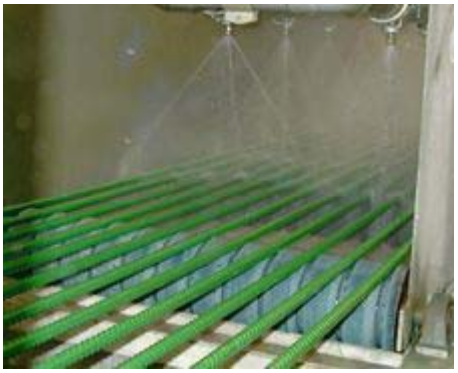

Figure 4.6. Quenching Process

4.2.1.3 Specifications

To provide adequate performance, specifications have been established addressing factors such as thickness, holidays, flexibility, adhesion, chloride permeability, abrasion resistance and impact resistance. The prescription based specifications coating requirements that have to be met are addressed by ASTM A 775/A775M – 04a.

1. Thickness: At least 90% of the measurements after curing shall be between 175 and 300µm (7 to 12 mils). More than 5% of the thickness measurements below 125µm (5 mils) shall be considered cause for

rejection. Furthermore, no single one measurement shall be less than 80% of the specified minimum or more than 120% of the specified maximum thickness.

2. Holidays: On average, there shall be no more than 3 holidays per meter (1 holiday per foot). For the purposes of rebar coatings, a testing equipment manufacturer Tinker-Rasor, defines holidays in thin coatings as: when a current of 500 or 700 (+/- 10/%) micro amperes flows in the circuit and actuates the audible signal.
3. Coating flexibility: The coating may not disbond, crack or otherwise visibly fail when bent around a mandrel within a specified time period. The mandrel size, bending angle and the time to test completion are specific to the tested bar size.
4. Adhesion: ASTM Test Method G 8 "Test Methods for Cathodic Disbonding of Pipeline Coatings" is specified. The average coating disbondment radius of three coated bars shall not exceed 4 mm (0.16 in.)
5. Chloride permeability: The accumulative concentration of chlorides permeating through the film shall be less than $1x10^{-4}$ mole per liter. The test was performed in accordance with ASTM C 1152 "Standard Test Method for Acid-Soluble Chloride in Mortar and Concrete."
6. Abrasion resistance: The weight loss cannot exceed 100 mg (0.0035 oz)/1000 cycles when the test is performed in accordance with ASTM Test Method D 4060 "Test Method for Abrasion Resistance of Organic Coatings by Taber Abrasor"
7. Impact resistance: When impacted with 9 Nm (80 in.lbs), the coating may not crack, shatter or disbond, except at the impact area. The test method specified is ASTM Test Method G 14 "Test Method for Impact Resistance of Pipeline Coatings (Falling Weight Test)"

4.2.1.4 Performance

Epoxy coatings protect the reinforcing steel by performing two basic functions: "first, to act as a barrier so that a complete corrosion cell cannot form; and second, to

prevent the spread of corrosion from an initial site of electrolyte penetration (Dickie, R.A. 1981)." These functions can be achieved through one or more of the following mechanisms (Hare, C.H. 2000; Revie R.W. 2000; Brown M.C. 2003):

1. Resistance inhibition. In this case, the film acts as an ionic filter, ensuring that the moisture passing through has high electrical resistance.
2. Oxygen deprivation. The coating limits the oxygen diffusion to the corrosion site, thereby eliminating one of the necessary corrosion cell elements.
3. Cathodic protection. A more anodic (less noble) metal is introduced in the coating to serve as a sacrificial anode.
4. Inhibition or aestivation. Uses the moisture diffusing through the coating as a delivery medium. "Soluble inhibiting moieties supplied from the coating film may be carried to the metal where they may stimulate the establishment of passive films (Hare, C.H. 2000).

Epoxy coatings primarily rely on one or both of resistance inhibition and oxygen deprivation to minimize or stop the corrosion process. These tasks are therefore limited by two coating properties: adhesion and permeability. Later research has shown, however, that not only is the epoxy coating permeable to oxygen and, but the total absence of defects, which is essential for the barrier to perform as designed, is unachievable under practical construction conditions (Clear, K.C. et al 1995). Therefore, the epoxy coated reinforcing steel is not as well protected as originally thought, with some instances where the structure reinforced with epoxy coated steel degraded far sooner than its bare bar reinforced counterparts. To add to the ongoing controversy, there are significant differences in recorded coating performance between laboratory test results and field data.

Most laboratory research as well as the field studies regarding the performance of ECR were prompted by the fallout from the severe corrosion induced distress observed in the Florida Keys bridges in 1986, barely 6 years after construction. Severe corrosion as well as concrete cover spalling and coating disbondment were observed (Pianca, F. et al

2006). It was reasoned that the severe corrosion was a result of pre-installation coating damage due to manufacturing and transportation coupled with a severe environment. A key finding of that study was the evidence of "coating disbondment at almost all of the structures examined" even in the absence of visible corrosion activity (Kessler, R. and Powers, R. 1987). Prior to 1986, a limited number of studies were conducted on ECR reinforced structures in Virginia, Maryland, Minnesota and Pennsylvania. The age of these structures at the time of investigation ranged between 1 to 10 years old. Based on those studies, the protection afforded by the fusion bonded epoxy coating was deemed adequate with some reservations (Munjal, S.K. 1986). Since then, a number of reports have confirmed the presence of visible corrosion damage or severe coating deterioration in ECR reinforced structures both in the US as well as Canada.

The initial good performance reviews of ECR reinforcement – in spite of clear evidence of coating disbondment and degradation (Clear, K. 1994 and Pianca, F. 1999) – based solely on the absence of concrete cover delaminations, and to a certain extent limited corrosion activity, was later attributed to the quality of the concrete (Pianca, F. 2006). More recent field performance studies conducted in Pennsylvania and New York concluded that " due to the low average age of the sample population (10 years), the performance of epoxy coated rebar with respect to either failure mechanism at an acceptable confidence level could not be statistically ascertained (Sohanghpurwalwa, A.A. and Scannell, W.T. 1999)." Finally, a study conducted in Virginia by Weyers and Pyc concluded that the coating will debond from the steel before chloride arrival thereby providing little to no additional service life (Pyc, W.A. 1998).

Initial laboratory studies performed under accelerated conditions generally had positive results indicating a substantial service life increase. One test going as far as claiming a 46 to 1 increase in time for the same amount of steel consumed between ECR and bare bar reinforcement (Virmani, Y. P. et al 1987). Between 1983 and 1988, Threadway and Davies conducted a study of ECR performance. The authors concluded that the epoxy coating provided a significant reduction in the rate of corrosion (Treadway, K.W.J. and H. Davies, H. 1989).

Later studies conducted by Romano in 1988 and Sagüés in 1989 began to investigate the effects of fabrication and service conditions. The authors concluded that adhesion loss was not only caused by corrosion activity at the coating-steel interface, but that corrosion and coating disbondment were more pronounced in the bent areas of the bars (Romano, D.C. 1988; Sagüés, A.A. and Zayed, A.M. 1989). Researchers also began to investigate other parameters that could potentially influence the coating performance. In 1990, Sohanghpurwala and Clear concluded that the source of tested ECR was the only variable that had a significant influence on the epoxy coating effectiveness. The authors also recognized, based on resistance measurements that the coating was deteriorating with time (Sohanghpurwala, A.A and Clear, K.C. 1990). In 1990, Sagüés determined that surface damage was one of the main causes of the adhesion loss of the epoxy coating to the steel surface (Sagüés, A.A. 1991).

Further studies, in spite of claiming a moderate to substantial service life increase, confirmed the fact that under constant exposure to the wet concrete environment the coating debonds from the steel substrate. More recent studies demonstrated that ECR, currently used in highway structures, will not provide long-term corrosion protection, over 50 years, in deicing salt and marine environments (Pyc, W. 1998). Despite promising accelerated exposure test results, countries outside North America have been reluctant to adopt ECR. This caution may stem in part from the initial conflicting reports and more recent negative field performance reports coming from North America.

In 2001, Virmani reported that 49 states used epoxy coating reinforcing steel extensively, with the exception of Florida, which discontinued its use after the Long Key Bridge showed signs of corrosion deterioration after only six years (Virmani, P. et al 2001). Presently, however, some U.S. states as well as Canada have discontinued using ECR or are investigating other corrosion protection methods. ECR is still being used in Virginia, but other corrosion abatement methods are being investigated.

4.2.1.5 Failure Mechanisms

A common conclusion of both laboratory and field investigations of ECR was the loss of adhesion experienced by even undamaged coatings in wet environments. To address this issue, several disbondment mechanisms have been proposed. Often quoted are Leidheiser and Funke who describe the coating disbondment mechanism as follows (Leidheiser, H. and W., Funke, 1987): 1) Water and ions diffuse through the coating. 2a) Chemical disbondment – the coating-oxide bonds are replaced by water-oxide and possibly coating-water bonds. 2b) Mechanical disbondment – caused by osmotic pressures due to ion concentration gradients. The process is illustrated in Figure 4.7. In addition, further research has shown that coating disbondment is assured in moist environments. The secondary bond energy between the coating and the oxide layer approximately 10 to 26 kJ/mole is exceeded by the activation energy of 32 kJ/mole associated with the disbondment of the epoxy by water (Pyc, W.1998 and Brown, M.C. 2003). The work done by Pyc supports previous research by Gledhill and Kinlock, which showed that the measured work of adhesion of the ferric-oxide changes from 291 mJ/m2 to -255 mJ/m2 between dry and wet environments, respectively (Gledhill and Kinlock, 1974).

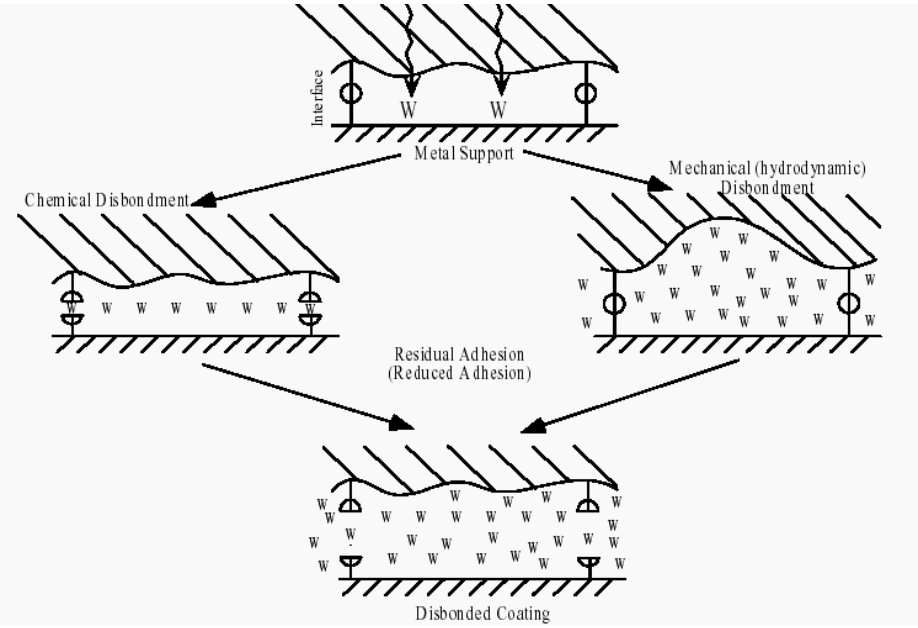

Figure 4.7 Coating Disbonding Mechanism

In a recent study, Tinh Nguyen and Jonathan W. Martin from the National Institute of Standards and Technology (NIST) investigated some of the causes leading to the failure of the epoxy coating. The purpose of this particular study was, as the authors indicate, "to reexamine the effectiveness, as well as to provide a better understanding of the degradation behavior, of fusion bonded epoxy-coated steel panel and rebars exposed to a marine concrete environment." The authors were able to show that the undamaged, unscribed, test specimens suffered water-induced adhesion loss, which was partially recovered after drying. The presence of water as the adhesion damaging agent was confirmed through the Fourier Transform Infrared (FTIR) spectra collected, which showed that the "thickness of the water layer at the coating/substrate interface increased with exposure." The authors stress that the adhesion loss is recoverable by drying the specimen, which would indicate the water can move freely through the protective coating (Nguyen, T. and Martin, J.W. 2004). Even before epoxy coatings were commonplace in the construction industry, in 1967, six years before the first bridge was constructed with ECR, P. Walker "found that initial coating adhesion values were typically maintained up to 1000 hours at relative humidity 0 to 50%." At higher relative humidity, adhesion loss occurred between 300 to 500 hours for epoxy esters.

Other possible disbonding mechanisms are anodic and cathodic adhesion loss. These mechanisms, which may or may not be simultaneously present, are a direct result of the corrosion process and can occur in damaged as well as undamaged films. As sufficient water diffuses to the steel-coating interface, the corrosion process is initiated. The area immediately under the blister will become anodic while the edges of the blister cathodic. One of the products of the reactions at the cathode is hydrogen. The evolution of protons causes the pH to decrease leading to further delaminations and blister growth. The difference for damaged coatings is the lack of blister formation. This process is illustrated in Figure 4.8.

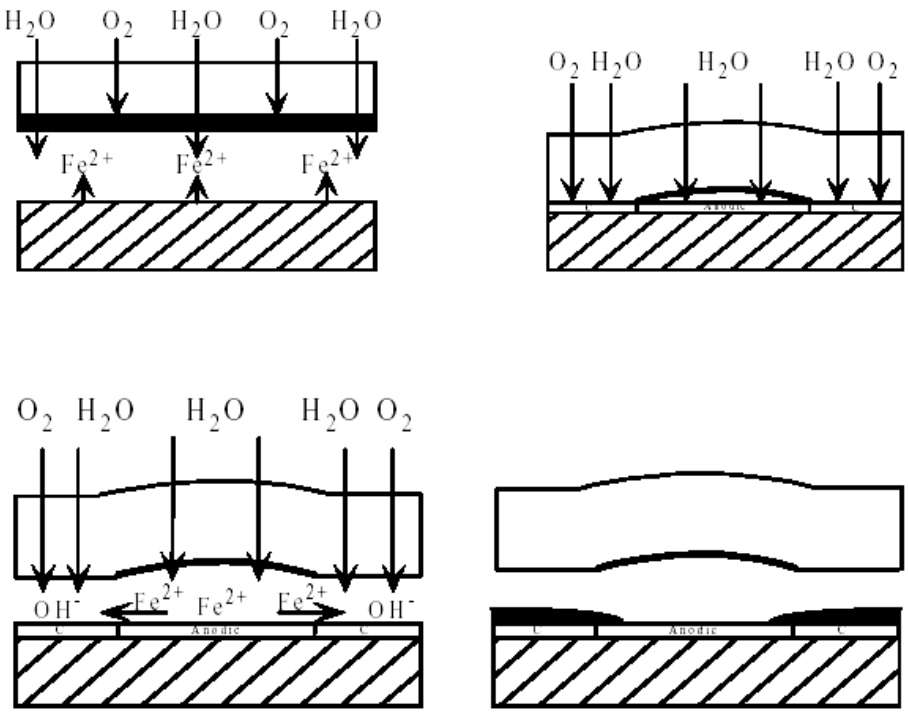

Figure 4.8 Cathodic Disbondment

Recognizing the effects of water induced adhesion loss; Bajat et al studied the effects of steel surface modification with zinc. Bajat was able to show that an electrodeposited Zn-Fe alloy could improve the corrosion stability of the protective system. The Zn-Fe alloy was deposited galvanostatically at 2.0, 4.0 and 10.0 A dm^{-2} on steel panels. The epoxy coating was electrodeposited and the measured thickness was 25μm ± 1μm. Based on the test results, Bajat concluded that sample treated with the Zn-Fe alloy at 4.0 A dm^{-2} showed the most improvement over the untreated steel coated sample. The parameters measured were electrochemical activity, H_2 evolution, water absorption and contact angle of the liquid epoxy with the steel substrate. The diffusion coefficient of water decreased from 7.83 to 3.70 (x 10^{10} cm^2s^{-1}), the water content from 0.40 to 0.37 (wt%) and the contact angle from 48° to 0°, or complete wetting of the surface, for the untreated steel and the Zn-Fe alloy treated, respectively (Bajat, J. B. et al 2002).

Gonzalez et al performed a similar experiment, but used commercially available galvanized steel. Three epoxy coating thicknesses were tested: 100, 300 and 500 μm.

Gonzalez concluded that "changes in the impedance characteristics of the systems were found to occur as a function of the exposure time in all the three cases, though their evolution with time showed marked differences which derived directly from the different thicknesses of the coatings. With the thinnest coating considered, the primer film could not provide an effective protection for the metal that underwent corrosion as a result of the delamination process. On the contrary, when the coating film was sufficiently thick, effective protection of the metallic substrate was provided by the epoxy-polyamide film (Gonzalez, S. et al, 2000)."

4.2.2 Water/Cement ratio

Another way to increase the service life of a bridge deck is to delay the initiation of reinforcing steel corrosion by decreasing the chloride diffusion constant (D_c). Virginia has lowered the maximum allowable w/c ratio from 0.47 to 0.45. Decreasing the specified w/c ratio decreases the permeability of the concrete and therefore increases the time for the chlorides to diffuse to the reinforcing steel. Kirkpatrick and others have shown that the decrease in w/c ratio may account for approximately 40% increase in service life (Kirkpatrick, T.J. et al 2002).

4.2.3 Pozzolans

Pozzolans have no stand alone cementing properties; however, they do hydrate in the presence of water and calcium hydroxide released during the hydration of Portland cement. Since the pozzolanic hydration process is not only much slower than the hydration of Portland cement, but is also dependant on the calcium hydroxide released by the hydrating Portland cement, the pozzolanic hydration products fill the already existent capillary spaces in the cement paste (Zemajtis, J. 1998). This process increases the strength and reduces the permeability of the final product. By reducing the permeability of the Portland cement concrete, the ingress of chlorides is significantly reduced and therefore, the corrosion of the reinforcing steel is delayed. It is important to note that the pozzolanic admixtures do not eliminate the capillary porosity, but reduce the pore size and lower the volume fraction of calcium hydroxide; at the same time, increasing the

total amount of calcium silicate hydrates (Bentz, D.P. et al 1991). Two commonly used pozzolanic admixtures are flyash and micro silica.

4.2.4 Slag

Also known as ground granulated blast furnace slag (GGBFS), it is a byproduct of the steel production industry. During steel production, the liquid slag is rapidly quenched in water forming a glassy, granular, non-metallic product consisting of silicates and aluminosilicates of calcium and other bases (Mehta, P.K. 1993). Unlike flyash and micro silica, GGBFS has stand alone cementitious properties. In addition to its benefits with respect to the corrosion of reinforcing steel such as decreased porosity and permeability (Lewis, D.W. 1985), GGBFS has also been used because it improves the workability and reduces the water requirements of the fresh Portland cement concrete mixture (Fulton, F.S. 1974).

4.2.5 Corrosion inhibitors

Corrosion inhibitors are chemical admixtures used to retard or delay the corrosion of reinforcing steel in concrete (Zemajtis, J. 1998). Many of these inhibitors are organic compounds; they function by forming an impervious film on the metal surface or by interfering with either the anodic or cathodic reactions or both (Fontana, M.G. 1986). There are three types of corrosion inhibitors: anodic, cathodic and mixed. Anodic inhibitors react with the corrosion products on the steel and form a protective film on the surface, and cathodic inhibitors react with the hydroxyl ions to precipitate insoluble compounds on the cathodic site and prevent the access of oxygen (Zemajtis, J. 1998). Anodic corrosion inhibitors may be nitrates, nitrites, chromates, silicates, phosphates, molybdates and borates. Cathodic corrosion inhibitors consist of arsenic, bismuth, antimony, and salts of zinc, magnesium or calcium (Trethewey, K.R. et al 1988).

4.2.6 Clear cover depth

Inadequate cover is invariably associated with areas of high corrosion risk due to both carbonation and chloride ingress through sound and cracked concrete. Therefore, there can be little doubt that an effective way of protecting steel which is embedded in concrete is to provide it with an adequate clear cover depth of low permeability concrete free from depassivating ions such as chlorides. By surveying the surface of a structure with an electromagnetic cover meter the low cover high-risk areas can be easily identified. A cover survey of newly completed structures would rapidly identify likely problem areas and permit additional protective measures to be taken.

American Association of State Highway and Transportation Officials (AASHTO) specifies a minimum cover depth of 50 mm, while the Virginia Department of Transportation (VDOT) requires a clear cover depth between 63 mm to 76 mm, but no less than 63 mm (Weyers, R.E. et al 2003, AASTHO 1994, VDOT 1994). Increasing the cover depth not only increases the chloride diffusion path leading to longer service life, but also leads to longer times to cracking caused by expansive corrosion products (Weyers, R.E. et al 1998).

4.3 Corrosion Detection Methods

Since it has been determined that chlorides are at the crux of reinforcing steel corrosion in concrete (Clemeña, G. G. 1992), several invasive and non-destructive methods have been developed to assess the level of corrosion taking place or the potential for corrosion. Because corrosion is an electrochemical process, some of the most commonly used non-destructive field methods for measuring corrosion activity are: resistivity of concrete, half-cell potentials, and linear polarization of the steel reinforcement. The invasive or destructive corrosion assessment methods consist of chloride content analysis from powdered samples, chloride permeability tests and gravimetric loss of steel specimens.

Individually, non-invasive methods have been used quite successfully to monitor corrosion activity of reinforcing steel in concrete. The invasive methods mentioned above have also been used for many years to model bridge deck service life. One common service life model for the chloride induced corrosion of reinforcing steel in concrete involves two time periods. The first is the time for chloride ingress to reach a concentration necessary to initiate corrosion. The second is the time for corrosion activity to the end of functional service life (Weyers, R.E. et al. 1993). The end of functional service life is defined as: "when 12 percent of worst span lane of a bridge deck has deteriorated (Fitch, M.G. et al. 1995)." This service life model is based on Fick's second law of diffusion, which uses an apparent diffusion process. A model solution which is used to determine the time for chlorides to "reach and initiate corrosion at first repair and rehabilitation", is described mathematically as follows (Crank, J. 1975):

$$C_{(x,t)} = C_o\left(1 - erf\frac{x}{2\sqrt{D_c t}}\right) \qquad \text{Equation 4.12}$$

$C_{(x,t)}$ = chloride concentration at depth and time (kg/m^3)

C_o = surface chloride concentration (kg/m^3)

D_c = apparent diffusion coefficient (mm^2/year)

t = time of diffusion (years)

x = concrete cover depth (mm)

erf = statistical error function

When $C_{(x,t)}$ is set equal to the chloride corrosion initiation concentration, and the equation is solved for time, t, the time for diffusion of chlorides to the chloride corrosion initiation concentration can be determined (Kirkpatrick, J. 2001). Weyers and Kirkpatrick, incorporating the statistical nature of the factors affecting the corrosion initiation process, further refined the modeling procedure (Kirkpatrick, J. 2001).

4.3.1 Concrete Resistivity

A non-destructive testing procedure that is becoming increasingly popular due to its low cost and ease of implementation, is measuring the concrete resistivity by the Wenner method, as shown in Figure 4.9.

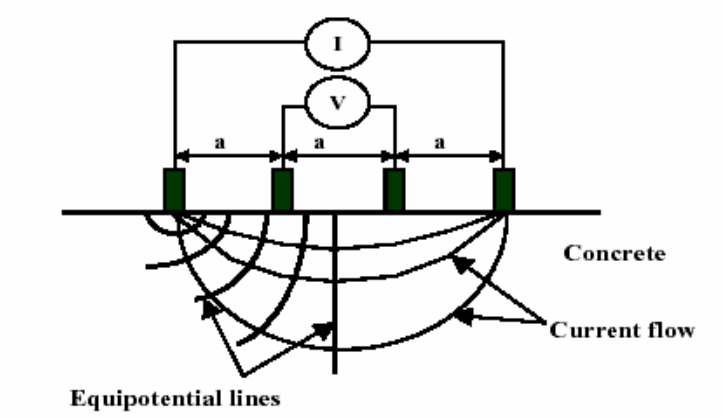

Figure 4.9 4 – point Wenner Resistivity Apparatus

Originally developed to measure the resistivity of soils by Wenner in 1916, this method uses four equally spaced probes. Although resistivity cannot be used to determine the rate of corrosion, it can be used to assess other concrete properties such as permeability to chlorides and its ability to sustain corrosion.

To minimize the polarization effects to the reinforcing steel, "a small alternating current is applied between the outer electrodes while the potential is measured between the inner electrodes (Nagi, M.A. and Whiting, D.A. 2003)." Thus, we are able to measure the electrical resistance of concrete, which affects the ionic current flow between the anode and the cathode, and the rate at which corrosion can occur (Gowers, K.R. et al 1999). Resistivity is then calculated as follows:

$$\rho = 2\pi aR \qquad \text{Equation 4.13}$$

ρ = Resistivity in units of ohm-cm or ohm-in

a = spacing between the four probes in cm or in

R = actual measured resistance in ohms

A high concrete resistivity decreases the current flow and impedes the corrosion process. Since concrete resistivity is affected by chlorides (mostly from deicing salts) and other ions, concrete resistivity by the Wenner method has been used to assess other concrete properties such as permeability. A study completed in 2001, by Weyers and Bryant, correlated the permeation properties of low permeability concrete, which is commonly used in the construction of bridge decks in the Commonwealth of Virginia, with the resistivity values obtained using the 4-point Wenner method. The study showed that "electrical resistivity measurements may be able to give an indication of the present penetrability properties of as-built structures (Bryant, J.W. 2001);" however, more research is necessary to better define the procedure. Currently, there is no agreement in interpretation guidelines. Bungey recommends the following guidelines (Bungey, J.H. 1989):

> 20	kΩ-cm	Low corrosion rate
10-20	kΩ-cm	Low to moderate corrosion rates
5 -10	kΩ-cm	High corrosion rate
< 5	kΩ-cm	Very high corrosion rate

Whereas others recommend (Feliu, S. et al, 1996):

>100 to 200	kΩ-cm	Negligible corrosion, or concrete too dry
50 to 100	kΩ-cm	Low corrosion rate
10 to 50	kΩ-cm	Moderate to high corrosion rate
<10	kΩ-cm	Resistivity does not control corrosion rate

And (Manning, D.G. 1985):

>12	kΩ-cm	Corrosion unlikely
5 to 12	kΩ-cm	Corrosion probable
<5	kΩ-cm	Corrosion certain

4.3.2 Potentials

Unlike resistivity, half-cell potentials can in fact indicate the potential of corrosion taking place on the reinforcing steel embedded in concrete. The basic process for the corrosion of steel in concrete is the development of micro and macro cells. That is the coexistence of passive and corroding areas on the same bar or separate bars, respectively. A short-circuited galvanic element with the corroding area as anode and the passive area as cathode is formed (Elsener, B. et al, 1994). The direct measurement is the potential difference created between the metal in the half-cell and the steel in concrete (Broomfield, J. P.1997). Therefore, places on the reinforced structure with higher concentrations of iron in solution – in this case the concrete pore solution – will exhibit higher, or more negative, potential differences. The measurements are obtained using a high impedance voltmeter. The illustration below shows the typical apparatus as described in ASTM 876-91.

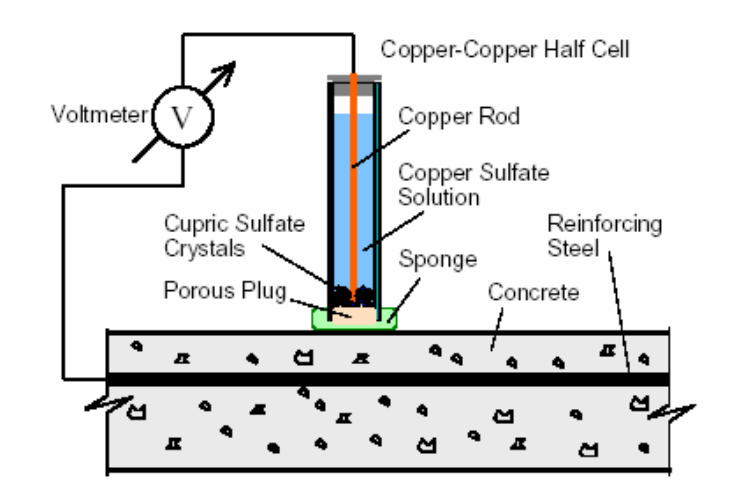

Figure 4.10 Half-Cell Potential Apparatus

There are several types of half-cells commercially available: Copper/copper sulphate (CSE), silver/silver chloride (Ag/AgCl), mercury/mercury oxide (Hg/HgO) and saturated calomel electrode (Broomfield, J.P. 1997). It's important to note what type of half-cell is used to perform the test, since the interpretation of results from half-cells other than CSE will have to be offset based on their respective chemical composition.

The ASTM interpretation criteria for tests performed using a CSE half-cell on structures reinforced with bare steel is presented in the table below (ASTM 876-91):

Table 4.1 Potentials Interpretation Guidelines

Voltmeter Reading	Interpretation
Greater than -200mV	90% probability of no active corrosion
Between -200mV and -350mV	Uncertain
Less than -350mV	90% probability of active corrosion

The limitations of this method, particularly with respect to ECR, arise from the common assumption that the epoxy coating is dielectric; and therefore, would prevent the creation of a continuous electrical circuit necessary in the measurement process. Therefore, prior to engaging in half-cell potential testing or mapping, a continuity test is performed on the reinforcing steel in the structure. Field measurements, however, have shown that it is possible to obtain reasonable data on ECR reinforced concrete bridge decks (Ramniceanu, A. 2003).

4.3.3 Linear polarization

A more sophisticated inspection method is the three electrode linear polarization (3LP). The 3LP device appears to be a convenient tool for measuring corrosion current densities. It yields reinforcing steel corrosion current densities that correlate reasonably well with metal losses observed in reinforcing steel specimens extracted from the decks (Clemeña, G.G. 1992). A typical unguarded linear polarization instrument and set-up are illustrated in Figure 4.11, below.

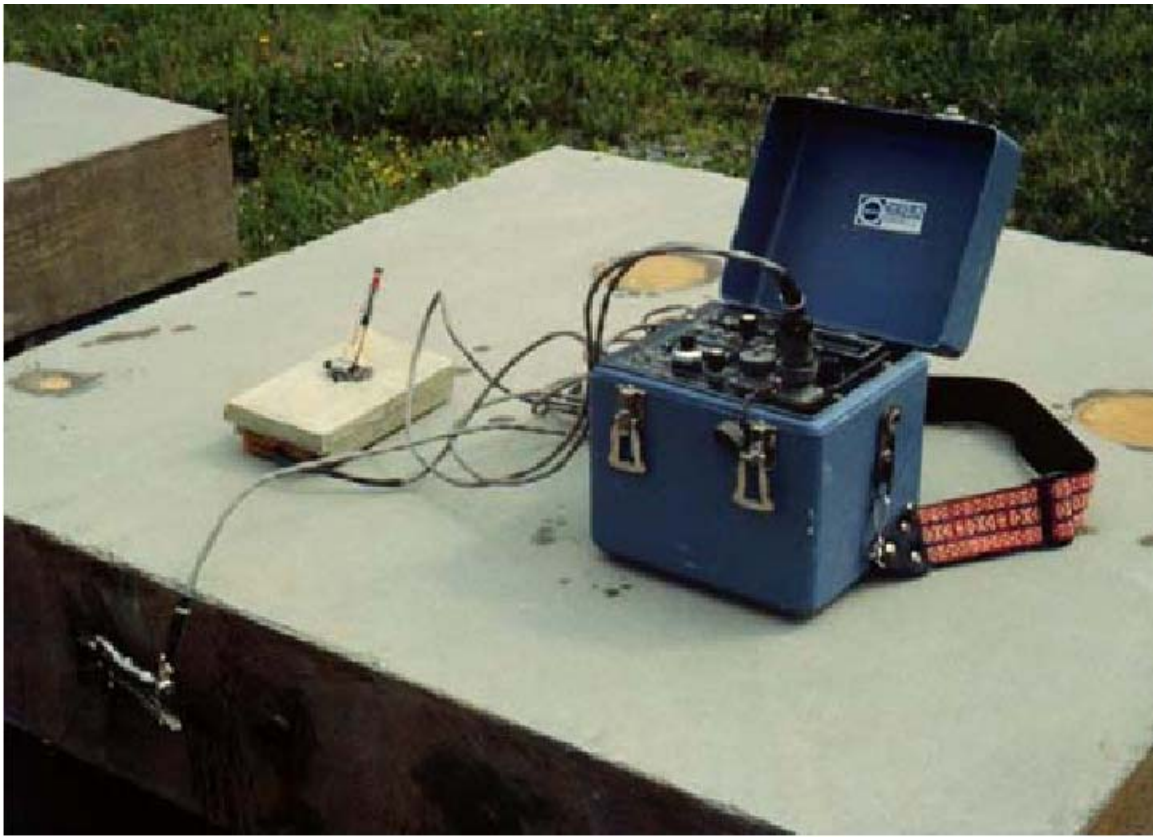

Figure 4.11 3LP Test Apparatus

"The technique is based upon the fact that a DC current applied to alter the natural electrical half-cell potential of the steel a few millivolts, is proportional to the natural corrosion of the steel. If a high current is required, the corrosion [current density] is high; and vice versa." The development of this device was based on the Stern-Geary equation (Clear, K.C. 1989):

$$I_{corr} = \frac{\Delta I_{appl}(\beta_a \beta_c)}{2.3\Delta\phi(\beta_a + \beta_c)} \qquad \text{Equation 4.14}$$

I_{corr} = corrosion current in mA

I_{appl} = DC current required to cathodically polarize the bar from its natural electrical half-cell potential

$\Delta\varphi$ = Absolute value of cathodic polarization potential minus the natural electrical half-cell potential

βa = Anodic Tafel constant = 150 mV/decade

βc = Cathodic Tafel constant = 250 mV/decade

One problem with this method of determining corrosion rates is the fact that it is considered to be inapplicable to epoxy coated reinforcing (ECR) steel just as with half-cell potentials. This inability to apply the linear polarization test to epoxy coated steel stems from two assumptions: the assumption that the coating is dielectric, and therefore continuity would be impossible to achieve; and should continuity be possible, the fact that the test interpretation is based on an assumed steel surface area. Since the epoxy coating is considered dielectric, as mentioned earlier, any measurements obtained would be from isolated bare areas, the size of which would be unknown (Brown, M.C. 2002). Another limitation of these methods is that "they detect the instantaneous corrosion rate which can change with temperature, RH and other factors. (Broomfield, J.P. 1997)" The generally accepted guidelines for interpreting the data obtained using the 3LP test apparatus for bare bar only is shown in Table 4.2 below (Clear, K.C. 1989):

Table 4.2 3LP Corrosion Rates

Corrosion State	**Corrosion Current Density ($\mu A/cm^2$)/ (mA/ft^2)**
No Corrosion Damage Expected	< 0.20
Corrosion Damage Possible in the Range of 10 to 15 Years	0.2 – 1.0
Corrosion Damage Expected in 2 to 10 Years	1.0 – 10
Corrosion Damage Expected in 2 or Less	> 10

It must be noted also that these interpretation guidelines are not exact even when applied to structures reinforced with bare bars. Research by Liu and others has shown that the unguarded linear polarization instruments such as the 3LP overestimate the corrosion rate (Liu, Y. 1996). Other studies support these findings showing that the weight loss calculated using this method may be as high as 110% (Law, D.W. et al 2003).

4.4 Summary

The literature review revealed that there is no consensus regarding the laboratory performance of ECR while the field performance is questionable at best. Furthermore, there appears to be a lack of understanding regarding the condition of ECR prior to embedment in concrete, reflected by the degree of cure as well as holiday and damage density. These parameters are currently believed to be adequate based on manufacturer recommendations and ASTM specifications. Additionally, while there is agreement in the scientific and engineering community regarding loss of coating adhesion, it may be more severe, extensive and of a more permanent nature than the literature review reveals.

The goal is to gain insight regarding the ECR condition prior and post embedment in concrete by examining new as well as extracted specimens. We will also correlate the coating condition data with the observed and measured corrosion activity.

5.0 METHODS AND MATERIALS

A total of 27 bridges in Virginia were selected for study, see Table 5.1. The bridges were built between 1984 and 1991 with a specified maximum water/cement of 0.45. The indicated maximum water/cement ratio is the applicable specification at the time of construction. However, it is most likely not the actual w/c used in the construction of each of the selected bridge decks. Also, the information regarding the inclusion of fly ash or GGBFS was indicated by the appropriate Engineering District personnel and later verified by petrographic analysis. The sample was then divided into two groups: one with flyash or slag as a supplemental cementing material and one with only Portland cement. Furthermore, the bridge decks selected for the project were distributed throughout the six Virginia climate regions, see Figure 5.1. The sampled bridge details are presented in Table 5.1

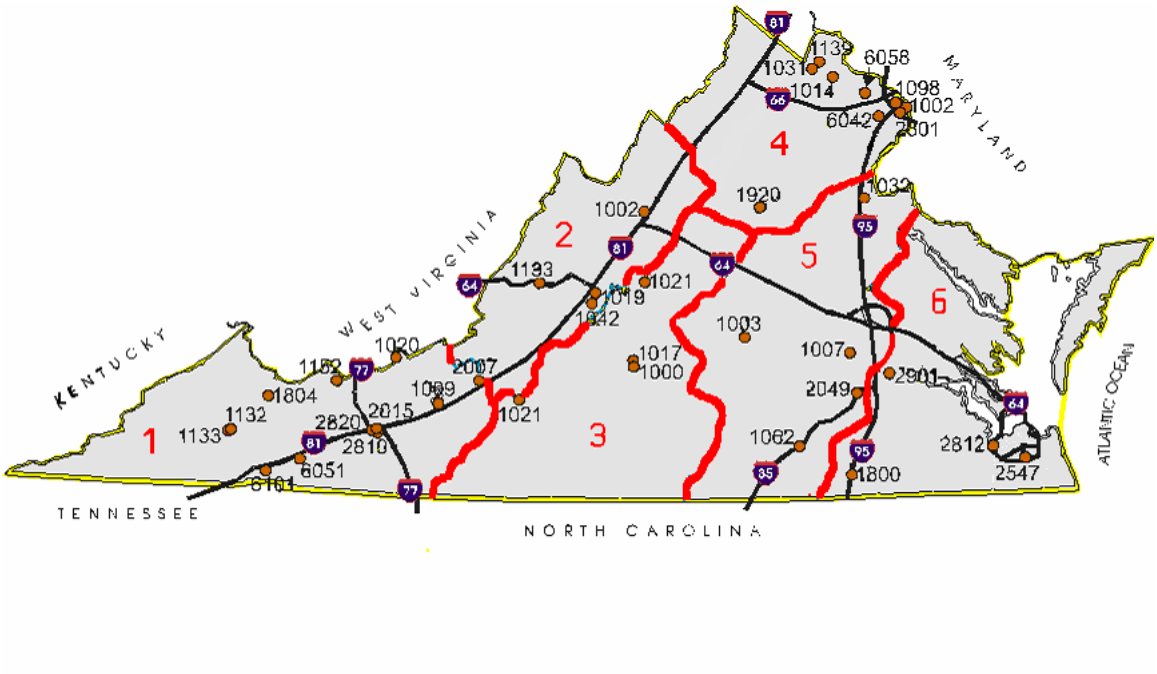

Figure 5.1 Bridge Locations

Table 5.1 Bridges selected for study

District	County	Structure Number	Year Built	Age at Survey (Years)	Climate Region	Specified Concrete
4	Prince George	2901	1991	12	6	0.45 w/c
7	Orange	1920	1991	12	4	
9	Loudoun	1031	1990	13	4	
1	Russell	1132	1988	15	1	
2	Franklin	1021	1988	15	1	
3	Cumberland	1003	1988	15	5	
1	Tazewell	1152	1987	16	1	
8	Alleghany	1133	1987	16	1	
9	Loudoun	1139	1987	16	2	
1	Wytheville	2815	1986	17	1	
1	Wytheville	2820	1986	17	1	
2	Giles	1020	1986	17	1	
5	Chesapeake	2547	1984	19	5	
8	Rockbridge	1019	1984	19	2	
3	Campbell	1000	1991	12	3	0.45 w/cm
5	Suffolk	2812	1991	12	6	
9	Fairfax	6058	1991	12	4	
1	Smyth	6051	1990	13	1	
3	Campbell	1017	1990	13	3	
4	Chesterfield	1007	1990	13	5	
8	Rockbridge	1042	1990	13	2	
1	Russell	1133	1988	15	1	
8	Augusta	1002	1988	15	2	
9	Arlington	1098	1988	15	4	
9	Arlington	1002	1987	16	4	
9	Loudoun	1014	1987	16	4	
1	Wytheville	2819	1986	17	1	

The chloride exposure data per climatic region presented in Table 5.2 was drawn from a previous study conducted by Dr. R.E. Weyers at Virginia Tech (Weyers, R.E., 2004). The average chloride exposure per climatic region was measured over a three year period in terms of an average annual kg-Cl^- /lane-km.

Table 5.2 Chloride Exposure by Environmental Zone

Zone #	Climatic Zone	Kg-Cl⁻/lane-km
1	Southwestern Mountain (SM)	688
2	Central Mountain (CM)	671
3	Western Piedmont (WP)	220
4	Northern (N)	4369
5	Eastern Piedmont (EP)	530
6	Tidewater (TW)	225

5.1 Sampling of Epoxy Powder and New ECR

5.1.1 Epoxy Powder

Three epoxy powder manufacturers were represented in the powder analysis. The manufacturers were 3M Scotchkote 413, Valspar Greenbar 720A009 and DuPont FBE Rebar. One sample of approximately 5 lbs from the three manufacturers was provided by VTRC, while one sample of Valspar Greenbar 720A009 was obtained from a site visit at a coating facility located in North Carolina.

5.1.2 New ECR

ECR samples from three currently ongoing projects in Virginia were collected for this study. The projects were the north bound span of I-81 over Buffalo Creek, Woodrow Wilson Bridge over the Potomac River and Route 123 Bridge over the Occoquan River in Northern Virginia. The sample from the Buffalo Creek project (BFC) and one sample from the Woodrow Wilson project (WWB1) were collected by the author. The second sample from the Woodrow Wilson project (WWB2) and the sample from the Occoquan River project (OBP) were supplied by VDOT project representatives. During the site visits, it was observed that the ECR bars were generally stored off the ground and were covered with a commercially available tarp. No other damage mitigation measures were noted. Interviewed site personnel indicated that the turn-over rate for ECR bars was approximately 2 weeks for BFC and a few days for WWB. We were unable to determine the age of the bar as delivered to the construction sites.

Additionally, an ECR sample was collected from Bay Shore precast plant located in Cape Charles, on the Eastern Shore of Virginia. The sample available for collection had been exposed to the elements approximately 12 month. Finally, ECR samples from four coating manufacturers were tested. One sample was provided for testing by the Hall Hodges plant located in Chesapeake, Virginia. A sample from three construction sites representing coaters Free State Coaters, Florida Steel and Lane Enterprises were stored at the Virginia Tech testing facilities from a previous study (Pyc, W. 1998 and Zemajtis, J. 1998). The ECR bars had been stored indoors, supported off the floor and individually separated using wooden spacers and covered with a black plastic tarp.

5.2 Bridge Deck Samples

The 27 study bridge decks were located on primary and secondary routes. The sample included bridge decks from the following populations of structures:

1. Built between 1984 and 1991 with a specified maximum w/c ratio of 0.45 with Portland cement only, and a clear cover depth of 63mm (2.5 in) minus zero, plus 13mm (0.5 in), 14 bridges.
2. Built between 1986 and 1991 with a specified maximum w/cm ratio of 0.45 with flyash or slag as a supplemental material, and a clear cover depth of 63mm (2.5 in) minus zero, plus 13mm (0.5 in), 13 bridges.

None of the bridges chosen for this study had been overlaid; however, during the deck inspection portion part of the study it was observed that one deck had been treated with a polymer sealer, structure 1020-2 in Giles County.

5.3 Deck Survey

The field survey was limited to one traffic lane, generally selected on the basis of traffic and surface drainage conditions for each individual deck. Under field conditions, however, the right traffic lane was selected for safety and practicality, as this is normally the lane with the most traffic and subsequently the one deteriorating first. The field survey of each deck included a visual inspection, non-destructive testing of cover depths,

half-cell corrosion potentials, corrosion current densities, concrete resistance measurements (later used to calculate the resistivity of the concrete) as well as general structural information which included the deck as well as its support structure. Core samples from the decks measuring 102 mm (4 in) in diameter and containing an epoxy coated reinforcing bar (ECR) were also collected.

5.3.1 Visual Inspection

As part of the visual inspection procedure:

1. The length and the width of the right traffic lane were measured.
2. The deck was "sounded" with a chain drag to determine delaminated area(s).
3. A visual determination of the wheel path locations was made.
4. A crack survey was performed. It consisted of recording the number, length, width and orientation of the cracks in each span.
5. Other structural data included the type of deck support structure (i.e. steel, prestressed or cast-in-place concrete), structure type (continuous or simply supported), and the girder spacing. The presence of stay-in-place forms was also recorded. The super-elevation condition and the skew angle of the deck were also measured.
6. Year built and traffic data were provided by the Virginia Department of Transportation.

5.3.2 Cover Depths

Clear cover depth measurements of the top reinforcing steel mat were performed at four-foot intervals in both wheel paths, for a total of 40 measurements per span. If the span length did not allow for the collection of 40 measurements, the measurements were taken at two-foot intervals. The data was collected using two Profometer 3 instruments.

5.3.3 Half-cell Potentials

Half-cell potential measurements were collected at the same locations as the cover depth measurements. A copper-copper sulfate half-cell was used, and the test was performed in accordance with ASTM 876-87.

5.3.4 Linear Polarization

Based on the half-cell potential values and the bridge deck length, four to six corrosion current density measurements were performed. The test was carried out using an unguarded three electrode linear polarization (3LP) instrument, and the data was usually collected from the right wheel path of the right lane for safety reasons. Generally, the tests were performed at two locations determined to have the most negative potential values, two locations with the least negative potential values and if deck length permitted, at two locations with potential values midway between the most and least negative values.

5.3.5 Concrete Resistivity

Generally, the test was performed at nine locations using a four-probe Wenner apparatus. Four to six of the nine locations selected were at the same locations as the corrosion current density measurements, while three locations selected were the same locations from which cores were obtained for petrographic analysis and contained no reinforcing steel. Five measurements were obtained at each test location using due diligence not to conduct the measurements directly over the reinforcing steel bar. For the purpose of calculating the resistivity of the concrete, the spacing between the four probes was maintained at 50.8 mm (2 in).

5.3.6 Core Samples

Generally, 12 core samples were collected from each bridge deck. Core drilling was performed with a water cooled diamond set drill bit. Six cores were drilled at the same locations where the corrosion current density measurements were performed, and contained an ECR section. Three core samples obtained included the reinforcing steel, but were located over a crack. Also, three un-cracked “companion” cores were drilled

adjacent to the cracked cores. The "companion" cores contained the next parallel reinforcing steel bar that was not cracked. Each specimen measured 102 mm (4 in) in diameter by approximately 152.4 mm (6 in). After extraction, each specimen was allowed to air dry only long enough for surface moisture to evaporate. The samples were then wrapped in multiple layers, consisting of a layer of 102-μm (4 mils) polyethylene sheet, followed by a layer of aluminum foil, and another layer of polyethylene sheet. Finally, the specimen and protective layers were wrapped tightly with duct tape. The purpose of the immediate wrapping of the cores was to maintain as closely as practical the in-place moisture condition of the concrete during transport and storage (Brown, 2002).

5.4 Concrete Tests

The Virginia Transportation Research Council at their facility located in Charlottesville, Virginia have conducted the following laboratory tests on the concrete samples:

1. Chloride content analysis.
2. Resistivity measurements using a two probe method across the diameter of the specimen at various depths.
3. Concrete percent saturation.
4. Concrete moisture content.
5. Electrical resistance as an indicator of chloride penetrability.

5.5 Reinforcing Steel Tests

In addition to the tests listed above, the condition of the ECR samples was assessed. The visible ECR corroded surface area was measured. The colors of both the epoxy coating and the corrosion products present under the coating were recorded. Additionally, for a limited number of samples, the steel substrate was also examined using the scanning electron microscope (SEM).

5.6 Epoxy Tests

The following tests were performed both at Virginia Tech and VTRC. The laboratory performing each test is specified in each test's description below. The samples on which the tests were performed are also indicated for each individual test. Specifically, whether the sample was ECR extracted from the cores (EECR), new ECR or epoxy powder.

5.6.1 Coating Thickness

The coating thickness was measured in accordance with ASTM G-12 "Nondestructive Measurement of Thickness of Pipeline Coatings on Steel." The test was carried out using the same Elektro-Phisik Minitest 500 coating thickness gauge on the EECR as well as the new ECR samples at Virginia Tech.

5.6.2 Coating Adhesion

The coating adhesion test was performed on the EECR field samples at the VTRC facilities. The peel or knife test is performed as follows: an x-cut is made in the coating between the bar lugs and the steel substrate is exposed by inserting the blade of an X-acto knife underneath the coating. A number between 1 and 5 is assigned to each test based on the size of the exposed area and represents a degree of residual adhesion (RA) of the epoxy to an oxidized steel surface layer. A total of 6 adhesion tests were performed on each ECR specimen and the average adhesion was calculated for each specimen. The interpretation guidelines are presented in Table 5.3 (Pyc, W.A. 1998).

Table 5.3 Adhesion Rating

Residual Adhesion Number (RA)	**Exposed Area**
1	Unable to insert blade tip under coating
2	Total exposed area < 2 mm^2
3	2 mm^2 < Total exposed area < 4 mm^2
4	Total exposed area > 4 mm^2
5	Blade tip slides easily under the coating. Levering action removes the entire section of coating

The test was attempted at Virginia Tech on the new ECR samples. The adhesion of the epoxy to the iron oxide layer, for ECR that has not been exposed to the moist/wet

concrete environment, is greater than the cohesive strength of the epoxy coating. We were therefore unable to produce RA test results.

5.6.3 Coating Damage Assessment

The coating damage was assessed using three different techniques: 1) by counting the number of defects visible to the unaided eye. 2) By assigning a subjective coating cracking from 1 through 4 based on the scanning electron microscope (SEM) micrograph guidelines illustrated in Figure 5.2.

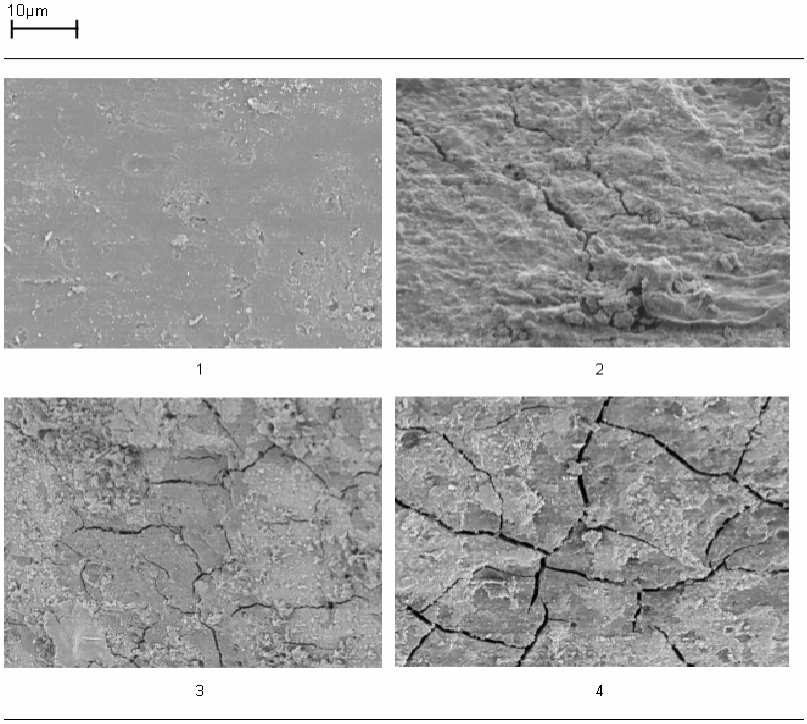

Figure 5.2 SEM Micrographs at 2k magnification

3) Finally, by using the image analysis program ImageJ on images collected during the SEM investigation. ImageJ is a shareware image analysis program developed by the National Institutes of Health (NIH). A 5k magnification SEM micrograph is converted to a binary image, which is then used to quantify the surface coating damage. The damage is recorded as a percentage of the surface area. Unlike technique 2, which takes into account only cracks, all damage types (cracks, pores, gouges) are included, using this method. Figure 5.3 illustrates a typical SEM 5k micrograph and its accompanying binary image.

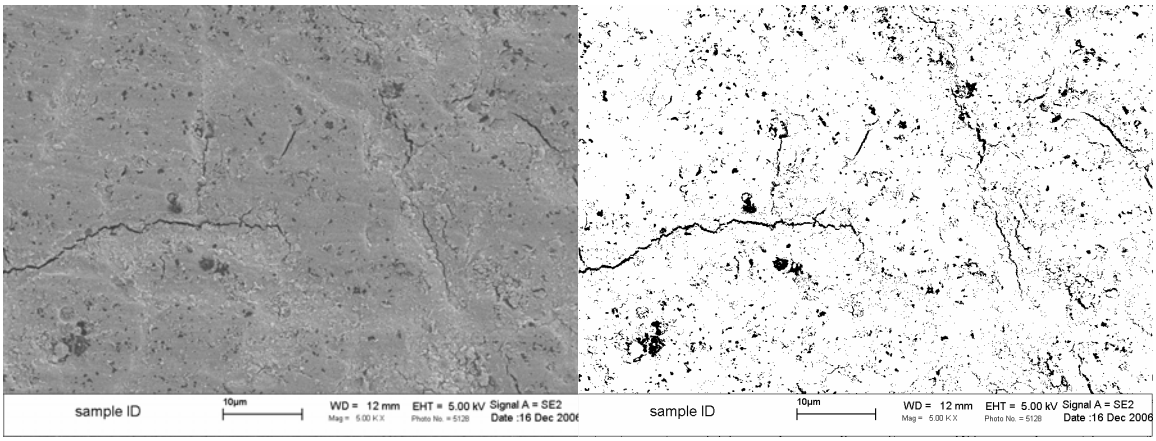

Figure 5.3 Structure 1019-8 C-4 5Kx SEM Micrograph and Binary

The color of the steel surface under the coating at the RA test locations was noted, and based on the interpretation criteria noted in Table 5.4, a value from 1 to 5 was assigned to each specimen (adapted from Pyc, WA 2001).

Table 5.4 Corrosion product interpretation

Number	Steel Surface Color
1	Shining
2	Gray, shining
3	Dark gray, shining
4	Black, Shining
5	Black

Because the RA tests were performed by VTRC, we at Virginia Tech were not able to perform EDAX analysis on the freshly exposed steel surface. Therefore, the surface chemical composition of freshly exposed steel surface corresponding to each steel surface color in Table 5.4 was obtained from a previous study and is presented in Table 5.5 (Pyc, WA 2001).

Table 5.5 Rebar surface chemical composition

Element	Weight %				
	Shining (1)	Gray shining (2)	Dark gray shining (3)	Black shining (4)	Black (5)
Fe	97.7	93.9	92.1	93.6	83.7
Mn	1.7	2.1	1.1	2.3	n/a
Cr	0.7	1.2	0.5	n/a	< 0.2
Ti	n/a	0.7	n/a	0.6	n/a
Ni	n/a	n/a	n/a	0.2	n/a
Al	n/a	n/a	< 0.2	n/a	0.4
Si	n/a	0.3	0.6	n/a	6.7
Cu	n/a	0.4	2.7	0.8	2.5
Ca	n/a	0.3	n/a	n/a	n/a
K	n/a	n/a	n/a	0.4	1.3
O	n/a	1.0	3.2	2.3	5.4

In addition to the color of the steel surface under the coating at the time of investigation, the color of the epoxy coating itself was also recorded. This was carried out based on the observation that the epoxy coating degradation (increase in brittleness) under certain exposure conditions is accompanied by color change. Five typical coating colors were observed. The colors are presented in Table 5.6 along with the values assigned.

Table 5.6 Coating color

Value	Coating color
1	Glossy green
2	Green
3	Light green
4	Dull green
5	Pale green

Both the new ECR and the EECR samples were investigated as described at Virginia Tech facilities.

5.6.4 Holidays

Holidays are flaws in the coating indiscernible to the naked eye. These discontinuities are detected by testing the continuity of the coating. The test was

performed on the EECR samples at the VTRC facilities. The new ECR samples were tested at the Virginia Tech facilities. In both cases, the tests were performed using the same Tinker & Rasor Model M-1 holiday detector according to ASTM G 62 "Holiday Detection in Pipeline Coatings".

Kentucky Department of Transportation, one of many state transportation agencies that use this test regularly, describes the procedure as follows: Wet the sponge until it is damp, but not dripping wet. Connect the wire lead to an uncoated spot on the bar and then move the sponge up and down the bar from one end to the other. The holiday detector will beep when a holiday or bare area is touched.

5.6.5 Differential Scanning Calorimetry

A TA DSC Q1000 v5.1 instrument was used to determine the initial and final glass transition temperature (T_g) of the samples and thereby assess the level of curing of the epoxy coating. 83 EECR samples and 18 new ECR coating samples, weighing approximately 12mg were tested. 10 powder samples weighing approximately 12mg were also tested to determine the curing temperature and Tg value of the three unadulterated powder coatings. The testing regimen imposed is presented in Table 5.7.

Table 5.7 DSC Process

Step	Process
1	Equilibrate to 25°C
2	Ramp 10°C/min to 250°C
3	Isothermal 30 seconds
4	Equilibrate to 25°C
5	Ramp 10°C/min to 250°C
6	Terminate process

5.6.6 Thermo-gravimetric analysis

A TA TGA Q100 instrument was used to determine the moisture content of the of the same number of coating samples as the ones for which the T_g values were obtained. Coating samples weighting approximately 15 mg were heated to 160 °C. The

temperature was then held constant for 30 minutes to ensure all moisture was removed. The pan was flame-dried over a Bunsen burner prior to each test, and each test was performed in an air atmosphere. The weight loss was recorded both as a function of time as well as temperature.

5.6.7 Scanning electron microscopy (FE-SEM)

Micrographs of the coating samples were obtained using a LEO 1550 FE-SEM at an accelerating voltage of 5Kv. Micrographs were taken at 100x, 500x, 2Kx, 5Kx and 10Kx. The condition of the epoxy surface was examined for evidence of cracking, porosity and other damage. The chemical composition for all specimens imaged was determined using Energy Dispersive X-ray Microanalysis (EDAX) and was performed by an Iridium Microanalysis (I/RF) System. Sample preparation included: 1) cleaning the specimens with acetone and ethanol to remove any oils from the machining process, and 2) the specimens were subsequently sputter-coated with a palladium/gold alloy 10μm thick.

5.6.8 Energy dispersive spectrometry

Energy dispersive X-Ray microanalysis (EDAX) was also performed to determine the chemical composition of the samples, specifically the presence of Cl^-, which is a critical element in the corrosion process of reinforcing steel. The chemical analysis composition was performed concurrently with scanning electron microscope (SEM) image analysis, which insured that the image was indeed that of the epoxy and not artifacts such as cement paste or steel oxidation products present on the coating sample.

5.6.9 Fourier Transform Infrared Spectrometry (FT-IR)

Spectra from four powder samples were collected. The samples were provided by coated bar suppliers to VDOT. The coating powder manufacturers represented were 3M Scotchcote 413, two Valspar samples, and DuPont. The spectra were obtained directly from the powder samples, with no additional preparation, using the attenuated total reflection technique (ATR).

5.7 Data Analysis

Since the effects of the different coating parameters on corrosion activity are not entirely understood, the aims of this study are to identify the probability of parameter inter-relationship and possibly create a regression model that will correlate the coating parameters with the observed corrosion activity. Should this simple stochastic model prove to be reasonably accurate, it can then be used in creating a more complicated and accurate deterministic model through the use of Monte Carlo or other sampling techniques.

6.0 RESULTS

6.1 Epoxy Powder Test Results

Infrared spectra were obtained from the four powder samples. The superimposed results are presented in Figure 6.1. From the plot, it is clear that there are no discernible differences in the general structures of the different products.

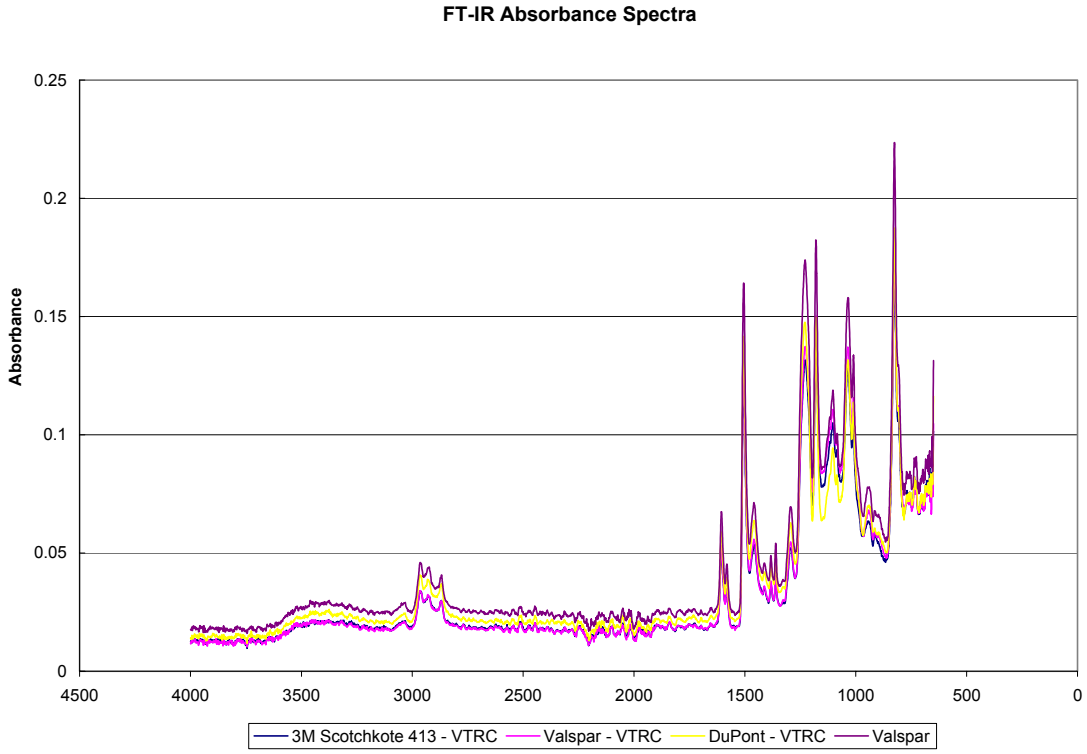

Figure 6.1 Fusion bonded epoxy powder FT-IR spectra

The glass transition temperature (T_g) was also determined. Three separate tests were performed from the samples available. The individual as well as the average values are presented in Table 6.1. The DuPont sample had the lowest T_g with a three test average value of 84.7°C, while the 3M Scotchkote sample collected from the coating plant presented the highest with a three test average value of 120.9°C.

Table 6.1 Epoxy Powder T_g values

Powder Sample	T_g1 (°C)	T_g2 (°C)	T_g3 (°C)	Average T_g (°C)
3M Scotchkote - VTRC	114.9	125.9	121.9	120.9
Valspar - VTRC	98.2	100.7	96.7	98.5
DuPont - VTRC	86.8	84.2	83.2	84.7
Valspar	103.1	97.4	102.3	100.9

6.2 ECR Rebar Samples

The samples collected by Virginia Tech consisted of one No. 5 coated bar 20 or 25 ft. cut into four or five 5 ft. length samples labeled S1 through S4 or S5, respectively. Samples WWBVTRC that were provided for analysis by VDOT representatives at the construction site were already cut to the 5 ft. length and wrapped when picked up, as were the OBP samples. The OBP samples were #3 bars, all other ECR project samples were #5 bars. Measurements performed on the epoxy coating taken from the new ECR samples were moisture content, determination of the glass transition temperature (T_g) before and after additional curing, coating thickness and residual adhesion.

The T_g values and moisture content are presented in Table 6.2. The initial T_g values ranged from a low of 84.6°C (BSCC – S3) to a high of 102.2°C (LNE – S4) while fully cured values ranged from a low of 96.8°C (OBP – S4) to a high of 102.2°C (LNE – S4). LNE – S4 was the only sample that was fully cured, exhibiting no change in T_g following a curing treatment designed to fully cure the film. The remaining samples exhibited changes in T_g ranging from 9.7°C (FSC – S2) to 15.9°C (WWBVTRC – S3). The moisture content ranged from a low of 0.34% (FSC – S4) to a high of 1.59% (BSCC – S1).

Table 6.2 New ECR coating T_g and Moisture Content

Specimen	Sample	T_g (°C)	Full T_g (°C)	ΔT_g (°C)	ΔT_g (°C) due to Moisture	Difference in ΔT_g	Moisture %
Woodrow Wilson - VT	S2	89.5	102.4	12.9	9.0	3.9	1.39
	S4	87.7	100.2	12.5	7.8	4.7	1.23
Woodrow Wilson Bridge -VDOT	S1	87.8	101.6	13.8	9.2	4.6	1.44
	S3	87.6	103.4	15.9	9.2	6.7	1.42
Hall Hodges Plant (HHP)	S2	88.4	102.2	13.8	7.3	6.5	1.13
	S4	89.1	102.6	13.5	7.9	5.6	1.22
Buffalo Creek (BFC)	S2	90.1	101.4	11.3	9.2	2.1	1.43
	S4	89.0	101.5	12.5	8.0	4.5	1.25
Bay Shore Cape Charles (BSCC)	S1	87.1	100.9	13.8	10.1	3.7	1.59
	S3	84.6	99.9	15.3	8.5	6.8	1.33
Florida Steel (FS)	S2	87.6	101.3	13.7	8.8	4.9	1.38
	S4	86.1	101.2	15.0	8.0	7	1.25
Occoquan Bridge Project (OBP)	S2	87.0	98.8	11.8	7.6	4.2	1.2
	S4	85.4	96.8	11.5	8.3	3.2	1.33
Free State Coaters (FSC)	S2	91.4	101.1	9.7	7.2	2.5	1.12
	S4	86.0	99.6	13.7	2.2	11.5	0.34
Lane Enterprises (LNE)	S2	89.0	99.3	10.4	4.0	6.4	0.63
	S4	102.2	102.2	0	5.3	-5.3	0.81

The column labeled "ΔT_g (°C) due to Moisture" represents the maximum change in T_g attributable to the level of moisture measured assuming that all of the moisture would contribute to a change in T_g. Only a small portion of the measured moisture may in fact be responsible for a decrease in the coating T_g, the remaining water being bulk water. The change in T_g was calculated using the Gordon-Taylor equation, presented below:

$$\frac{1}{T_g} = \frac{W_1}{T_{g1}} + \frac{W_2}{T_{g2}} \qquad \text{Equation 6.1}$$

Where: T_g = Glass transition temperature of the Coating/Water mix (Kelvin)

W_1 = Weight percent of water in the coating

T_{g1} = Glass transition temperature of water (136 Kelvin)

W_2 = Weight percent of coating

T_{g2} = Glass transition temperature of fully cured dry coating (Kelvin).

Figure 6.2 illustrates a typical DSC plot showing the difference in T_g due to additional curing. The initial T_g of sample LNE – S2 was 91.4°C as shown by the upper plot in the figure, with maximum additional curing occurring at 130.8°C. The fully cured T_g of this sample was 101.1°C, with the sample showing no additional curing as evidenced by the constant slope of the lower plot at 130.8°C.

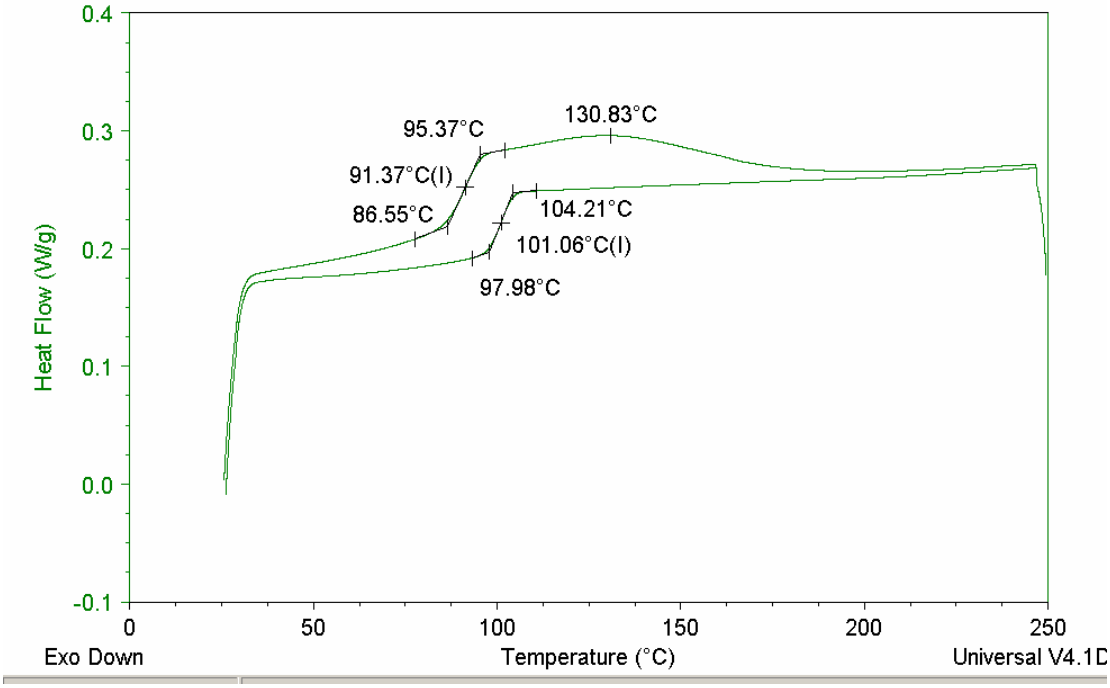

Figure 6.2 Sample LNE S2 DSC plot

In addition, ECR coating thickness, the visible damage number, holidays and the approximate age of the sample at collection time are presented in Table 6.3. The OBP samples had the least damage number at 0.1/304.8 mm as well as the least number of holidays with 0.0/304.8 mm. The LNE samples had the greatest damage number with 1.76/304.8 mm, while the holiday detector beeped continuously. The LNE holiday results were not used in further analysis because of continuous holiday detection. At collection time, the age of the samples, was noted as time in field because we could not determine the manufacture date. Also, the time in field represents information provided by construction personnel. The stated age at the time of collection was 1 week for the Woodrow Wilson Bridge projects and Hall Hodges Plant and 2 weeks for the Occoquan Bridge and Buffalo Creek projects. The Bay Shore Concrete sample was 68 weeks old, being exposed to the environment at the casting plant for that time period. The Virginia Tech Free State Coaters, Florida Steel, and Lane Enterprises samples were exposed to a field environment of 4 weeks plus 8 years in the laboratory covered by a black plastic tarp to protect the ECR from UV light.

Table 6.3 New ECR Sample Measurements

Specimen	Damaged Areas /304.8 mm	Thickness (µm)	Thickness Stdev (µm)	Holidays/304.8 mm	Time in Field (weeks)
Woodrow Wilson - VT	10.2	263	34	1.0	1
Woodrow Wilson Bridge	1.8	344	46	0.2	1
Hall Hodges Plant	20.8	263	39	4.0	1
Buffalo Creek	10.0	218	50	4.4	2
OBP	1.2	243	37	0.0	2
Bay Shore Cape Charles	7.8	321	60	0.8	68
FS	9.0	242	76	7.6	4*
FSC	12.6	251	62	2.8	4*
LNE	21.2	141	37	∞	4*

* - Plus additional 8 years laboratory storage

The thickness measurements were performed at 20 random locations along the bars. Three measurements were taken at each of the 20 locations and the results averaged. As illustrated in Figure 6.3, the thickness measurements were normally distributed. This conclusion is supported by the P-value 0.01that is greater than 0.05.

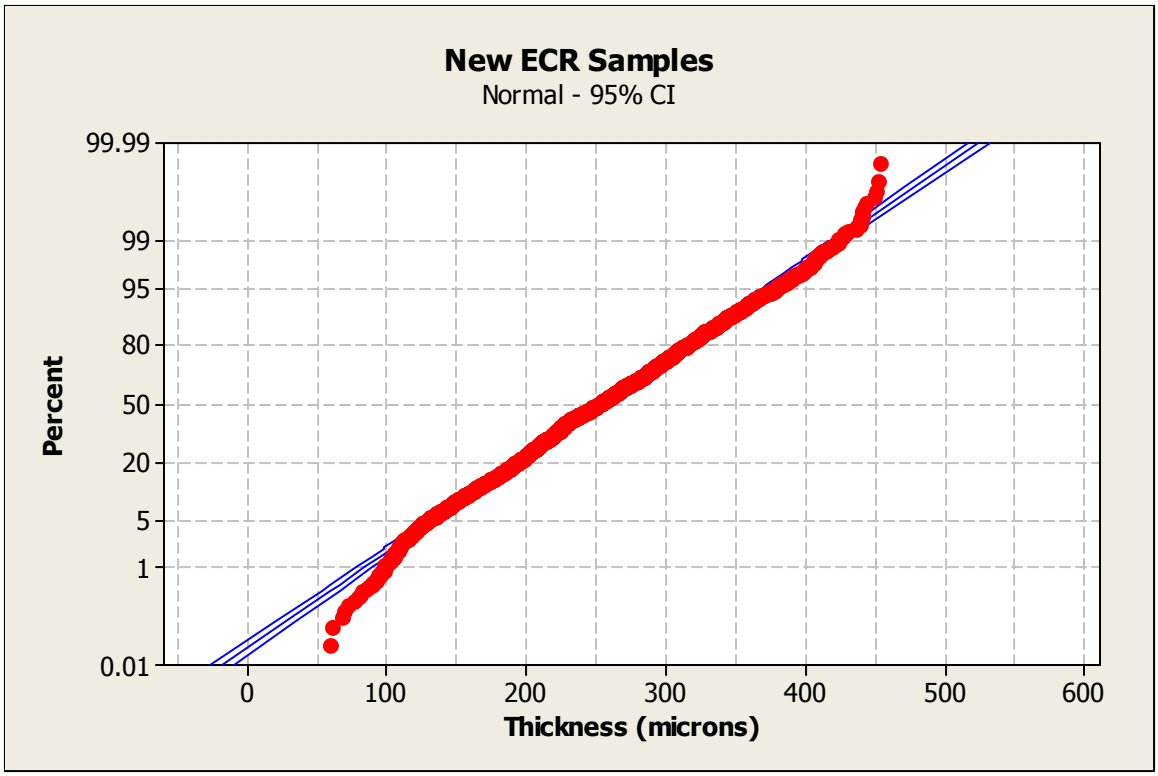

Figure 6.3 ECR Epoxy Coat Thickness Measurements Distribution

The average thickness measurements and the 95% confidence intervals are presented in Figure 6.4 for the individual samples with the minimum and maximum specified thickness represented by the two horizontal lines at 175 µm and 300 µm. Three sample sets, WWBVTRC, BSCC, and LNE failed to meet the current coating thickness specifications. The average thickness of WWBVTRC is 344 µm with a standard deviation of 46 µm, and the average thickness of BSCC is 321 µm with a standard deviation of 60 µm. The average thickness of both sample sets is above the maximum current specification. Inversely, the average thickness of LNE is below the current specified minimum of 175 µm at 141 µm with a standard deviation of 34 µm.

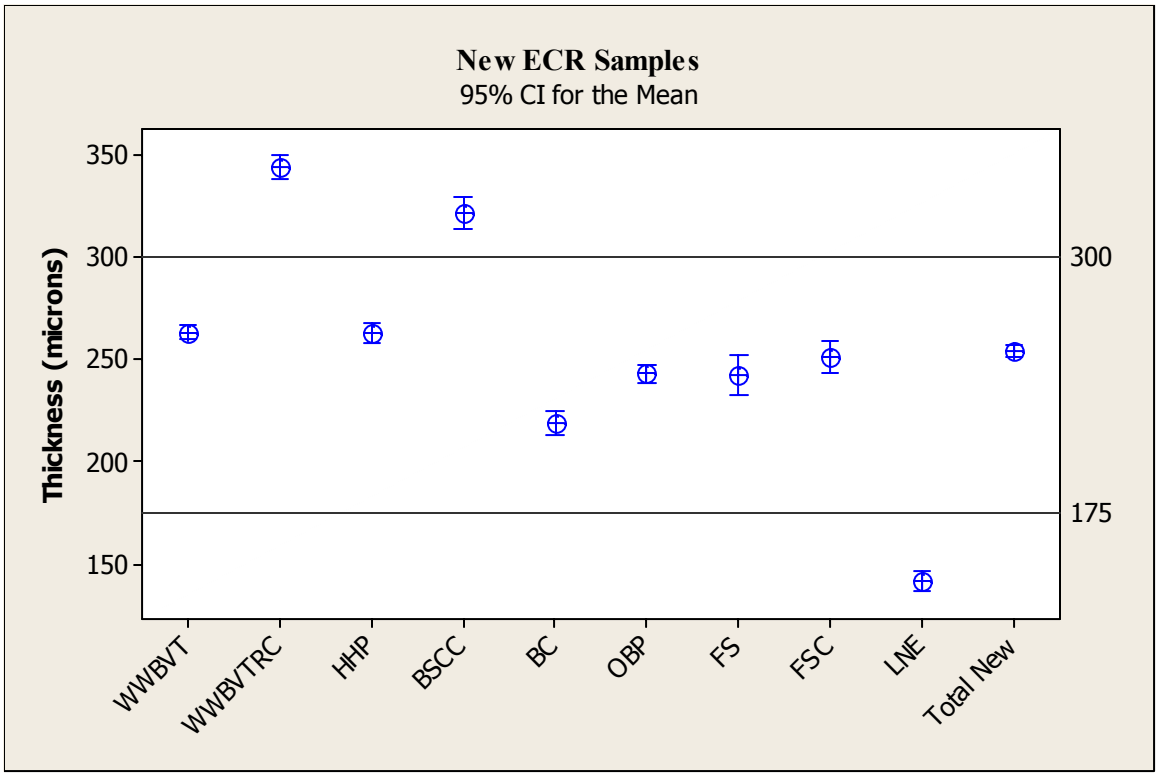

Figure 6.4 New ECR Coating Thickness

6.3 Extracted ECR Rebar Samples

The same tests and measurements performed on the new ECR samples were conducted on select specimens from the extracted ECR samples. The tests were limited to three random specimens from each structure investigated due to time and cost limitations. Since one of the goals of the study was to determine the condition and deterioration level of the coating, the samples obtained from cracked cores were not analyzed. ECR specimens from cracked concrete locations were excluded because the coating may have been damaged by the rapid ingress of chlorides and possible subsequent corrosion. The T_g and moisture content of the sampled specimens are presented in Table 6.4.

Table 6.4 Extracted ECR Coating T_g and Moisture Content

Structure	Core Sample	T_g (°C)	Final T_g (°C)	ΔT_g (°C)	ΔT_g (°C) due to Moisture	Difference in ΔT_g	% Moisture
1003-3	C2	*	*	*	*	*	1.75
	C7	*	*	*	*	*	*
	C1	99.1	112.8	13.7	10.4	3.3	1.50
1019-8	C1	99.2	111.5	12.3	10.7	1.6	1.57
	C4	99.5	111.0	11.4	11.0	0.4	1.62
	C5	98.2	110.9	12.6	10.2	2.4	1.50
1020-2	C1	87.0	111.3	24.3	8.7	15.6	1.27
	C3	102.1	113.3	11.3	8.8	2.5	1.27
	C6	102.1	115.1	13.1	9.6	3.5	1.37
1031-9	C1	86.6	112.5	25.8	9.6	16.2	1.39
	C4	94.3	110.5	16.2	10.1	6.1	1.48
	C5	105.5	113.3	7.8	8.5	-0.7	1.22
1132-1	C1	94.9	109.2	14.3	9.9	4.4	1.46
	C4	98.9	108.5	9.6	9.3	0.3	1.38
	C6	98.2	109.1	10.9	10.0	0.9	1.48
1133-8	C1	90.8	108.9	18.0	10.6	7.4	1.58
	C3	95.1	110.4	15.2	10.8	4.4	1.59
	C5	97.4	112.0	14.6	9.8	4.8	1.43
1139-9	C1	97.6	111.7	14.1	11.2	2.9	1.64
	C3	86.7	113.4	26.7	10.4	16.3	1.50
	C6	81.2	115.1	33.9	5.5	28.4	0.78
1152-1	C1	96.0	112.6	16.7	9.6	7.1	1.39
	C2	104.3	111.6	7.4	7.5	-0.1	1.09
	C3	103.2	112.7	9.4	7.4	2	1.06
2547-5	C1	86.9	113.1	26.2	12.2	14	1.78
	C2	84.2	110.1	25.9	11.0	14.9	1.62
	C6	87.2	102.3	15.2	6.8	8.4	1.04
2815-1	C1	103.7	114.6	10.8	8.6	2.2	1.23
	C3	98.6	113.3	14.8	11.2	3.6	1.62
	C6	78.9	113.4	34.5	8.4	26.1	1.21
1000-3A	C1	101.0	110.3	9.4	10.0	-0.6	1.47
	C2	99.5	109.7	10.2	8.8	1.4	1.30
	C4	99.9	109.5	9.6	9.0	0.6	1.33
1000-3B	C1	100.5	110.2	9.7	9.1	0.6	1.33
	C2	98.9	109.9	11.0	5.8	5.2	0.85
	C4	83.0	110.1	27.0	9.4	17.6	1.38
1002-8	C1	86.2	109.9	23.7	9.2	14.5	1.35
	C3	83.1	111.7	28.6	11.7	16.9	1.72
	C4	107.0	109.5	2.5	8.1	-5.6	1.19
1002-9	C2	96.0	110.6	14.7	7.9	6.8	1.16
	C4	87.6	110.6	23.0	9.1	13.9	1.33
	C6	98.4	109.8	11.4	10.4	1	1.53
1007-4	C1	99.6	111.0	11.4	10.0	1.4	1.47
	C3	83.8	108.7	24.9	11.6	13.3	1.73
	C6	101.6	108.5	6.9	10.3	-3.4	1.53
1014-9	C1	101.7	111.4	9.8	7.0	2.8	1.01
	C3	83.6	104.0	20.4	10.5	9.9	1.61
	C6	81.7	103.6	21.9	10.3	11.6	1.58
1017-3	C1	99.5	107.6	8.1	7.5	0.6	1.12
	C2	83.4	109.8	26.4	8.4	18	1.24
	C4	85.8	109.0	23.3	7.1	16.2	1.04

1042-8	C1	106.4	111.1	4.7	7.8	-3.1	1.13
	C3	103.2	111.1	7.9	7.7	0.2	1.12
	C4	99.9	109.2	9.4	8.7	0.7	1.29
1098-9	C2	101.9	101.0	8.1	7.8	0.3	1.22
	C4	101.0	110.9	9.9	8.5	1.4	1.24
	C7	104.2	111.0	6.8	7.5	-0.7	1.09
1133-1	C1	84.1	110.1	26.0	10.1	15.9	1.49
	C3	95.7	108.4	12.8	9.3	3.5	1.38
	C6	82.7	108.4	25.7	11.2	14.5	1.67
2819-1	C1	98.6	109.2	10.6	11.0	-0.4	1.63
	C3	96.2	108.4	12.2	9.0	3.2	1.34
	C5	97.2	107.6	10.4	11.8	-1.4	1.77
6051-1	C1	102.3	112.4	10.1	10.7	-0.6	1.55
	C4	99.5	109.2	9.7	8.5	1.2	1.25
	C6	86.8	109.6	22.8	11.6	11.2	1.73
2820-1	C1	100.2	111.0	10.8	10.0	0.8	1.46
	C4	98.7	108.3	9.6	12.6	-3	1.89
	C6	99.9	112.8	12.9	11.0	1.9	1.60
1021-2	C1	99.9	109.1	9.2	7.5	1.7	1.11
	C2	100.6	107.8	7.2	8.5	-1.3	1.26
	C4	104.2	110.3	6.1	7.0	-0.9	1.02
2901-4	C1	*	*	*	*	*	1.83
	C5	87.9	109.6	21.7	11.3	10.4	1.67
	C6	87.8	108.1	20.3	7.9	12.4	1.18
2812-5	C1	100.1	108.8	8.7	11.1	-2.4	1.66
	C4	84.2	111.1	27.0	10.4	16.6	1.52
	C6	83.6	111.3	27.6	12.0	15.6	1.76
1920-7	C2	102.4	112.6	10.2	10.4	-0.2	1.51
	C3	100.0	110.4	10.4	10.8	-0.4	1.59
	C6	98.5	111.7	13.2	9.9	3.3	1.44
6058-9	C1	93.4	97.9	4.4	7.0	-2.6	1.11
	C3	90.5	102.2	11.8	7.4	4.4	1.14
	C6	96.6	99.1	2.5	5.2	-2.7	0.82

Note: * - Unable to collect data from sample

The initial T_g values ranged from a low of 78.9°C (2815-1 C6) to a high of 107.0°C (1002-8 C4) while fully cured values ranged from a low of 97.8°C (6058-9 C1) to a high of 115.1°C (1139-9 C6). The EECR samples showed changes in T_g ranging from 2.5°C (1002-8 C4 and 6058-9 C6) to 27.6°C (2812-5 C6). The moisture content ranged from a low of 0.82% (6058-9 C6) to a high of 1.89% (2820-1 C4).

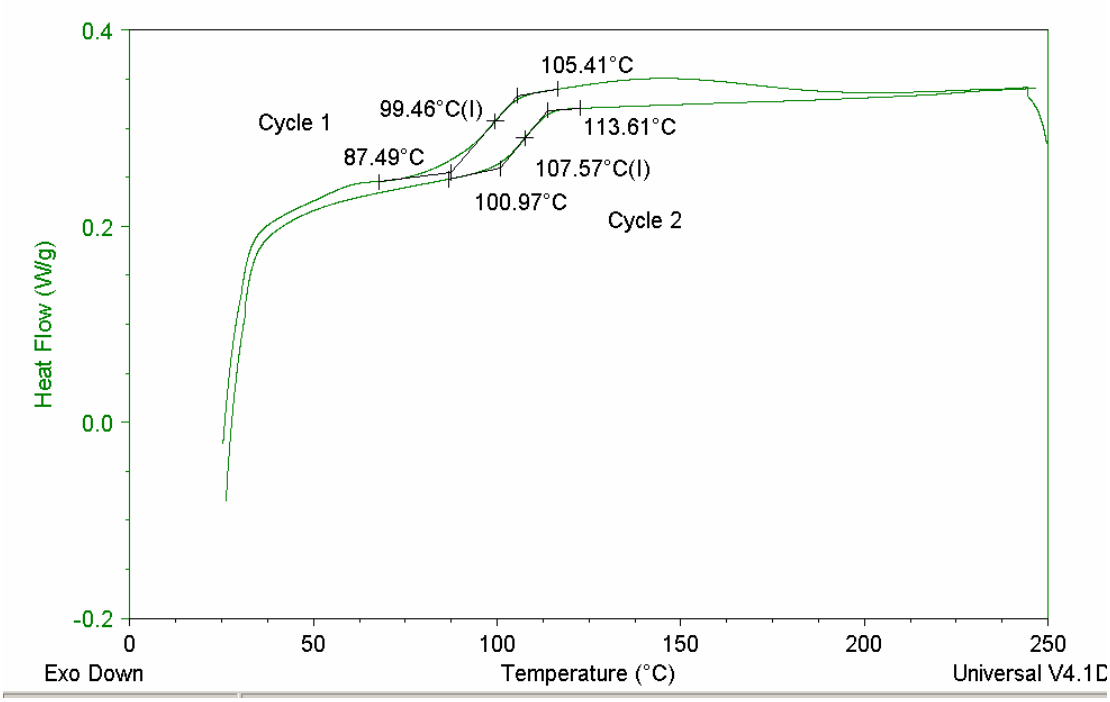

Figure 6.5 1017-3 C1 DSC Plot

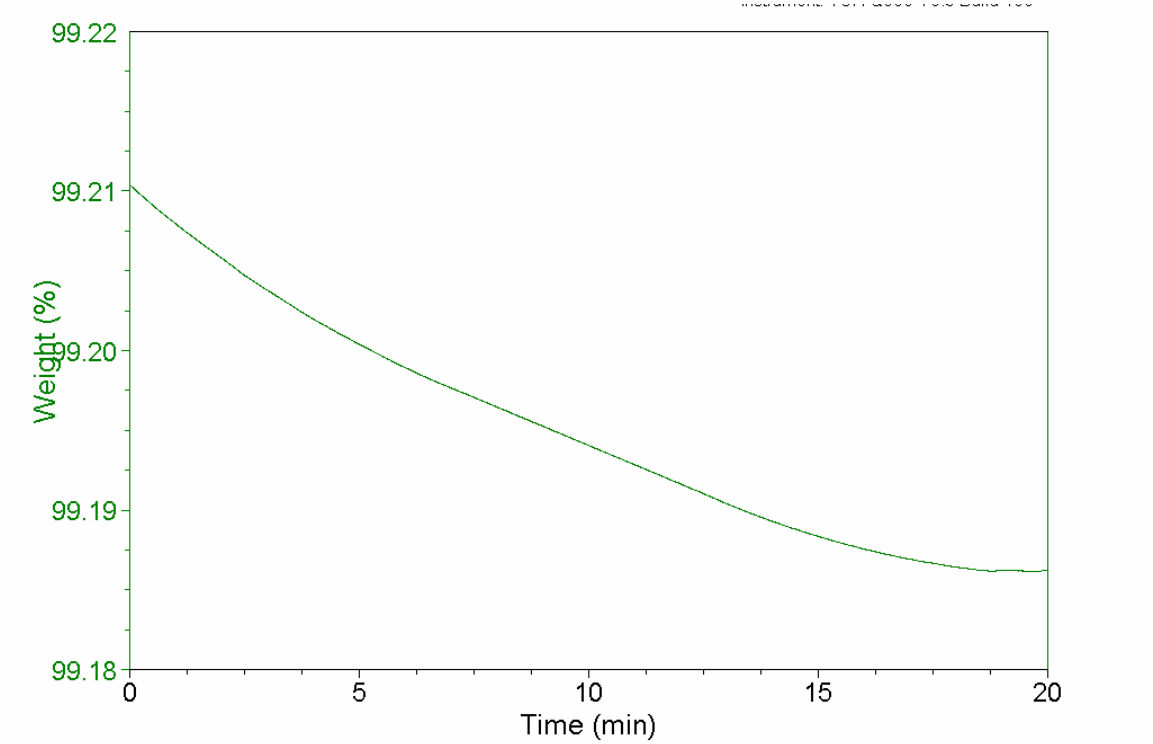

Figure 6.5 6058-9 C6 TGA Plot

Figure 6.5 illustrates a typical DSC plot showing the difference in T_g due to additional curing while Figure 6.6 illustrates the moisture weight loss plotted as a

function of time. The initial T_g of sample 1017-3 C1 was 99.5°C as shown by the upper plot in the figure, with maximum additional curing occurring at 150°C. The fully cured T_g of this sample was 107.6°C, with the sample showing no additional curing as evidenced by the constant slope of the lower plot at 150°C.

The average coating thickness, coating color, average residual adhesion, holidays, the number of damaged areas, % corroded area, the color of corrosion products under the coating, the coating cracking number, % cracking and porosity and % moisture content are presented in Table 6.5. The corrosion related measurements of concrete resistivity, half-cell corrosion potentials and linear polarization, as well as concrete chloride content at bar level are presented in Table 6.6.

Using the Gordon-Taylor equation, the potential change in the glass transition temperature of the coating was calculated, and the information is presented in the appropriate column. The difference between the measured change in T_g and the calculated change in T_g due to the measured moisture content is also presented to illustrate the fact that the coating is in fact not fully cured.

Table 6.5 Extracted ECR Test Data

Structure	Core Sample	Average Thickness (microns)	Coating Color	Average Residual Adhesion	Holidays/ 304.8 mm	# Damaged Areas/ 304.8 mm	% Corroded Area	Color of Corrosion Products	Cracking	% Cracking and Porosity
1003-3	C2	209	1	5.00	0.00	0.00	0.00	4.00	*	*
	C7	*	1	3.67	*	1.25	0.75	3.00	2	6.44
	C1	233	1	4.33	1.75	0.00	0.00	4.00	1	6.95
1019-8	C1	266	2	4.00	0.25	0.25	0.18	2.00	4	11.65
	C4	191	2	5.00	4.00	0.50	0.25	2.67	3	6.11
	C5	247	1	3.00	0.25	0.25	0.15	3.00	2	5.55
1020-2	C1	169	4	1.33	11.00	14.25	2.07	1.67	2	4.65
	C3	276	4	4.00	3.25	5.00	0.79	2.00	3	8.41
	C6	243	4	5.00	0.50	2.25	0.26	2.33	1	3.63
1031-9	C1	267	2	5.00	0.25	1.25	0.14	5.00	1	1.85
	C4	192	2	5.00	4.50	2.25	0.13	5.00	1	7.16
	C5	251	2	2.67	0.75	0.75	0.13	2.00	1	3.77
1132-1	C1	276	2	5.00	0.75	1.00	0.26	4.00	1	3.86
	C4	261	2	2.00	0.50	0.50	0.06	1.33	2	3.51
	C6	260	2	2.33	0.50	0.00	0.00	1.00	1	5.35
1133-8	C1	199	2	3.67	1.25	2.25	0.18	1.67	3	2.83
	C3	177	2	3.00	3.00	4.25	0.65	2.00	3	3.55
	C5	214	2	2.33	4.00	1.25	0.13	2.00	2	4.18
1139-9	C1	232	4	2.00	0.25	0.00	0.00	1.00	4	7.74
	C3	195	1	2.67	0.00	3.00	0.59	2.33	1	6.63
	C6	256	2	2.00	0.00	0.00	0.00	1.00	2	3.81
1152-1	C1	328	1	3.33	1.00	3.75	0.19	2.00	2	6.91
	C2	250	1	2.00	1.25	4.50	0.38	1.00	1	8.74
	C3	294	1	2.33	1.50	1.50	0.90	1.00	1	4.10
2547-5	C1	194	2	4.00	10.25	5.25	0.80	3.67	2	4.47
	C2	256	2	4.33	8.00	5.75	1.50	3.00	4	4.44
	C6	170	*	1.00	3.50	2.25	0.35	1.00	*	*
2815-1	C1	237	2	5.00	1.00	4.25	0.70	4.00	2	4.73
	C3	172	4	3.00	5.00	2.50	0.33	3.00	*	*
	C6	126	4	5.00	7.00	3.25	0.36	4.00	1	2.04
1000-3A	C1	246	2	5.00	0.50	4.75	0.74	4.00	2	8.76
	C2	294	2	3.67	1.25	1.00	0.19	3.00	1	15.80
	C4	253	2	3.67	0.25	2.75	0.38	3.00	1	8.50
1000-3B	C1	*	2	2.67	*	*	*	3.00	*	*
	C2	*	2	2.00	*	*	*	2.00	*	*
	C4	*	2	5.00	*	*	*	4.00	*	*
1002-8	C1	236	4	5.00	1.75	6.50	0.45	4.00	3	7.05
	C3	190	2	5.00	8.25	5.75	0.62	3.00	3	2.36
	C4	241	2	2.33	0.50	0.50	0.09	1.00	*	*
1002-9	C2	180	2	4.00	0.50	0.50	0.09	3.00	1	5.16
	C4	182	2	2.00	3.00	4.00	1.25	3.00	1	7.18

	C6	169	4	2.00	3.75	0.75	0.00	2.00	2	9.52
1007-4	C1	284	2	3.33	0.25	0.25	0.09	3.67	2	7.01
	C3	231	2	5.00	0.75	1.25	0.24	4.00	1	6.54
	C6	242	2	2.00	0.00	0.75	0.09	2.00	2	11.32
1014-9	C1	271	4	2.00	0.50	3.25	1.40	1.00	2	7.42
	C3	272	3	3.67	0.00	2.25	0.27	3.00	1	2.45
	C6	*	3	5.00	0.50	1.50	0.31	2.00	1	0.71
1017-3	C1	459	2	2.00	0.00	2.25	0.25	1.00	3	7.03
	C2	278	2	5.00	0.50	1.50	0.21	4.00	1	1.61
	C4	329	2	2.67	0.00	0.00	0.00	1.00	2	5.49
1042-8	C1	309	1	2.33	2.75	1.00	0.80	1.33	1	2.97
	C3	265	1	3.00	0.50	0.75	0.50	2.33	1	5.20
	C4	478	1	2.33	0.25	0.75	1.00	2.00	1	2.43
1098-9	C2	271	2	2.67	2.00	1.50	0.35	2.00	2	5.67
	C4	*	2	3.00	*	*	*	1.00	2	4.48
	C7	*	2	2.33	*	*	*	1.00	3	5.77
1133-1	C1	286	4	5.00	1.75	2.75	0.35	4.00	3	17.29
	C3	233	4	5.00	2.00	4.25	0.40	4.00	4	6.77
	C6	271	4	5.00	1.50	4.25	0.34	3.00	3	10.01
2819-1	C1	238	4	4.67	4.00	2.50	0.50	2.00	3	5.51
	C3	188	4	4.00	3.75	1.00	0.00	2.00	3	3.93
	C5	274	2	5.00	6.00	11.25	12.00	5.00	*	*
6051-1	C1	300	2	3.33	0.50	0.25	0.07	4.00	1	6.20
	C4	277	2	4.00	0.25	0.00	0.00	4.00	3	4.77
	C6	271	4	3.67	1.25	2.25	0.55	3.00	4	12.78
2820-1	C1	252	2	3.67	4.00	3.75	0.38	2.67	1	5.19
	C4	223	4	3.33	6.75	12.50	7.35	2.33	1	4.77
	C6	227	2	4.33	0.00	4.25	0.40	3.00	2	3.79
1021-2	C1	305	2	2.00	0.00	0.25	0.10	3.00	*	*
	C2	266	4	2.00	2.50	2.50	0.35	2.00	4	9.45
	C4	246	2	2.00	2.00	0.25	0.05	2.00	2	5.88
2901-4	C1	288	4	5.00	2.25	2.75	0.42	3.00	2	1.68
	C5	259	4	5.00	1.25	2.75	0.78	4.00	2	3.05
	C6	235	4	5.00	1.25	8.25	1.87	4.00	4	8.10
2812-5	C1	229	4	5.00	0.75	2.00	0.51	4.00	*	*
	C4	151	4	5.00	3.00	2.00	0.53	4.00	4	3.01
	C6	225	4	5.00	0.50	2.25	0.42	4.00	4	6.14
1920-7	C2	337	4	4.00	3.00	5.75	0.88	4.00	2	9.53
	C3	*	4	3.33	*	*	*	3.00	3	1.78
	C6	296	4	2.33	0.00	1.75	0.23	1.00	1	3.82
6058-9	C1	316	5	3.00	0.75	5.25	0.83	3.00	*	*
	C3	318	5	3.00	0.00	2.00	0.31	3.00	1	1.76
	C6	248	2	2.67	0.50	0.75	0.52	2.00	1	2.28

Note: * - Unable to collect data from sample

The thickness measurements were performed at six random locations along the bar sample. Three measurements were taken at each of the six locations and the results averaged. As illustrated in Figure 6.7, the thickness measurements were normally distributed

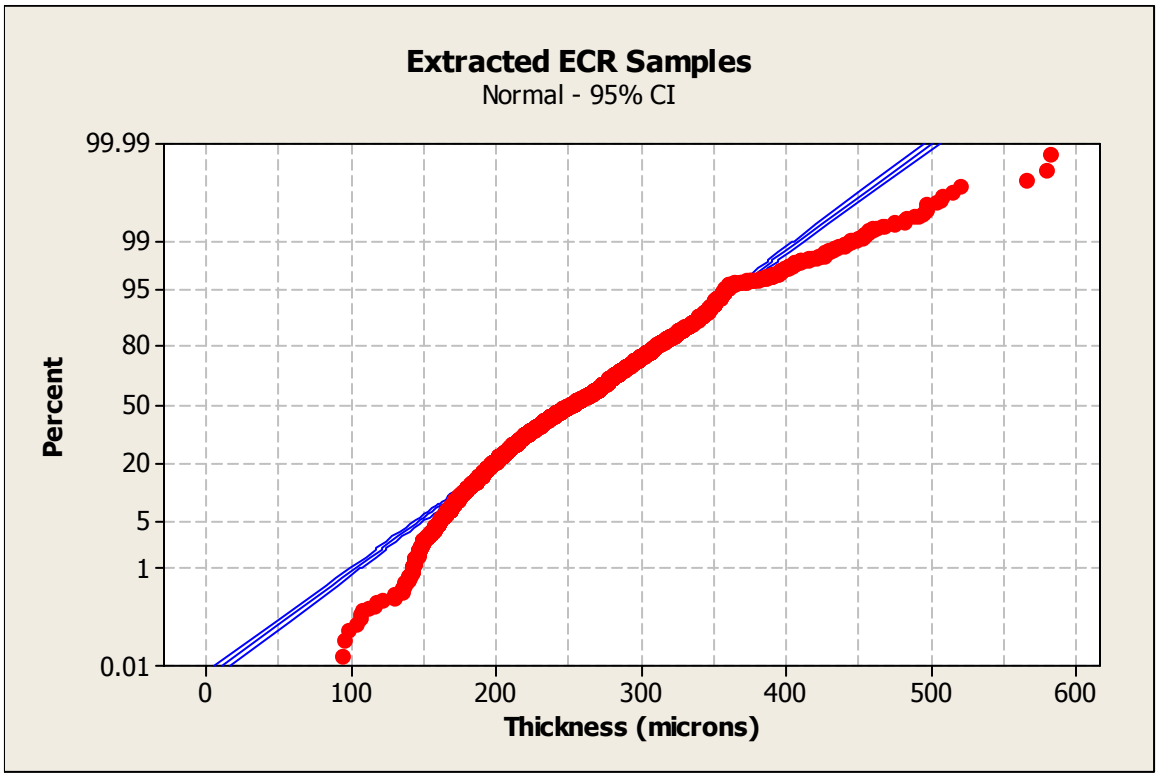

Figure 6.7 EECR Epoxy Coat Thickness Measurements Distribution

The average thickness measurements and the 95% confidence intervals are presented in Figure 6.8 with the minimum and maximum specified thickness represented by the two horizontal lines at 175 µm and 300 µm. Three sample sets, 1014-9, 1017-3, and 1042-8 failed to meet the current coating thickness specifications. The average thickness of 1014-9 is 310 µm with a standard deviation of 67.1 µm, the average thickness of 1017-3 is 322 µm with a standard deviation of 78.5 µm, and finally, the average thickness of 1042-8 is 335 µm with a standard deviation of 79.1 µm. The average thickness of both sample sets is above the maximum current specification. There were no samples failing the minimum specified thickness.

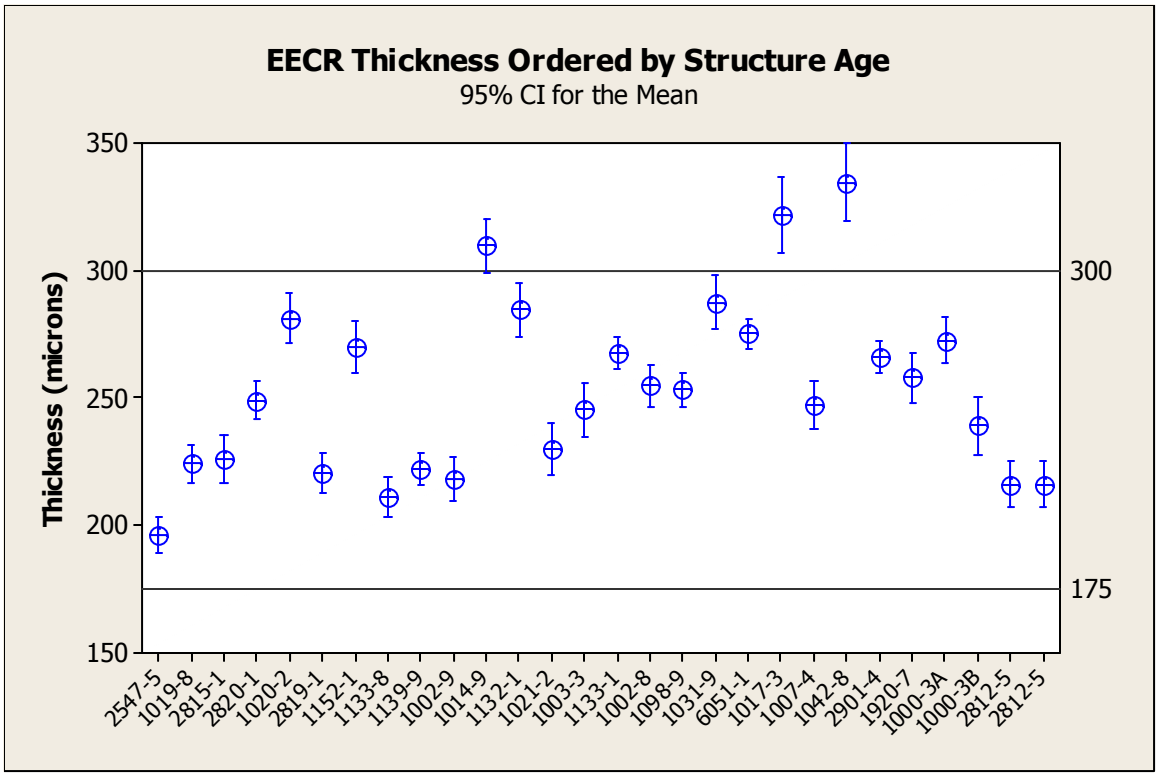

Figure 6.8 EECR Coating Thickness

Since a change in color from the original glossy green can be an indicator of coat degradation, this color change was recorded on a scale from 1 through 5, and the interpretation scale is presented in Chapter 5. From the sample population, the coating color of two structures showed no apparent change from new. The structures were 1003-3 and 1042-8. The remaining structures all presented some degree of coating color degradation with most experiencing loss of gloss rather than pigmentation. The distribution of color values is presented in Figure 6.9, while the mean and the standard deviation of each structure are presented in Figure 6.10.

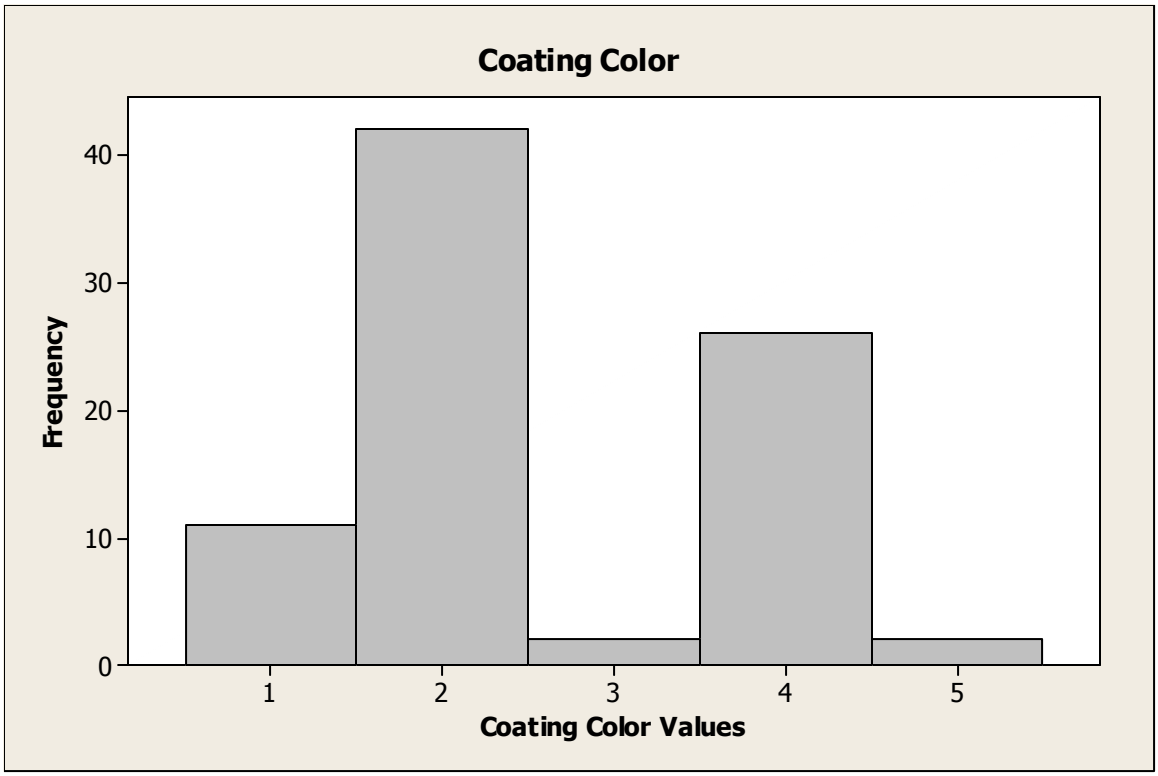

Figure 6.9 Coating Color Distribution

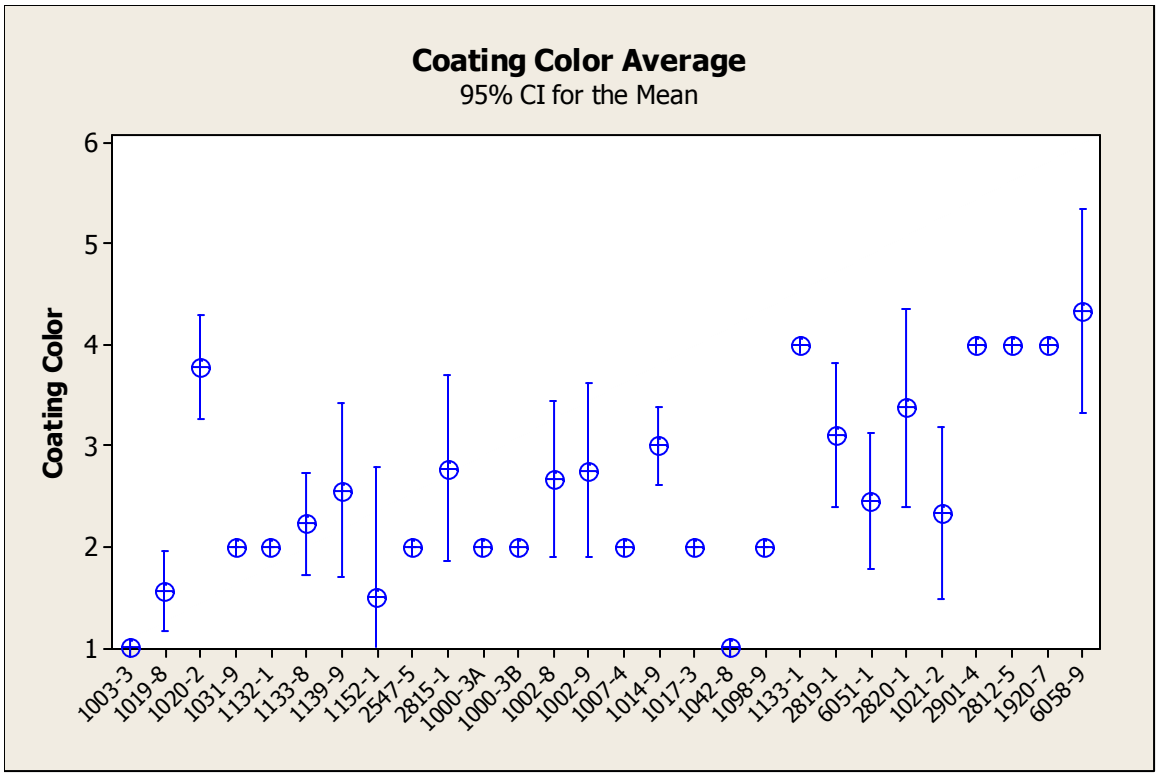

Figure 6.10 EECR Coating Color

Loss of adhesion between the coating and the rebar upon aging was significant. From a total of 666 measurements, only 18 exhibited no adhesion loss. From the remaining 648 measurements, 229 samples showed a complete loss of adhesion. All the remaining samples showed some level of residual adhesion loss ranging from 2 to 4. This information is illustrated in Figure 6.11 while the average and 95% confidence interval are presented in Figure 6.12. While there were a limited number of individual samples that showed no adhesion loss, every single structure investigated exhibited adhesion loss to a certain degree. Additionally, one structure, 2812-5, exhibited complete adhesion loss with an average of 5 and a standard deviation of 0, while six additional structures had residual adhesion averages greater than 4, indicating an almost complete loss of adhesion.

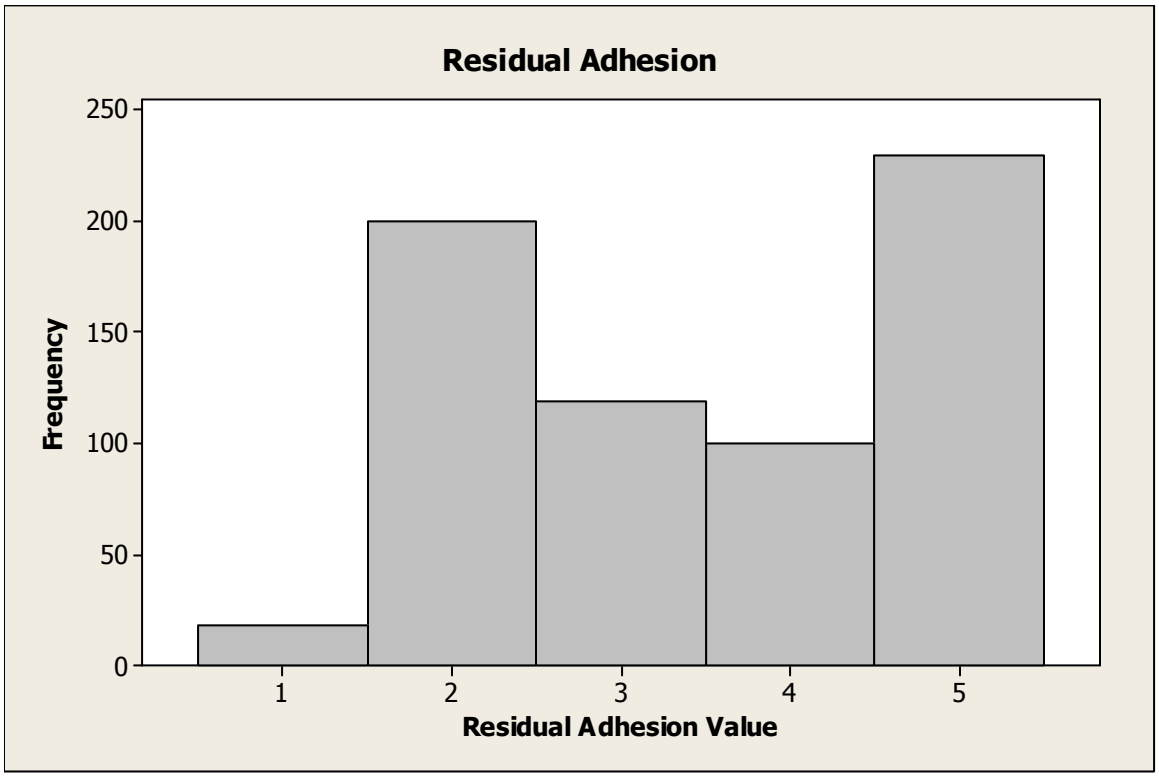

Figure 6.11 Residual Adhesion Distribution

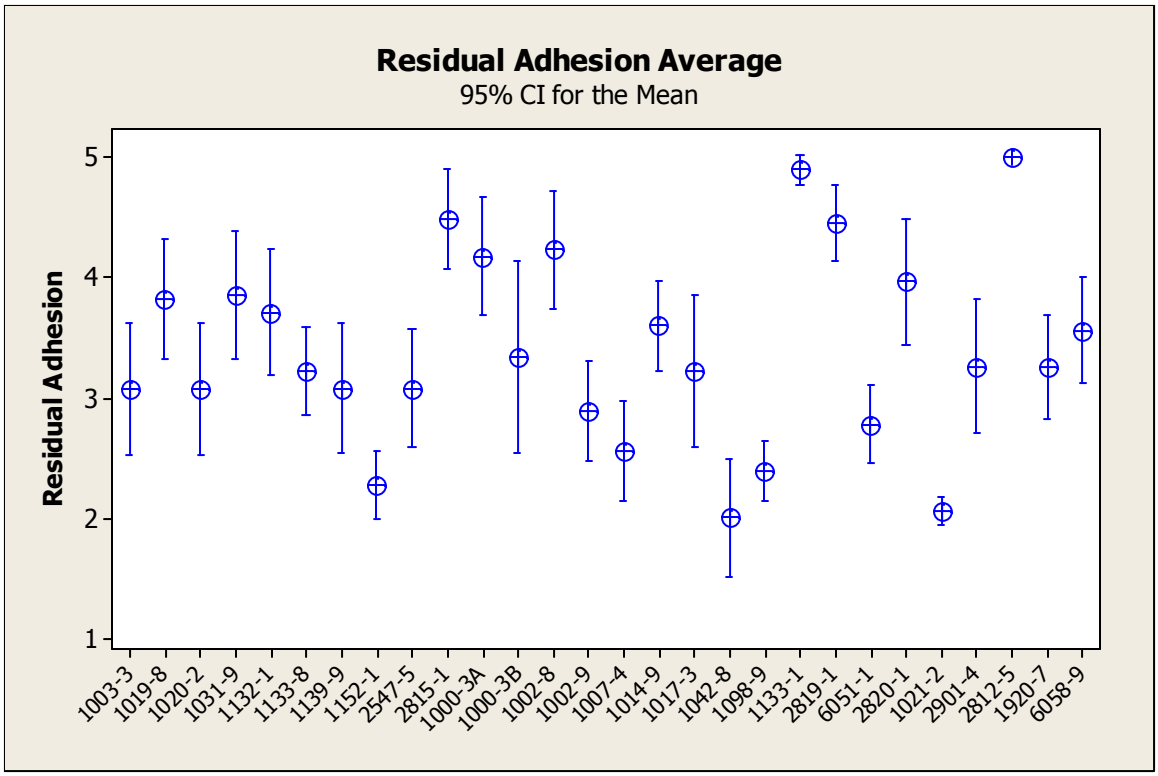

Figure 6.12 EECR Residual Adhesion

From a total of 244 individual specimens, 37 had no holidays while 74 had 1 holiday or less per 304.8 mm. The remaining 133 specimens had more than the allowable 1 holiday per 304.8 mm as currently specified. Conversely, out of 28 structures investigated, the average number of holidays per 304.8 mm of ECR bar of 18 structures failed to meet the maximum allowable number of holidays. Structure 1017-3 exhibited the lowest number of holidays with an average of 0.21 holidays/304.8 mm and a standard deviation of 0.25 holidays/304.8 mm. Structure 2547-5 exhibited the highest number of holidays with an average of 5.5 holidays/304.8 mm and a standard deviation of 3.9 holidays/304.8 mm. The average number of holidays/304.8 mm and the 95% confidence intervals are presented in Figure 6.12 with the maximum specified number of holidays/304.8 mm represented by the horizontal line at 1 holiday/304.8 mm. The number of holidays/304.8 mm is also highly positively skewed as shown in Figure 6.13.

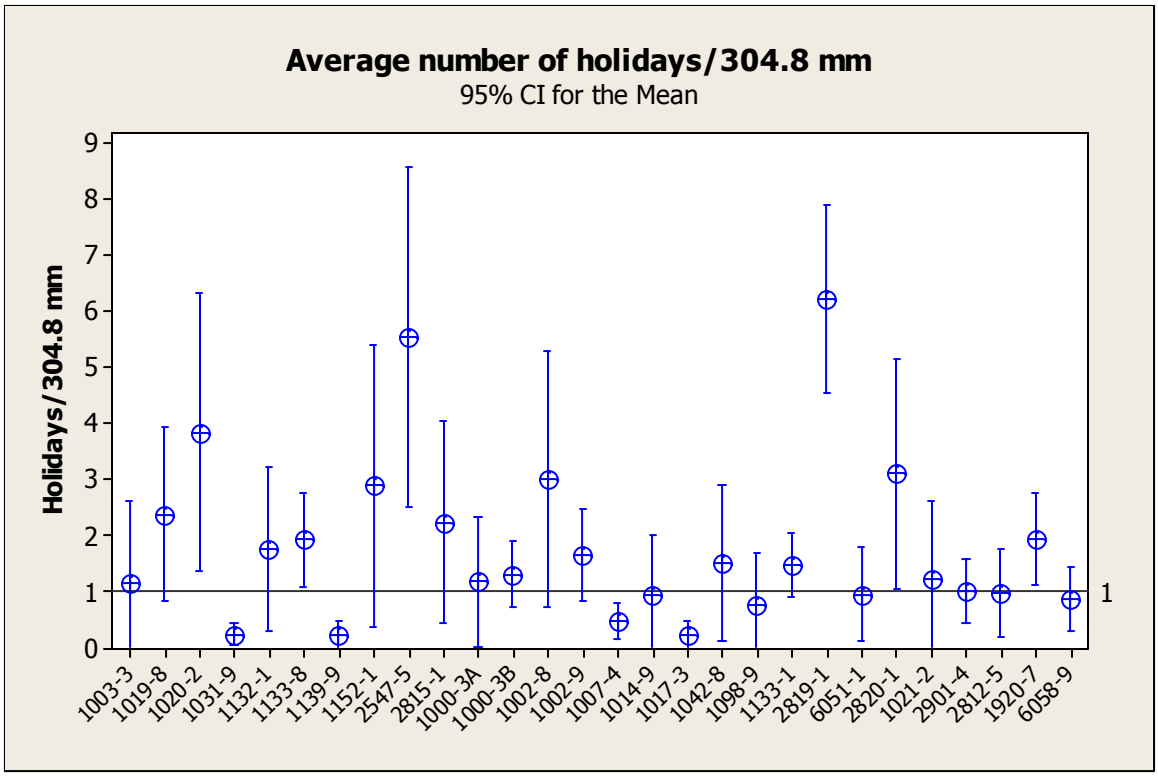

Figure 6.13 EECR Holidays

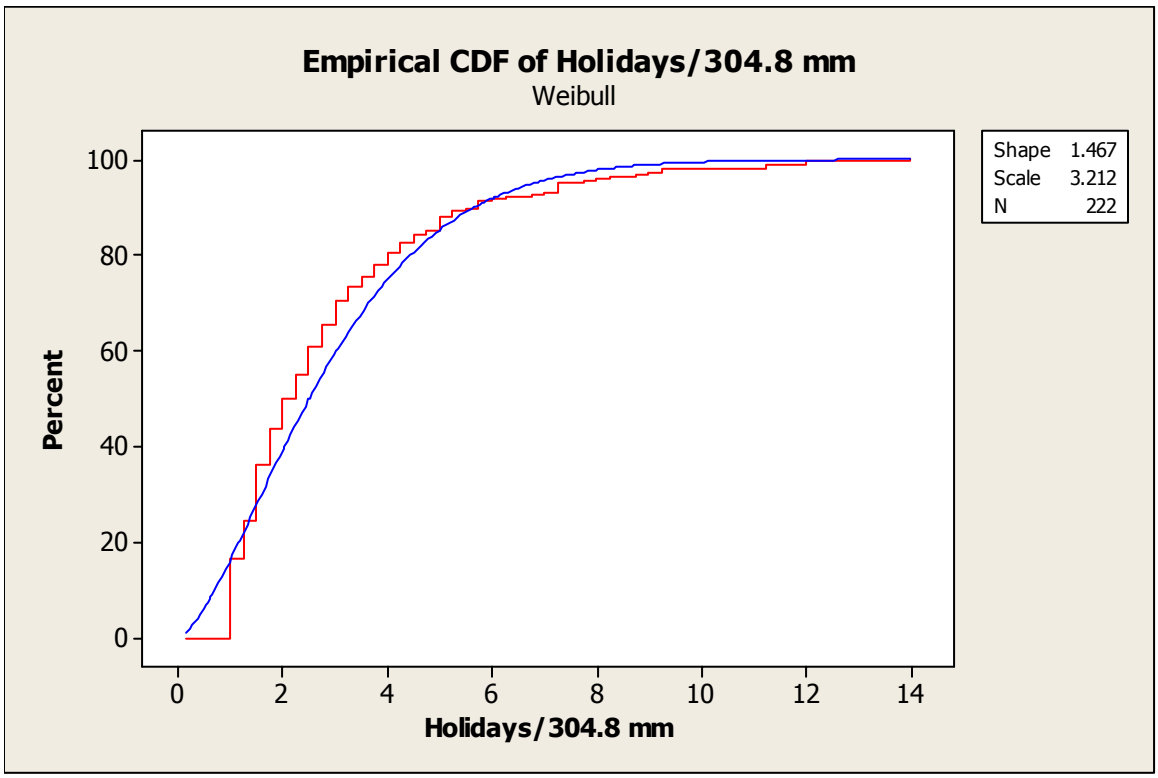

Figure 6.14 EECR Holiday CDF Plot

Similarly, the number of visible damages was also assessed. The number of damages follows a similar probability distribution as the holidays, as illustrated in Figure 6.14. Interestingly, there were no structures with zero damages per foot as shown in Figure 6.15. The lowest number of damages was shown by structure 1021-2 with 0.54 damages/304.8 mm and a standard deviation of 0.97. Structure 1019-8 had a similarly low number of damages with 0.56 damages/304.8 mm, but a significantly lower standard deviation at 0.50. The highest number of damages was exhibited by structure 1020-2 with 6.1 damages/304.8 mm and a standard deviation of 4.5. The average number of damages for the entire sample population is 2.45 damages/304.8 mm and a standard deviation of 2.48. There were however, individual bar samples with zero counted damages. Specifically, out of 244 individual samples, 26 samples had 0 damages/304.8 mm, while 46 samples had 1 damages/304.8 mm or less. This leaves 172 samples with more than 1 damages /304.8 mm and one sample with damages as high as 15.25 damages/304.8 mm.

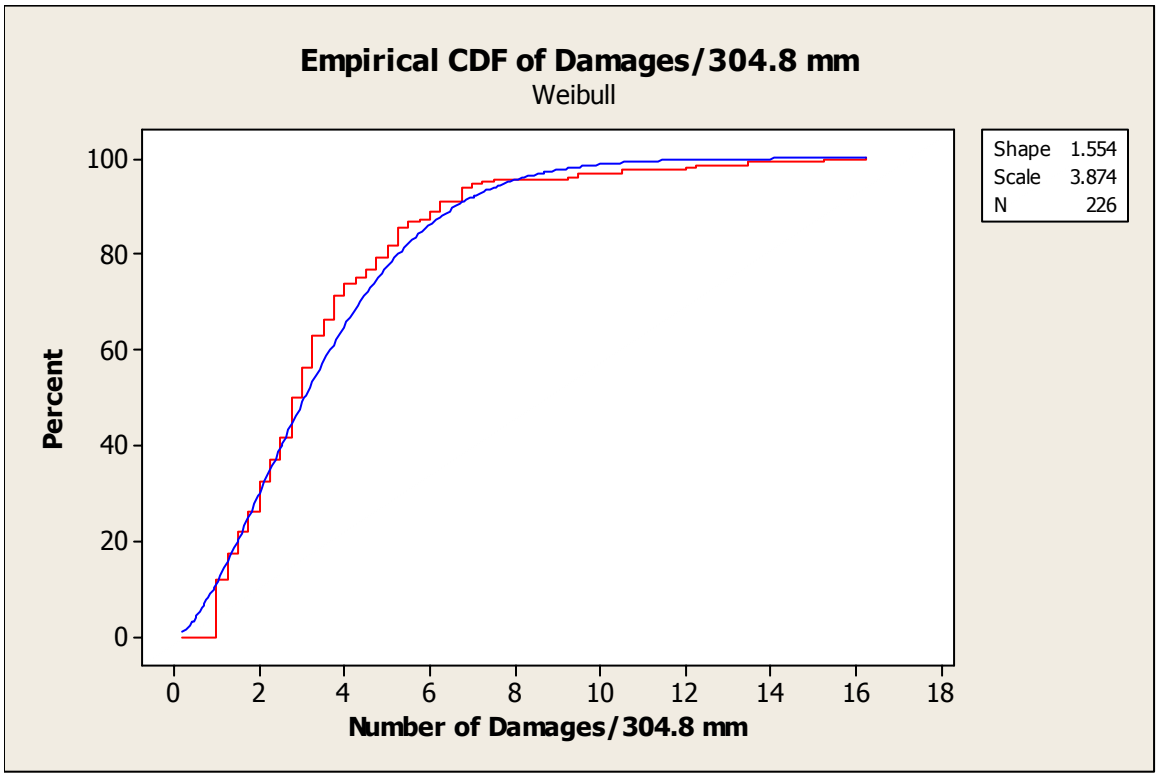

Figure 6.15 EECR Number of Damaged Areas CDF Plot

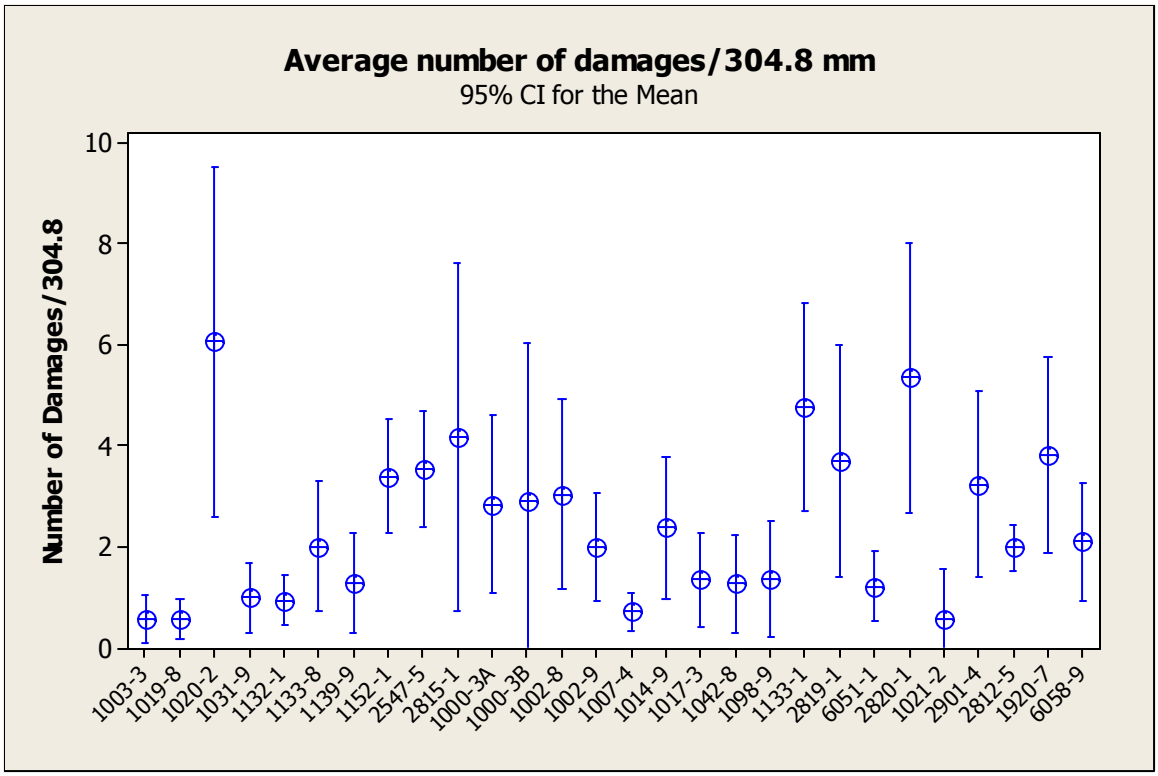

Figure 6.16 EECR Number of Damaged Areas

The probability distribution of the measured percent corroded area followed a pattern similar to the holidays and the number of damages as illustrated in Figure 6.17. Just as with the number of damages, there were no structures showing absolutely no signs of corrosion although there were individual bar samples the showed no visible signs of corrosion. The average percent corroded area and the standard deviation of each structure are presented in Figure 6.18. Out of 244 samples, 28 showed no visible signs of corrosion leaving 216 samples with corrosion ranging from a low of 0.05% to a high of 12%. From the investigated structures, 1132-1 showed the least average amount of visible corrosion with 0.15% corroded area and a standard deviation of 0.14. Structure 2820-1 had the greatest corrosion with an average of 3.57% corroded area and a standard deviation of 3.49. The total average for the sample population is 0.59% corroded area with a standard deviation of 1.22.

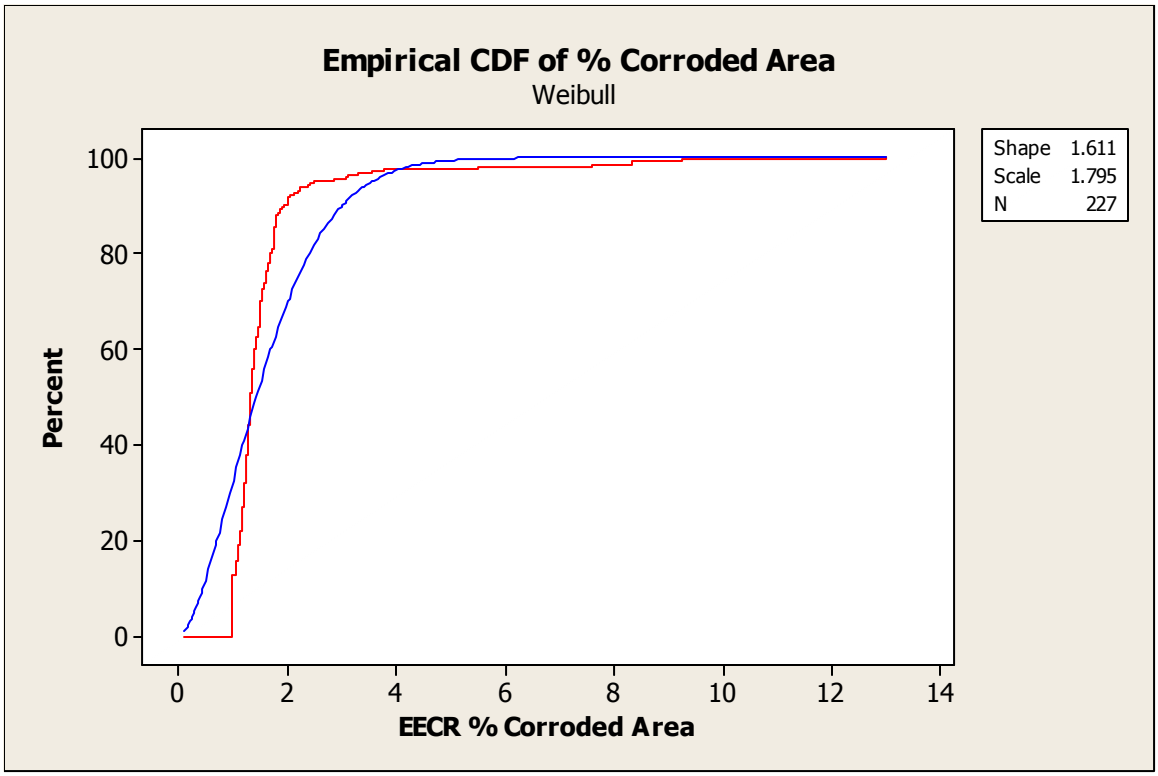

Figure 6.17 Percent Corroded Area CDF Plot

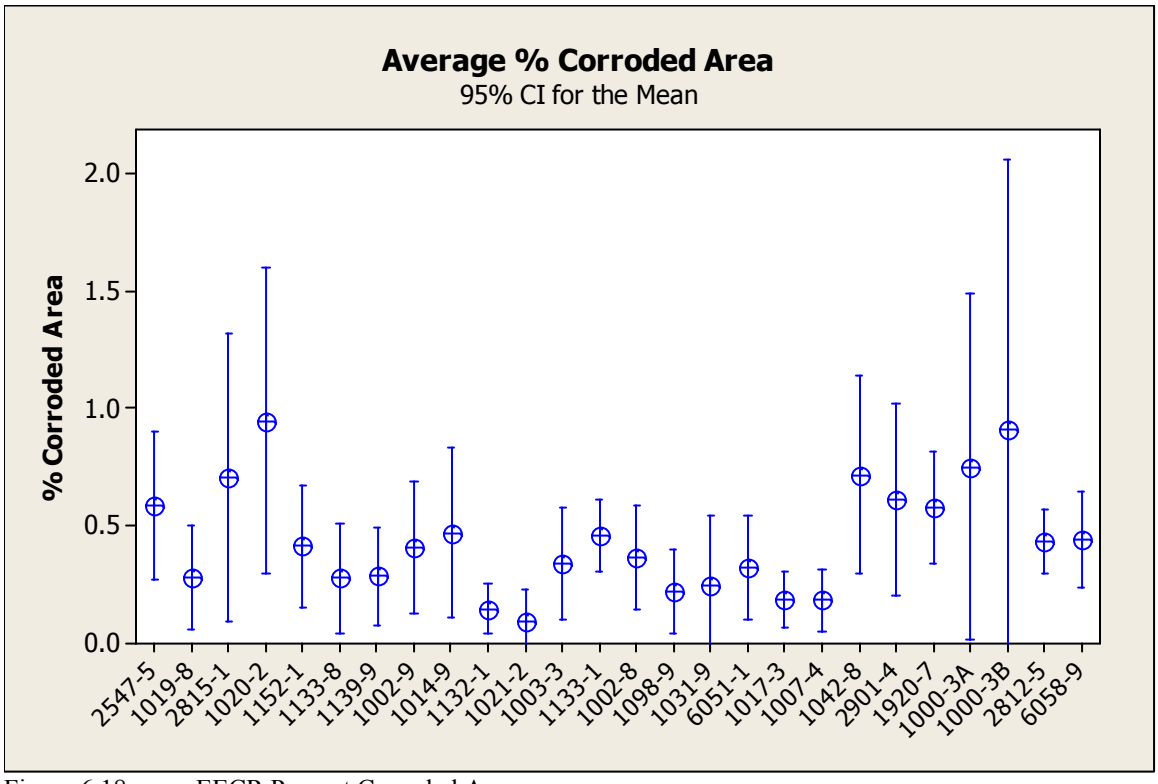

Figure 6.18 EECR Percent Corroded Area

A coating cracking value was assigned to each examined specimens using a 2000x magnification scanning electron micrograph. Figure 6.19 illustrates the average and 95% confidence interval for each structure. The coating samples of only three structures showed no cracking. Those structures were: 1031-9, 1042-8 and 6058-9. The remaining structures presented a mean of 2 with a standard deviation of 1.

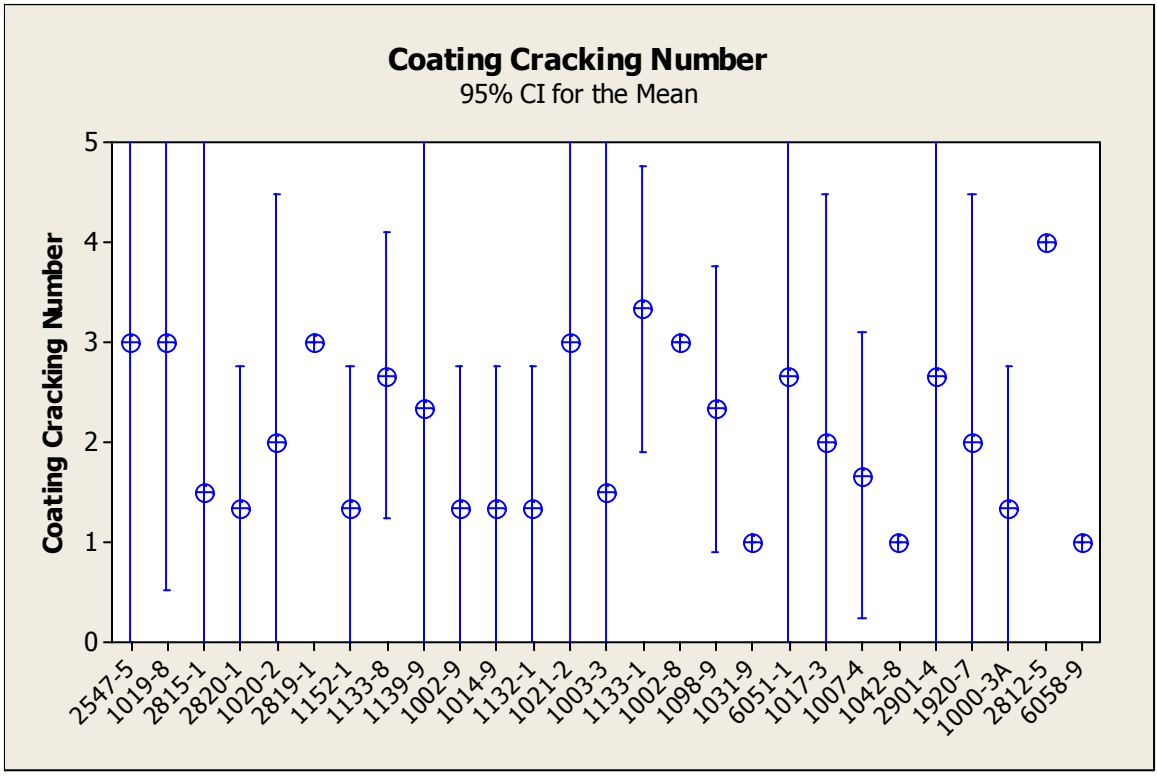

Figure 6.19 EECR Coating Cracking

The average percent cracking and porosity for each structure are presented in Figure 6.20. Structure 6058-9 had the lowest percent cracking and porosity with an average 2.017 and a standard deviation of 0.37. Structure 1133-1 had the highest percent cracking and porosity with an average of 11.36 and a standard deviation of 5.39. Out of the individual samples examined, sample 1014-9 C6 had the lowest percent cracking and porosity with 0.71, while sample 1133-1 C1 had the highest percent cracking and porosity with 17.29. The total average and standard deviation for the entire sample population were determined to be 5.77 and 3.16, respectively. Unlike holidays and the number of damaged areas, the percent cracking and porosity were normally distributed as illustrated in Figure 6.21.

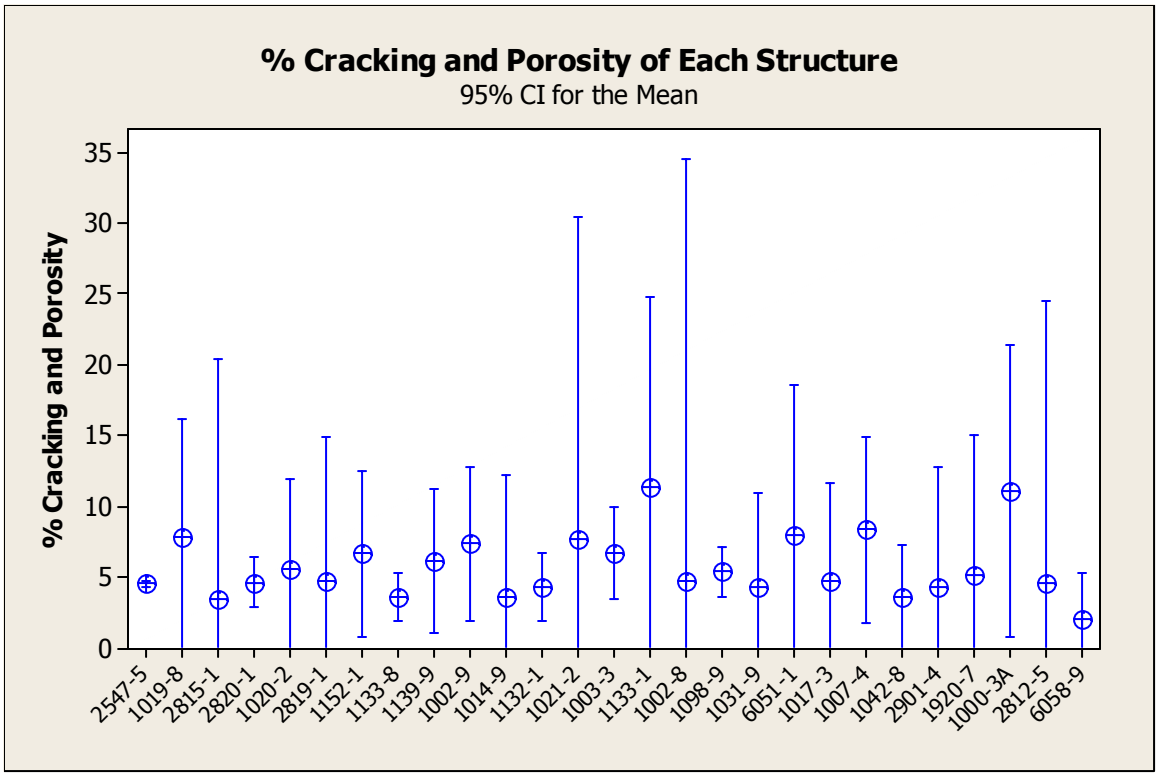

Figure 6.20 EECR Percent Cracking and Porosity

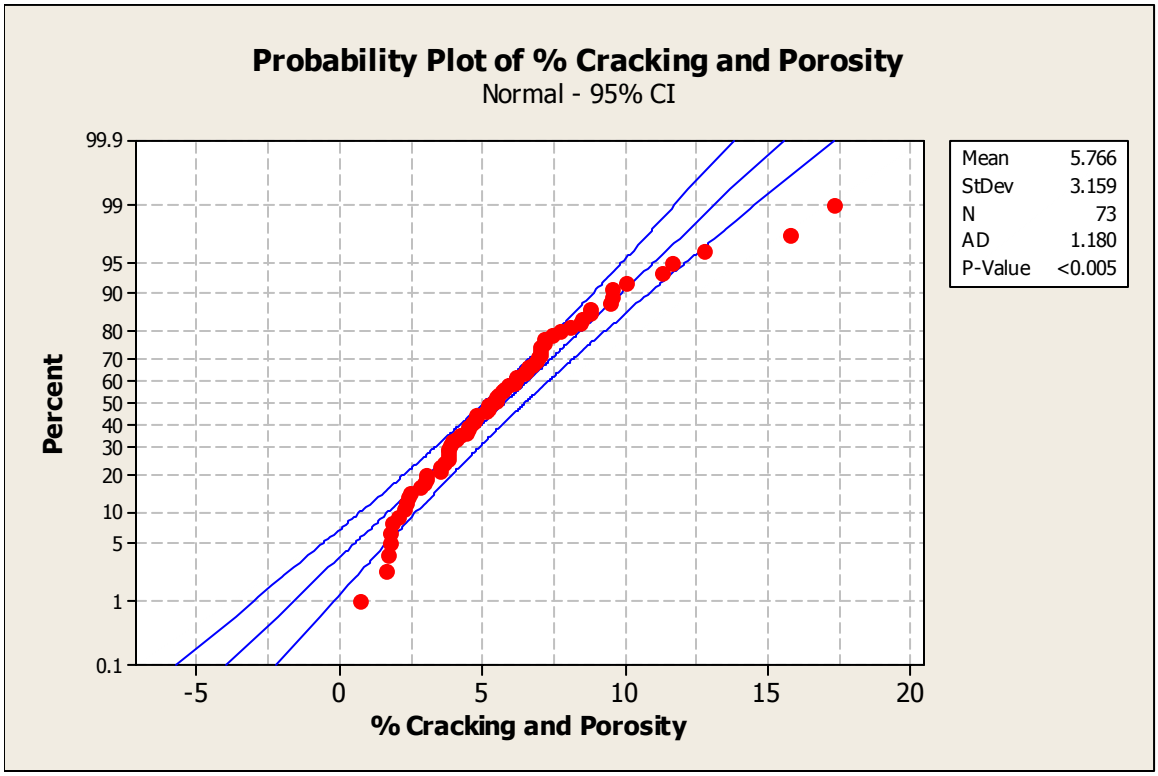

Figure 6.21 Percent Cracking and Porosity Probability Plot

The non-destructive corrosion activity data as well as the concrete chloride concentration at the level of the reinforcing bar are presented in Table 6.6. The relevant parameters particular to each are summarized following the table.

Table 6.6 Corrosion Measurements and Chloride Concentration

Structure	Core Sample	Ecorr (-mV)	R (kOhm-cm)	icorr (mA/ft2)	Cl at Bar Level (kg/m^3)
1003-3	C2	284	17.7	7.29	0.86
	C6	295	12.5	15.7	0.10
	C1	200	13.1	9.52	0.14
1019-8	C1	331	33.5	2.22	0.00
	C4	341	29.9	3.18	0.29
	C5	364	30.2	2.63	0.18
1020-2	C1	243	76.2	7.23	0.50
	C3	296	140	0.41	0.00
	C6	387	61.0	13.0	1.79
1031-9	C1	257	30.5	0.76	0.45
	C4	260	16.2	0.77	1.26
	C5	452	28.0	0.71	0.10
1132-1	C1	251	12.8	16.1	1.07
	C4	298	16.2	17.6	0.97
	C6	435	10.7	23.7	2.34
1133-8	C1	124	30.5	1.66	0.00
	C3	220	30.5	1.94	0.00
	C5	172	29.9	2.12	0.00
1139-9	C1	386	24.7	0.85	0.00
	C3	527	18.3	1.04	0.00
	C6	273	30.5	0.74	0.00
1152-1	C1	245	143	0.52	0.05
	C2	107	162	7.92	0.11
	C3	328	143	2.20	0.07
2547-5	C1	131	51.8	1.67	0.00
	C2	118	64.0	1.51	0.00
	C6	*	79.3	*	0.02
2815-1	C1	290	296	2.45	0.00
	C3	318	204	8.92	0.00
	C6	313	305	2.81	0.00
1000-3A	C1	319	162	2.34	0.01
	C2	237	159	2.05	0.02
	C4	283	186	2.33	0.00
1000-3B	C1	*	*	*	*
	C2	*	*	*	*
	C4	*	*	*	*
1002-8	C1	334	70.1	4.99	0.00
	C3	256	97.5	3.62	0.01
	C4	320	64.0	4.91	0.00
1002-9	C2	161	30.5	2.01	0.06
	C4	308	30.5	4.61	0.00
	C6	265	61.0	3.64	0.00
1007-4	C1	380	15.6	0.38	0.20
	C3	294	25.3	0.82	0.00
	C6	265	48.8	3.24	0.06
1014-9	C1	289	82.3	2.53	0.05

	C3	159	70.1	2.62	0.00
	C6	262	64.0	1.81	0.00
1017-3	C1	313	125	0.74	1.35
	C2	277	143	0.71	1.60
	C4	242	125	0.91	0.00
1042-8	C1	697	30.5	2.78	4.57
	C3	393	36.6	6.08	0.02
	C4	*	30.2	*	0.02
1098-9	C2	309	113	1.20	0.15
	C5	299	137	1.43	0.15
	C6	270	82.3	1.37	0.07
1133-1	C1	403	12.8	5.78	1.35
	C3	208	15.2	3.86	0.16
	C6	313	12.8	25.0	2.82
2819-1	C1	168	122	8.33	0.14
	C3	188	168	9.08	0.35
	C5	202	88.4	9.91	5.02
6051-1	C1	193	14.9	0.55	0.18
	C4	285	10.1	0.34	0.87
	C6	305	11.3	2.46	0.25
2820-1	C1	154	168	10.7	0.00
	C4	141	165	9.74	0.00
	C6	210	159	5.96	0.00
1021-2	C1	285	152	0.64	0.03
	C2	328	131	0.58	0.04
	C4	277	152	0.40	0.07
2901-4	C1	342	36.6	7.52	0.64
	C5	315	36.6	10.9	0.00
	C6	277	39.6	11.7	0.06
2812-5	C1	222	33.5	6.87	1.28
	C4	262	33.5	6.98	0.01
	C6	290	51.8	3.14	0.08
1920-7	C2	287	22.0	26.5	1.84
	C5	437	30.2	0.62	0.94
	C6	405	33.5	0.52	0.71
6058-9	C1	278	64.0	0.89	0.00
	C3	255	51.8	0.24	0.00
	C6	264	42.7	0.25	0.01

Note: * - Data unavailable

For the resistivity range of values, the interpretation guidelines proposed by Feliu et al were chosen (Feliu, S. et al 1996) and are presented as the three horizontal lines at 10, 50 and 100 kΩ-cm in Figure 6.22. As previously stated, between 10 to 50 kΩ-cm the corrosion rate is high to moderate; between 50 to 100 kΩ-cm the corrosion rate is low; above 100 kΩ-cm the corrosion rate is negligible. Based on these interpretation guidelines, almost half of the structures investigated, 13 structures, lie within the high to moderate corrosion rate region while 5 structures are located in the low

corrosion rate region of Figure 6.22. The remaining 9 structures theoretically will have low corrosion rates or the concrete was too dry when tested.

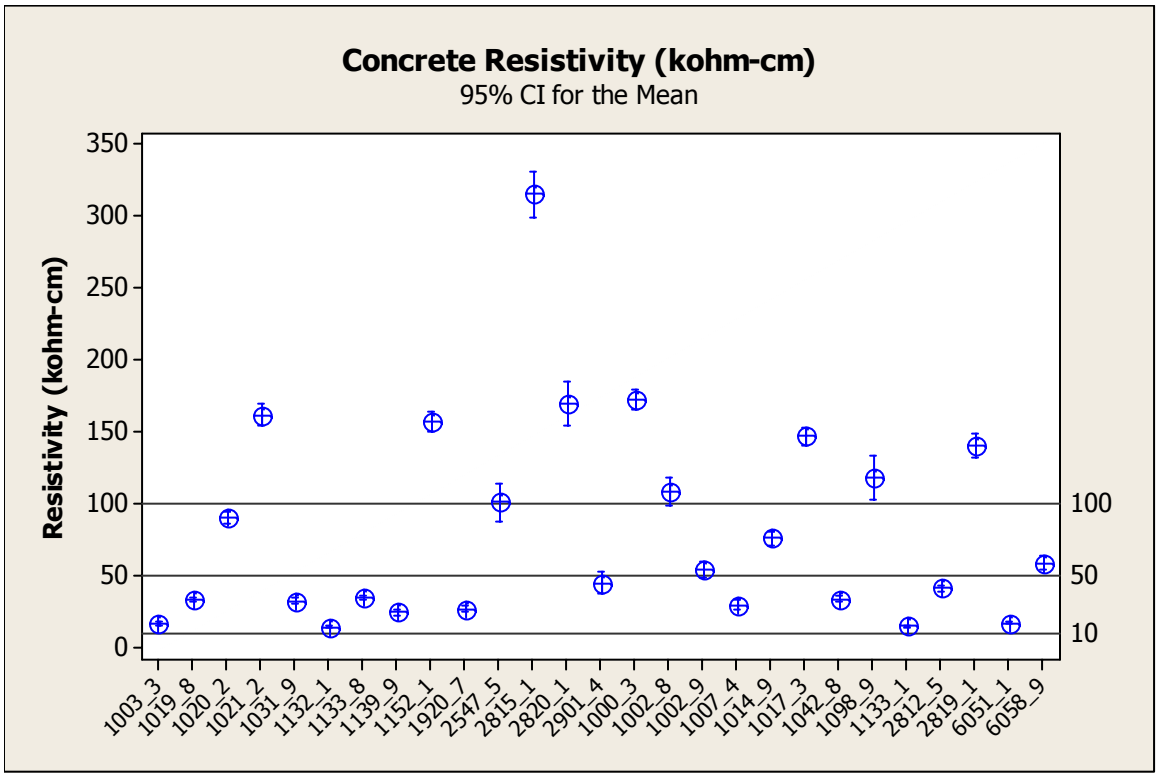

Figure 6.22 EECR Structures Concrete Resistivity

The corrosion half-cell potentials are presented in Figure 6.23 with the horizontal lines at -200 mV and -350 mV representing the current interpretation guidelines. The corrosion activity in the majority of the bridges investigated, based on half-cell potential measurements is uncertain. Three structures, 1139-9, 1142-8 and 1098-9 showed high probability of corrosion occurring with average half-cell potential measurements of -380 mV, -434 mV and -364 mV, respectively. Four structures, 1133-8, 2547-5, 2820-1 and 2819-1 showed very low probability of corrosion occurring with average half-cell potential measurements of -177 mV, -164 mV, -149 mV and -162 mV, respectively.

The corrosion rates obtained using an unguarded 3LP instrument are presented in Figure 6.24. The horizontal lines at 0.2, 1 and 10 $\mu A/cm^2$ represent the interpretation guidelines proposed by Clear, K presented in Table 4.2. From the figure, it is clear that the majority of structures investigated are located between 1 and 10 $\mu A/cm^2$. In that

region, damage to concrete due to corrosion activity is expected to take place between 2 to 10 years. Two structures, 1003-3 and 1031-9 presented significantly higher corrosion rates with values of 16.8 and 21.1 μA/cm^2, respectively. In these cases, concrete damage due to corrosion activity is expected to occur within 2 years or less. Five structures, 1021-2, 1031-9, 1139-9, 1017-3 and 6058-9 presented very low corrosion rates with damage due to corrosion activity expected between 10 to 15 years.

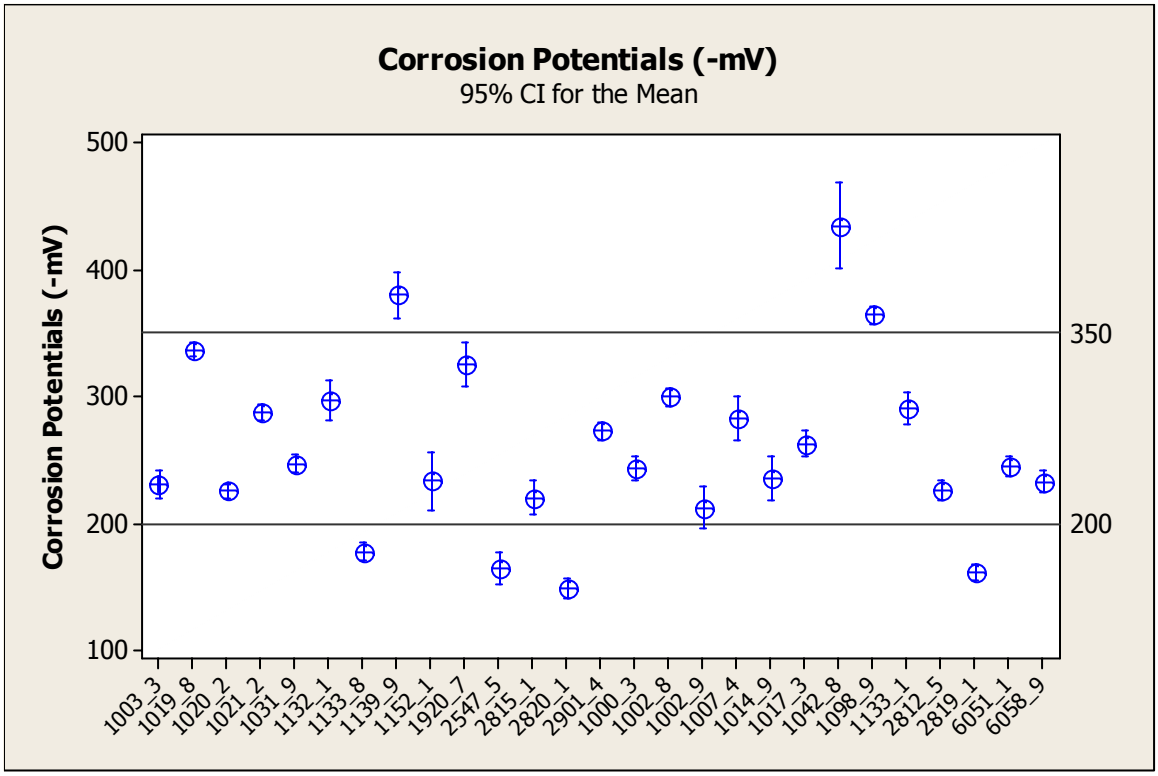

Figure 6.23 EECR Structures Corrosion Potentials

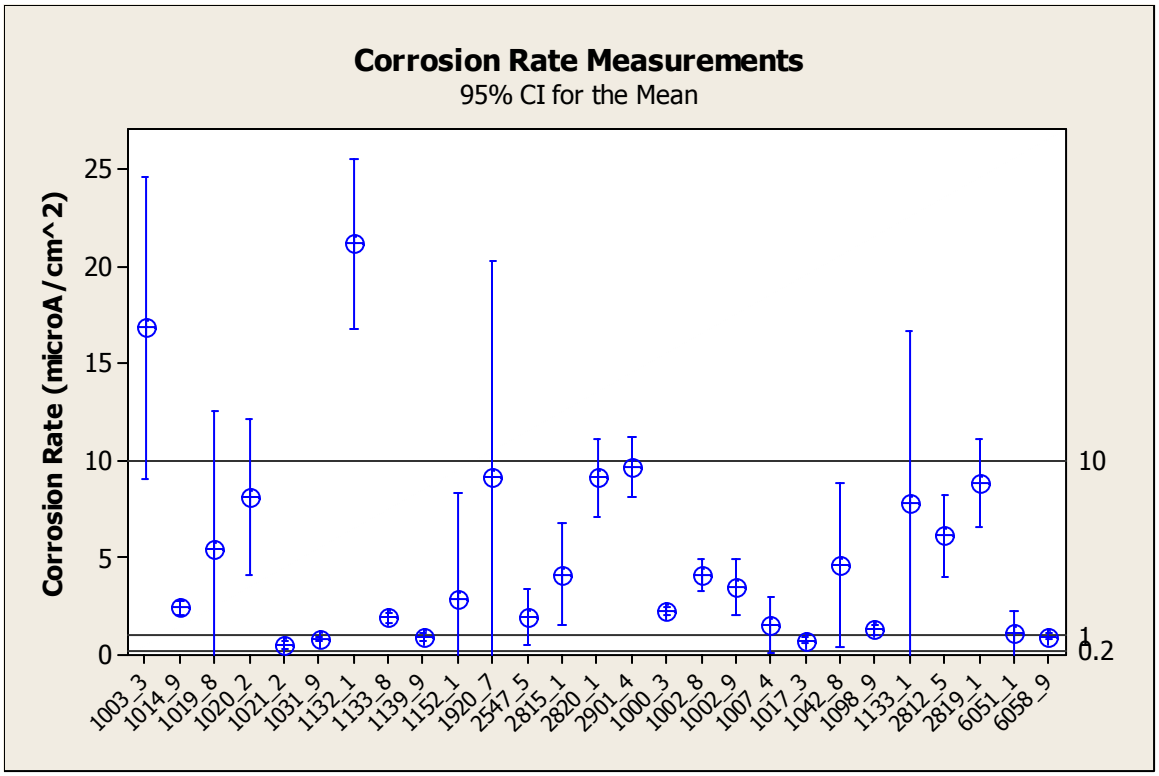

Figure 6.24 Corrosion Rate Measurements

Figure 6.25 illustrates the average chloride concentration at bar level, while the reference line at 0.71 kg/m^3 of concrete represents a corrosion initiation level. With the exception of five structures, the chloride concentration at bar level was below the commonly used corrosion initiation threshold of 0.71 kg/m^3 of concrete. The five structures that exhibited higher chloride concentrations were: 1132-1, 1133-1, 1920-7, 1042-8 and 1031-9. The average chloride concentration of these structures was 1.78, 0.99, 1.06, 1.54 and 0.71 kg/m^3 of concrete, respectively.

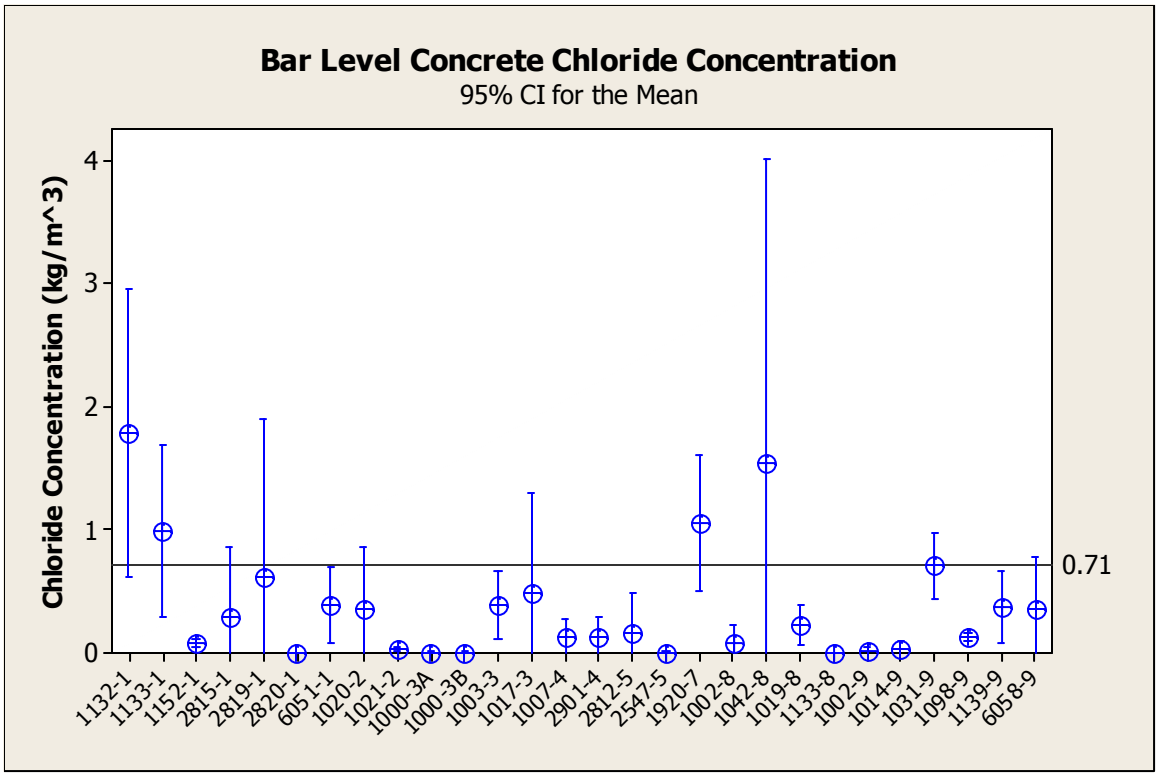

Figure 6.25 Concrete Chloride Concentration at Bar Level

Finally, SEM and EDS analyses were performed. Figure 6.26 illustrates an electron scanning micrograph of structure 1020-2 C6. The EDS spectra were collected at the numbered locations and are presented in Figures 6.27, 6.28 and 6.29.

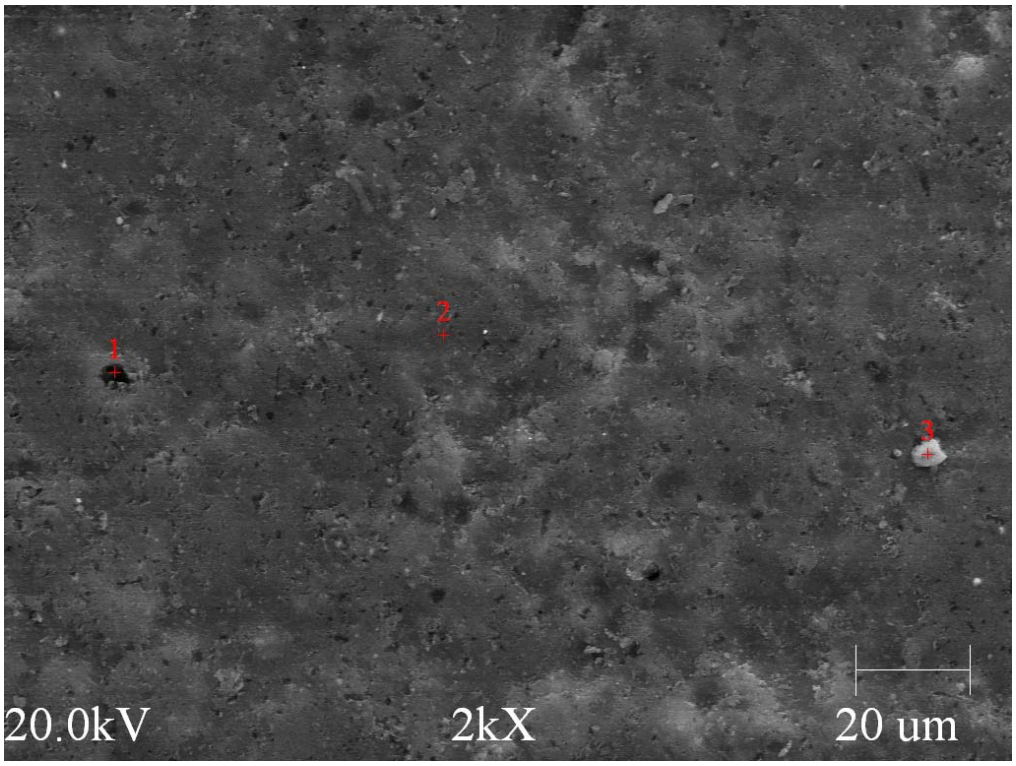

Figure 6.26 Structure 1020-2 C6 SEM Micrograph

The spectrum at location 1 (Figure 6.27) would indicate that the pore in the coating is continuous to the steel substrate. Although the signals are weak due to interference from the pore walls, iron still presents the strongest peak, followed by silica, chlorides, potassium and calcium, which may all be found in the concrete pore solution. Location 2 (Figure 6.28) spectra is dominated by the carbon signature as expected from an organic coating. There are traces of other elements that are commonly found in concrete or the concrete pore solution. This is due to adsorption of the pore solution on the coating surface. Finally, the third spectrum (Figure 6.29) illustrates the typical signature of cement. There is no carbon present, as expected from an organic coating, but the calcium and the silica signatures dominate.

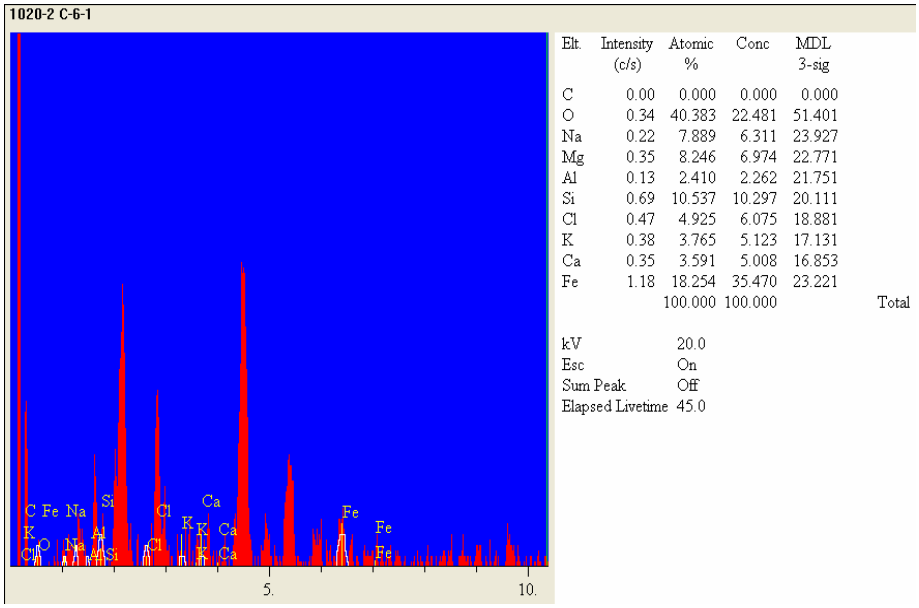

Elt.	Intensity (c/s)	Atomic %	Conc	MDL 3-sig	
C	0.00	0.000	0.000	0.000	
O	0.34	40.383	22.481	51.401	
Na	0.22	7.889	6.311	23.927	
Mg	0.35	8.246	6.974	22.771	
Al	0.13	2.410	2.262	21.751	
Si	0.69	10.537	10.297	20.111	
Cl	0.47	4.925	6.075	18.881	
K	0.38	3.765	5.123	17.131	
Ca	0.35	3.591	5.008	16.853	
Fe	1.18	18.254	35.470	23.221	
		100.000	100.000		Total

kV	20.0
Esc	On
Sum Peak	Off
Elapsed Livetime	45.0

Figure 6.27 EDS Spectra 1020-2 C-6-1

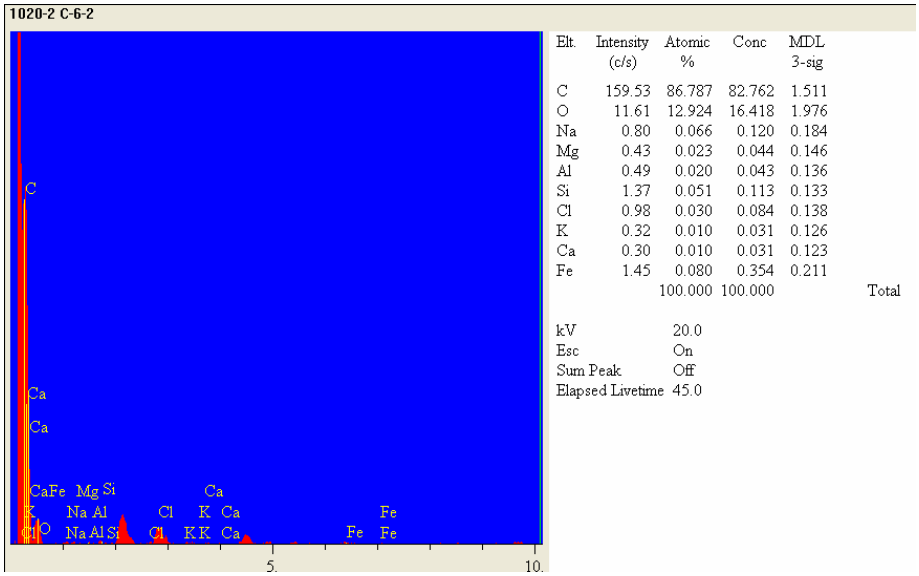

Elt.	Intensity (c/s)	Atomic %	Conc	MDL 3-sig	
C	159.53	86.787	82.762	1.511	
O	11.61	12.924	16.418	1.976	
Na	0.80	0.066	0.120	0.184	
Mg	0.43	0.023	0.044	0.146	
Al	0.49	0.020	0.043	0.136	
Si	1.37	0.051	0.113	0.133	
Cl	0.98	0.030	0.084	0.138	
K	0.32	0.010	0.031	0.126	
Ca	0.30	0.010	0.031	0.123	
Fe	1.45	0.080	0.354	0.211	
		100.000	100.000		Total

kV	20.0
Esc	On
Sum Peak	Off
Elapsed Livetime	45.0

Figure 6.28 EDS Spectra 1020-2 C-6-2

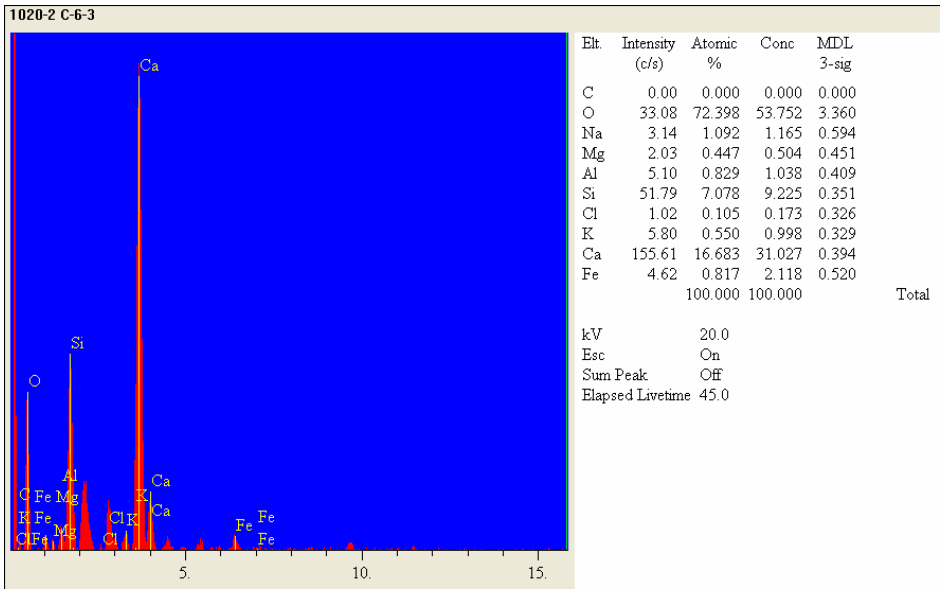

Elt.	Intensity (c/s)	Atomic %	Conc	MDL 3-sig	
C	0.00	0.000	0.000	0.000	
O	33.08	72.398	53.752	3.360	
Na	3.14	1.092	1.165	0.594	
Mg	2.03	0.447	0.504	0.451	
Al	5.10	0.829	1.038	0.409	
Si	51.79	7.078	9.225	0.351	
Cl	1.02	0.105	0.173	0.326	
K	5.80	0.550	0.998	0.329	
Ca	155.61	16.683	31.027	0.394	
Fe	4.62	0.817	2.118	0.520	
		100.000	100.000		Total

kV	20.0
Esc	On
Sum Peak	Off
Elapsed Livetime	45.0

Figure 6.29 EDS Spectra 1020-2 C-6-3

7.0 ANALYSIS AND DISCUSSION

Initial analysis of the data revealed several coating conditions; specifically, the extent of coating surface cracking, the insufficient degree of coating curing and the generalized loss of adhesion. The ramifications of these conditions as well as other correlations will be discussed in detail in the following subsections.

7.1 Coating Cracking

The presence of micro-cracks on the fusion bonded epoxy coating surface has been established by a previous study (Wheeler, M. 2003) that also provided a visual assessment guide. Several coating and exposure parameters were investigated during the course of this current study to determine if any correlations exist. The presence of cracking in new ECR samples before embedment into concrete as well as the extent of cracking in extracted ECR samples was confirmed and ranked.

With the exception of only one new specimen (WWBVT-S4), which is presented in Figure 7.1, no map-like cracking was noted in the remaining new ECR samples. Based on the interpretation guide, WWBVT-S4 was assigned a cracking value of 3. The colors in Figure 7.1 were inverted for better contrast. Unlike the new ECR samples, the majority of the extracted ECR samples showed surface coating cracking spanning the severity scale with a total average cracking value of 2. This significant difference between the new and the extracted ECR samples indicates that while it is possible that there are factors that may contribute to coating cracking prior to concrete embedment, the majority of the cracking occurs in concrete.

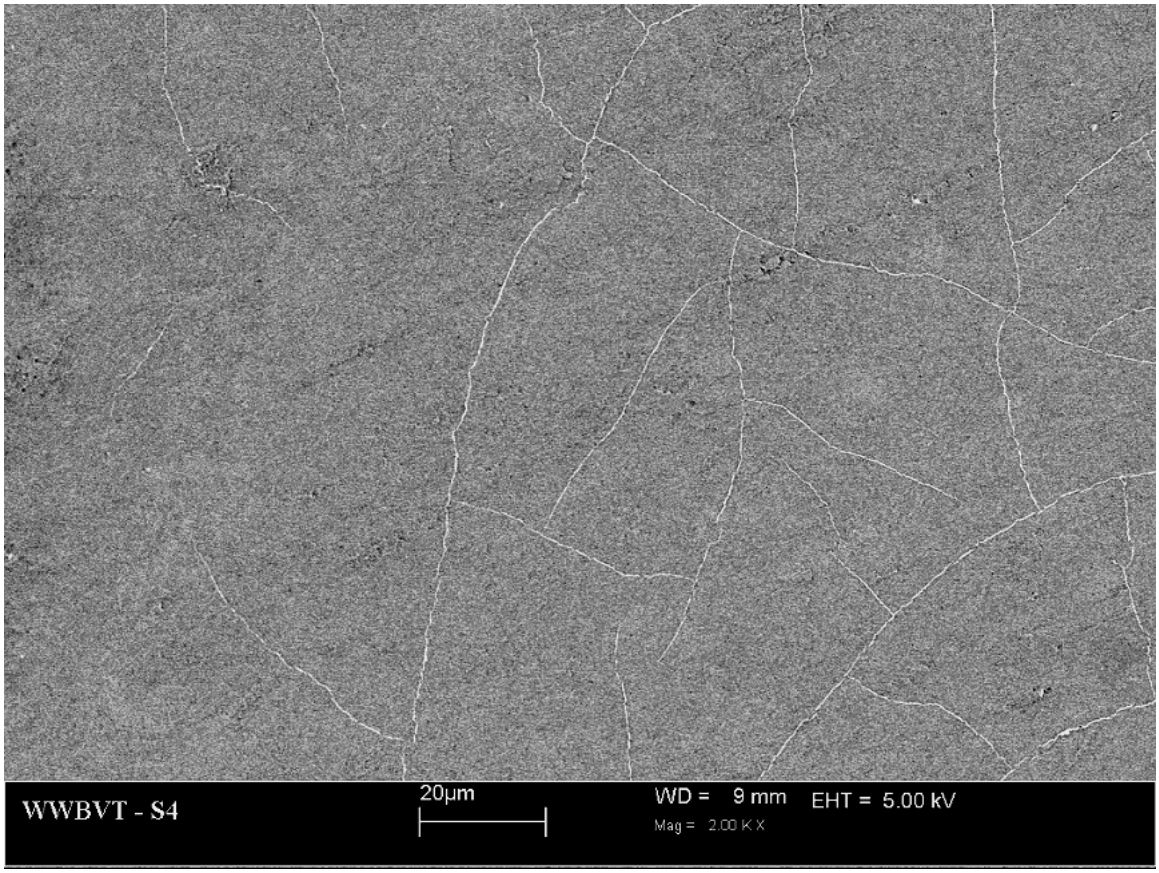

Figure 7.1 WWBVT – S4 Cracking (SEM Micrograph)

Using a confidence level of 80% allows for the inclusion of chlorides at bar level, adhesion, color of corrosion products and % moisture as cracking prediction parameters. The P-values were 0.171, 0.115, 0.118 and 0.186, respectively. Further regression performed using only the parameters with P-values ≤ 0.20 ultimately yielded only the coating color as the strongest predictor of coating cracking. At the 95% confidence level, the coating color P-value was 0.003. Based on individual correlations, excluding combined effects, the cracking value correlated with the % moisture, with a Pearson correlation value of 0.637 and a P-value of 0.001 (Figure 7.2).

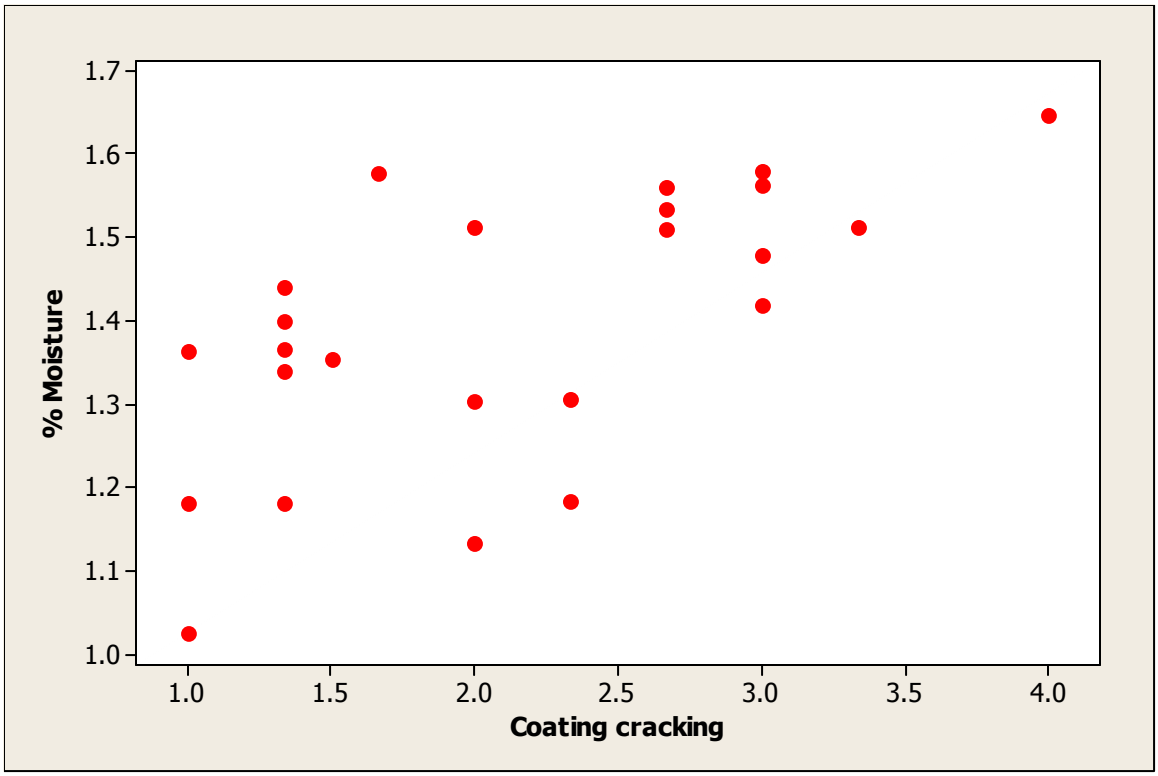

Figure 7.2 Scatter Plot of %Moisture vs. Coating cracking

While the change in coating glossiness and/or color, adhesion, and the color of the corrosion products under the coating may simply be a result of and not the cause of coating degradation; percent moisture content relationship points to hydrothermal degradation coupled with chloride induced ageing. Furthermore, prior exposure to UV light exacerbates the effect of hydrothermal ageing in the presence of chlorides (Kotnarowska, D. 1999). Apicella and others have also shown that in a DGEBA based epoxy "microcavities can be formed by effect of crazing in the plasticized system exposed to high temperatures" in the presence of moisture (Apicella, A. et al 2003). Although the ECR steel embedded in concrete may not necessarily be exposed to high temperatures as were the samples tested by Apicella and others (i.e. 100°C), bridge deck concrete at bar level commonly reaches 40°C (~ 104°F) in Virginia while the relative humidity of the concrete at bar level can vary between 75 and 100% (Liu, Y. 1996). Additionally, the bars themselves may be exposed to temperatures as high as 50°C (~ 120°F) prior to embedment in concrete. As such, hydrothermal ageing effects may not become evident for several years.

7.2 Degree of Coating Curing

Coating samples from both the new as well as the extracted specimens were not fully cured as demonstrated by the DSC data presented in the previous section. The new ECR samples show a minimal degree of improvement, but statistically there are no differences between the new and the extracted ECR samples as verified by the 2-sample T-test presented below:

	N	Mean	Standard Deviation	SE Mean
Extracted ECR ΔT_g:	81	14.83	7.57	0.84
New ECR ΔT_g:	17	13.00	1.70	0.41
Estimate for difference:	1.83			
95% CI for difference:	(-0.03, 3.69)			
T-Value =	1.96			
P-Value =	0.053			
DF =	95			

One of the consequences of the incomplete curing of the coating is its increased absorptivity. The correlation of the moisture content with the ΔT_g in the extracted ECR samples, as illustrated by Figure 7.3, is an indicator of the porous nature of the coating and not necessarily the plasticizing effects of water. The Pearson correlation of this relationship was 0.272 and the p-value 0.014.

While the effect of moisture on the T_g of the tested epoxy coating samples is not as trivial as some have suggested (Wheeler, M. 2003), nor are they so drastic that they explain the entire observed change in T_g. De'Nève and Shanahan were able to show that 1% moisture content leads to an approximately 8°C reduction in T_g; however, even based on this temperature reduction rate, there are still structures that exhibit differences in glass transition temperatures as high as 27°C indicating that the coating is indeed not fully cured. This conclusion is also supported by the Gordon-Taylor equation results presented in the previous section. Furthermore, not knowing the exact effects of moisture on our coating samples, the actual measured difference in glass transition was used in the statistical analysis.

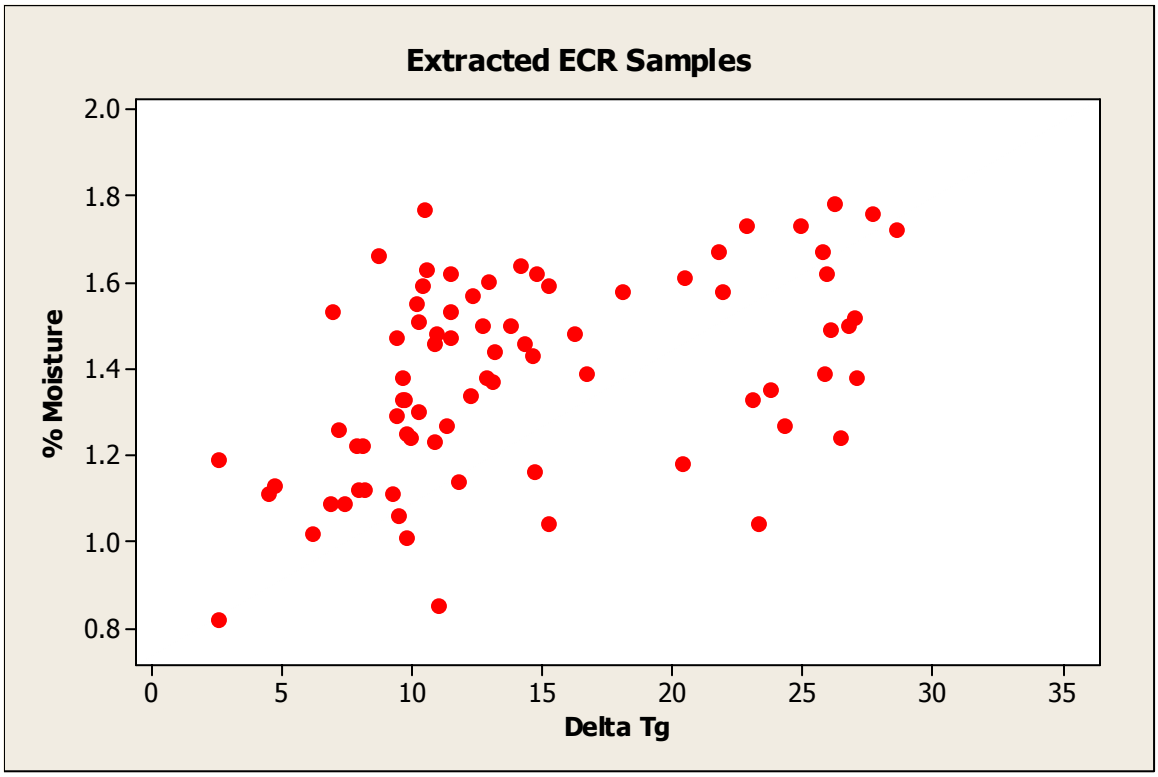

Figure 7.3 Scatter Plot of % Moisture vs. ΔT_g

The porous structure of coating samples collected from structures 1017-3 C-2 and 2820-1 C-4 is illustrated in Figures 7.4 and 7.5. The ΔT_g of sample 1017-3 C-2 is 26.42 °C while the ΔT_g of sample 2820-1 C-4 is 9.63 °C. Both coating samples present capillary-sized pores throughout the bulk of the coating. The size of the pores was 10.4 and 10.2 µm for the 1017-3 C-2 sample and 18.9 and 37.6 µm for the 2820-1 C-4 sample in addition to the multitude of pores 1 µm or less occupying the bulk of the coating. Since the examples of the porous structure presented were obtained from three structures only, we cannot conclusively state that this is a common condition. It is the opinion of the author, however, based on the random nature of the investigated samples, that this may in fact be the prevailing coating condition. Using the 1% moisture to 8°C conversion leads to ΔT_g due to insufficient curing of 16.50°C and -5.49°C, respectively. The -5.49°C in this case may be explained by the fact that some of the moisture is in fact free or bulk water, which has no plasticizing effect.

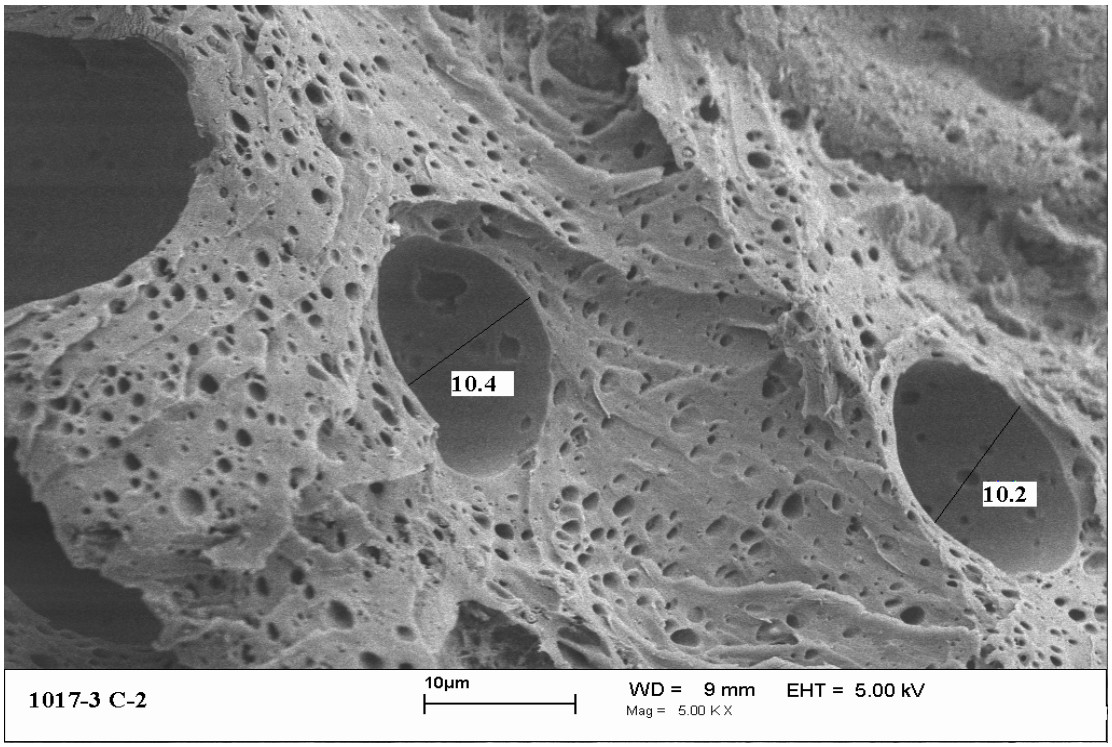

Figure 7.4 1017–3 C–2 5x SEM Coating Micrograph

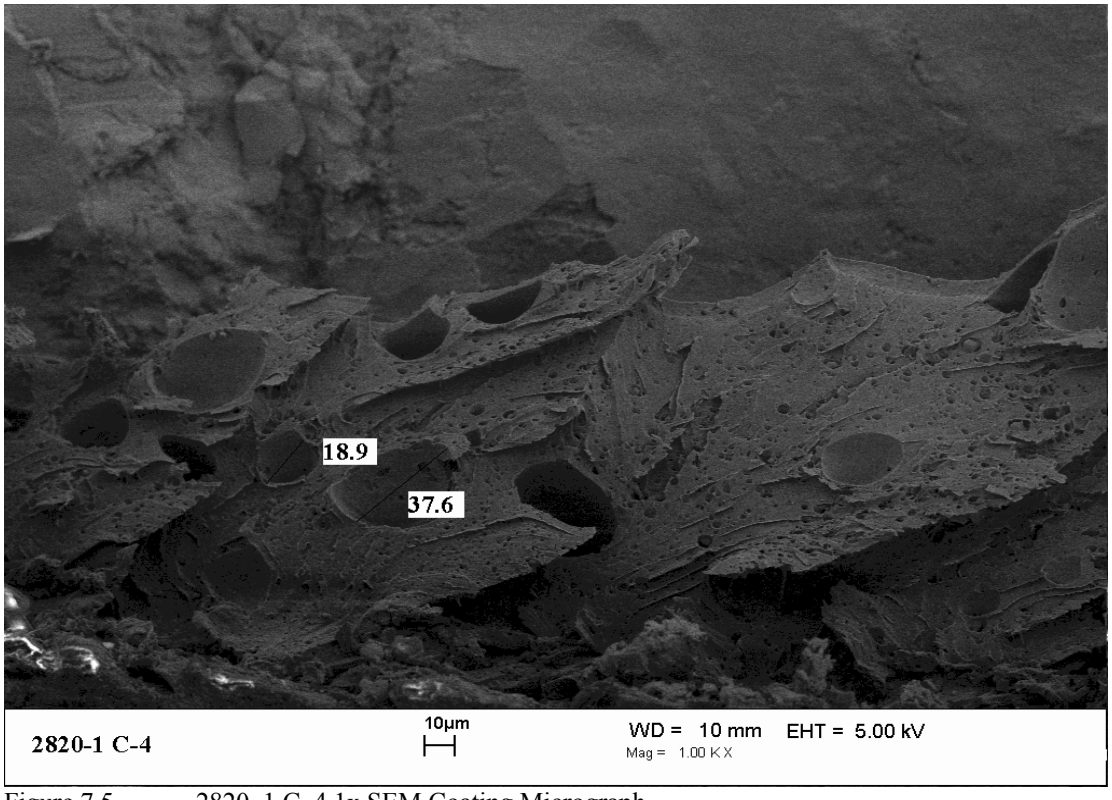

Figure 7.5 2820–1 C–4 1x SEM Coating Micrograph

The presence of this pore network throughout the bulk of the coating also makes the question of whether the cracks go to the steel surface irrelevant. The large capillaries providing not only open conduits for moisture, oxygen, and later chloride transfer between the concrete environment and the steel substrate, but also crevices which allow moisture to collect creating an ionic path.

In addition to % moisture, ΔT_g also correlated well with the coating thickness with a Pearson correlation value of -0.340 and P-value of 0.003. The data in Figure 7.6 leads to an influence that has not yet been fully discussed in literature: the coating speed at the ECR manufacturing facility. The negative Pearson correlation value and the scatter diagram indicate that thicker coatings are more fully cured than thinner ones.

Since the degree of curing is independent of the material thickness, the relationship can be explained as follows: greater manufacturing speeds produce low and uneven heating of the bar element. Following the heating of the bar element, the greater speed not only impedes the adhesion of sufficient epoxy powder to the bar, but it also limits the time available for the fusion bonded epoxy to cure leading to a more porous and therefore more permeable coating structure. The LNE data deviates from this conclusion with a ΔT_g of zero indicating a fully cured coating, yet exhibiting the thinnest coating and continuous holiday detection. In this case, the bar may have in fact been overheated, flash-curing the powder coating without allowing sufficient time for the fluid to flow and fully coat the bar.

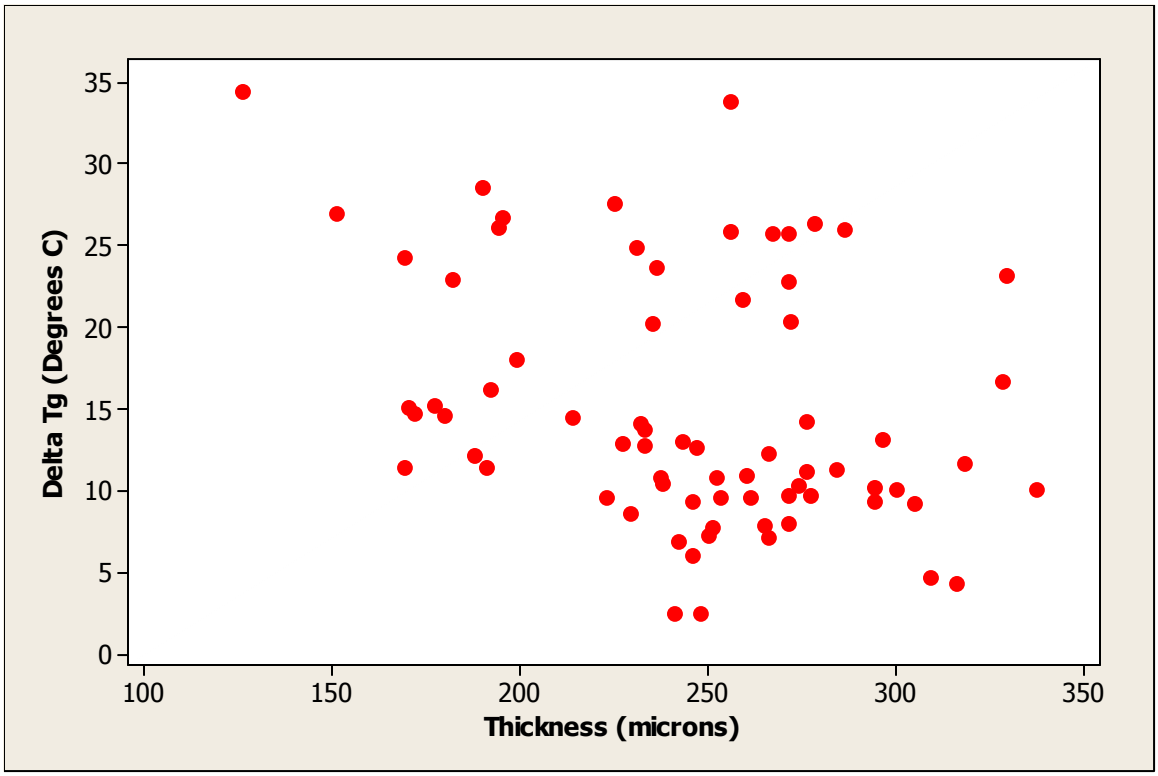

Figure 7.6 ΔT_g vs. Thickness (µm)

Another parameter affected by insufficient curing is the number of holidays per unit length of bar. The Pearson correlation value is 0.282 and the P-value of this relationship is 0.014, however the highly variable nature of the data makes this conclusion tenuous at best.

Finally, the color of the corrosion products also correlated reasonably well with the coating degree of curing with a Pearson correlation value of 0.341 and a P-value of 0.002 (Figure 7.7). The same relationship can also be seen between % moisture and the average steel surface color with a Pearson correlation value of 0.422 and a P-value of 0.000 (Figure 7.8), which would indicate that the moisture present in the coating plays an active role in the corrosion activity under the coating. The gross classification of the steel surface color in this case possibly being an indicator of the hydration level of the oxide layer present on the steel surface.

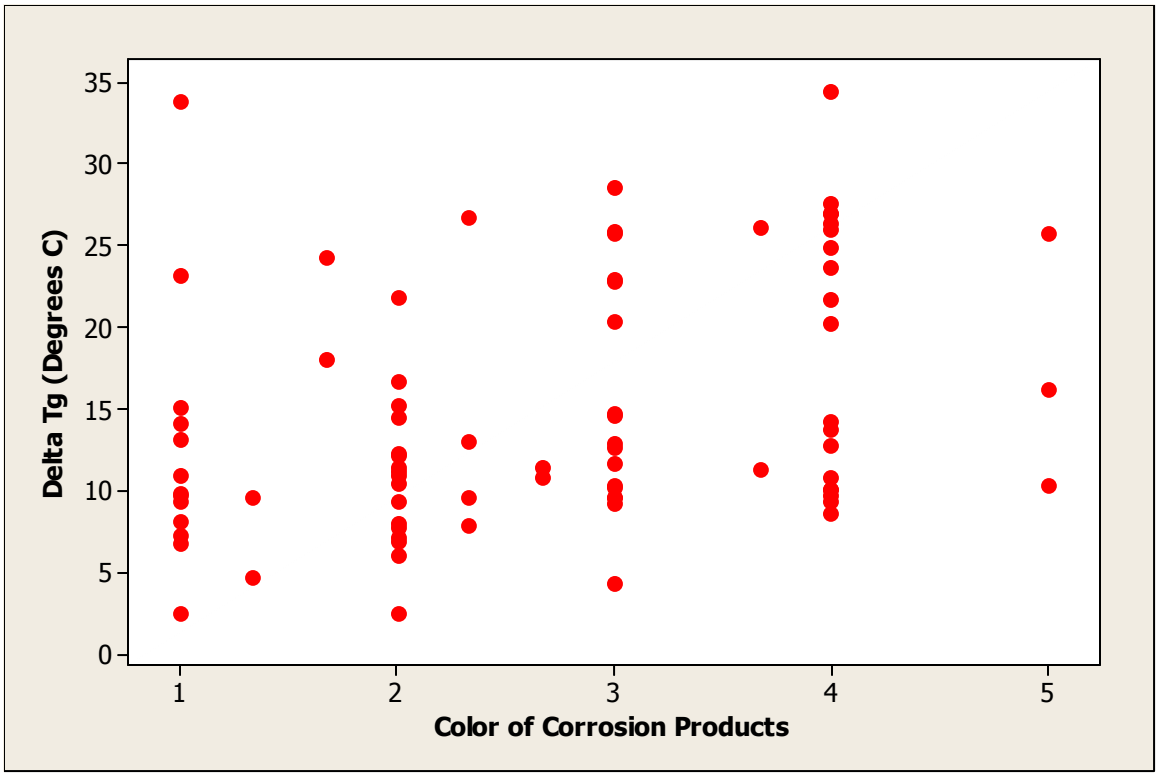

Figure 7.7 ΔT_g vs. Steel Surface Color

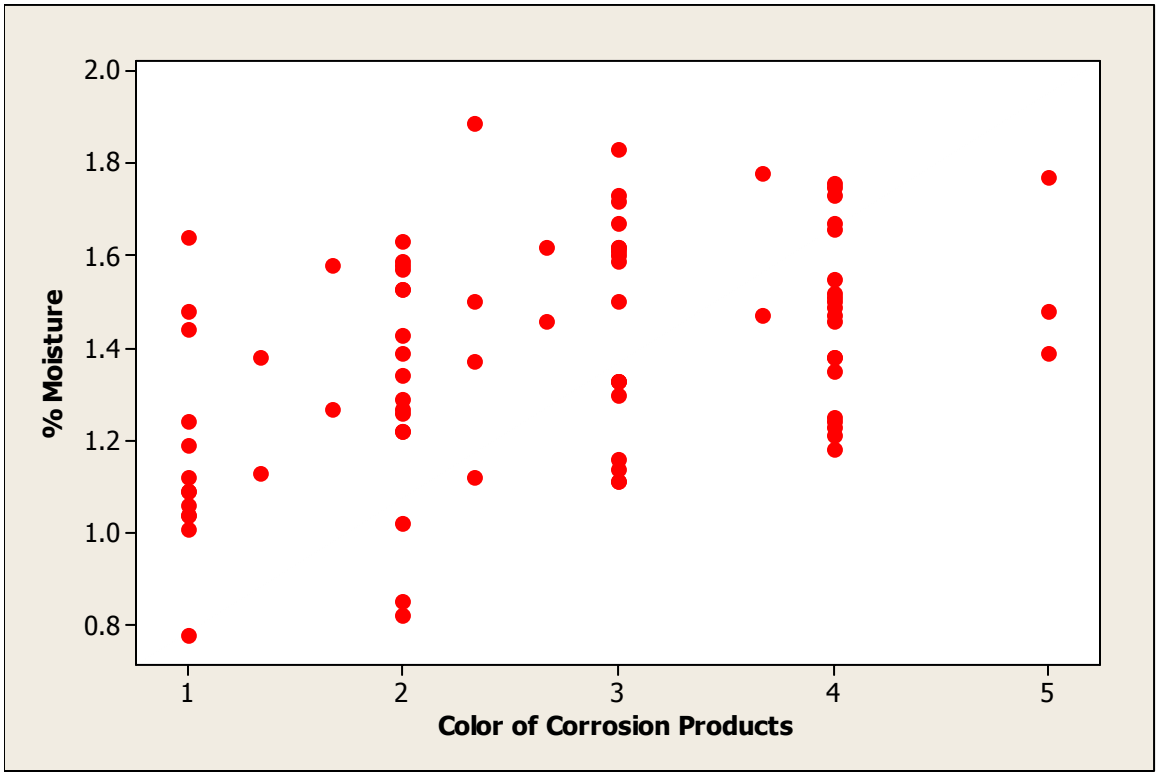

Figure 7.8 % Moisture v. Steel Surface Color

7.3 Residual Adhesion

The residual adhesion correlated well with three parameters: ΔT_g, the % coating moisture and the steel surface color. The Pearson correlation values were 0.416, 0.522 and 0.764 respectively. Conversely, all the P-values were 0.000. The relationship of ΔT_g with the residual adhesion is presented in Figure 7.9. This relationship is relevant only insofar as the absorption is concerned. The prevalent thought in the industry was that cross-link density had a significant effect on adhesion based on the availability of hydroxyl pendants. Rouw, however, showed that the effect cross-link density has on adhesion is in fact minimal (Rouw, A.C. 1998). This leaves coating permeability as the parameter most affected by the degree of curing.

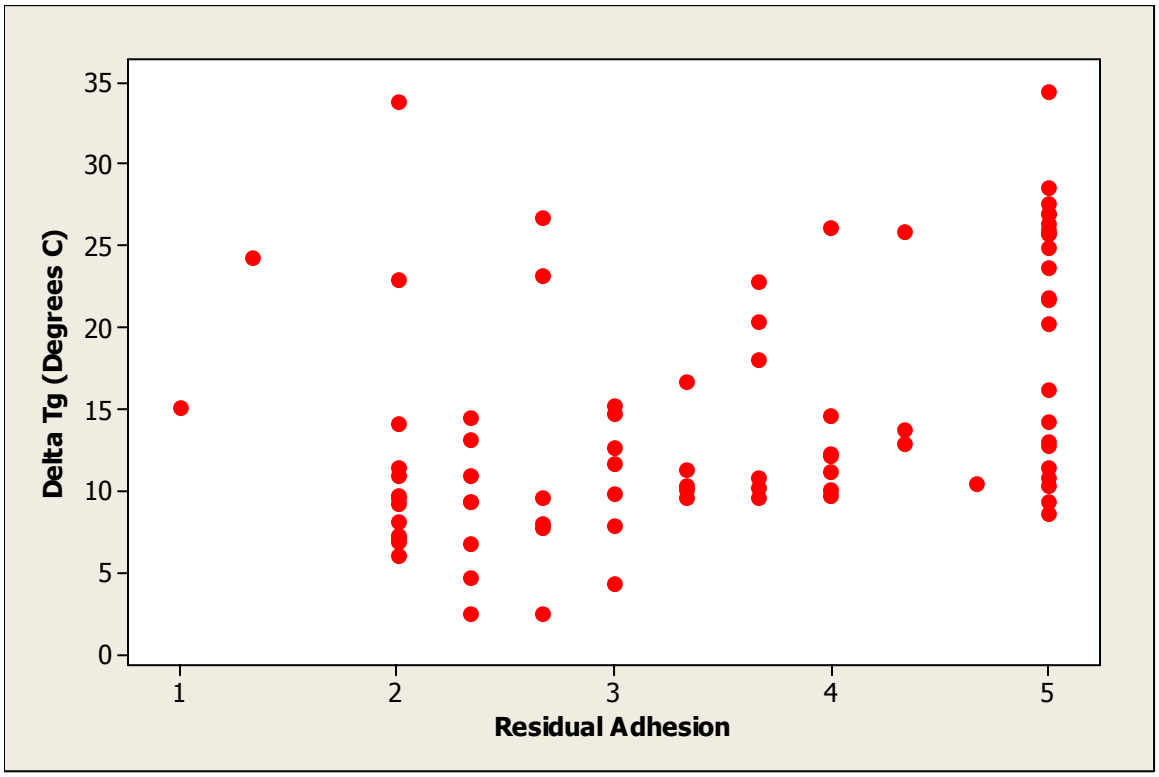

Figure 7.9 ΔT_g vs. Residual Adhesion

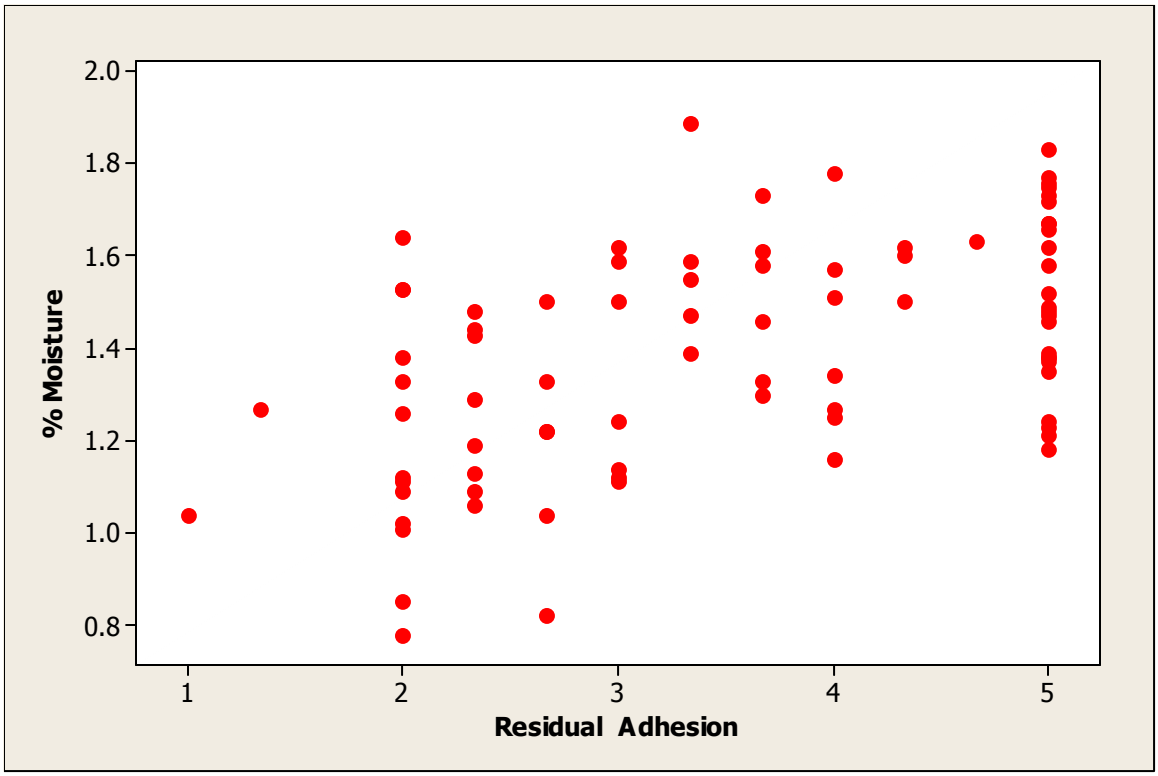

Figure 7.10 % Moisture vs. Residual Adhesion

Pyc, Sagüés, Powers and others have shown that epoxy coatings lose adhesion upon exposure to wet environments (Pyc, W.A 1998; Sagüés, A.A. and Powers, R.G. 1990). This study supports those findings (Figure 7.10). We also observed that upon removal from concrete, the coating does not regain adhesion as others have observed in laboratory studies; but instead, the adhesion loss is permanent. The ability of the coating to regain adhesion upon drying after short-term exposure to wet environments as well as the permanent adhesion loss exhibited upon long-term exposure would seem to suggest that while mechanical interlocking between the coating and the steel surface may occur on a limited scale, in fact it contributes little to the overall adhesion of the coating to the steel substrate. This is illustrated in Figure 7.11 and supported by EDAX spectra in Figures 7.12, 7.13 and Table 7.1. The spectra in Figures 7.12 and 7.13 were obtained from locations 2 and 3 in Figure 7.11. The high carbon content present at location 2 and presented in Table 7.1 supports the conclusion that the observed material is indeed an epoxy coating fragment. Location 3, however, presents no carbon signal, but the iron signal is exceptionally strong indicating a complete absence of epoxy. In fact there is an

approximately 20 µm gap between the coating fragment and the steel surface which may indicate that the coating never adhered to that surface.

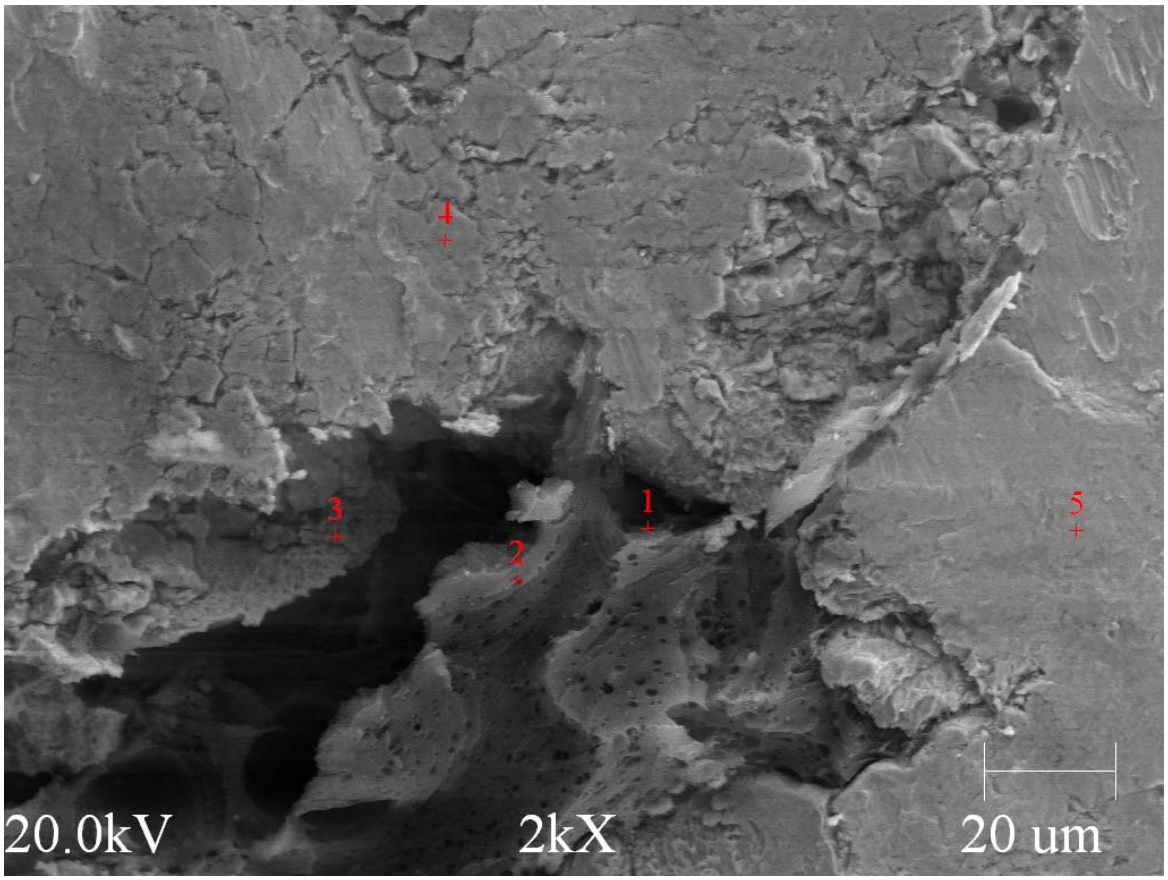

Figure 7.11 Structure 1133-1 C-6 SEM Micrograph

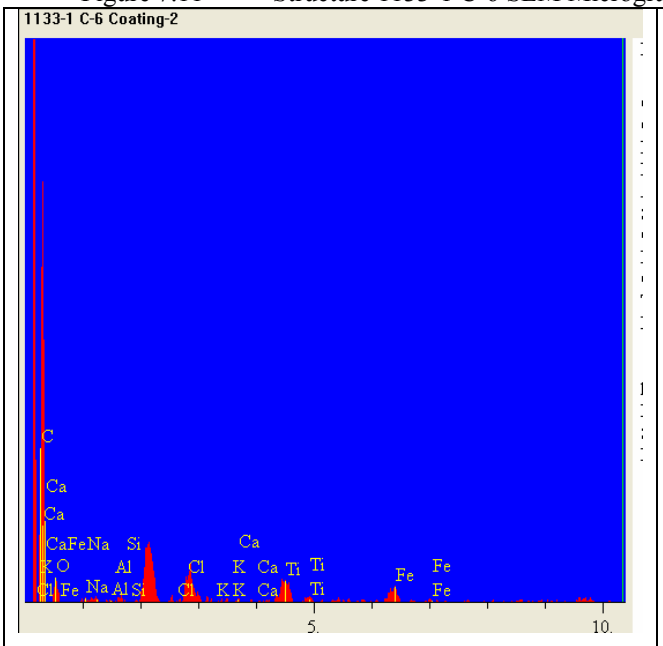

Figure 7.12 Structure 1133-1 C-6 EDS Coating Spectrum

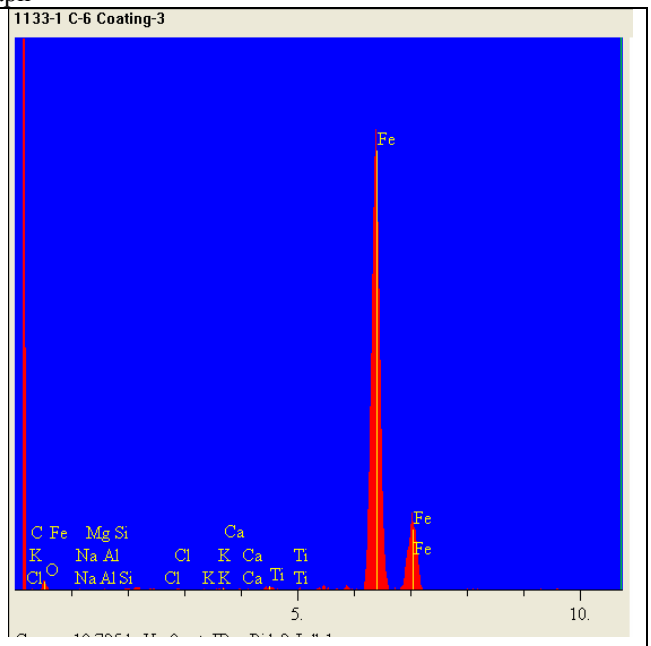

Figure 7.13 Structure 1133-1 C-6 EDS Metal Spectrum

Table 7.1 Structure 1133-1 C-6 EDS Chemical Composition

	Test Location 2			Test Location 3		
Element	Intensity (c/s)	Atomic %	Concentration	Intensity (c/s)	Atomic %	Concentration
C	38.61	84.825	76.564	0.000	0.000	0.000
O	3.57	12.844	15.443	1.56	4.621	1.377
Na	0.72	0.212	0.366	0.17	0.409	0.175
Mg	0.74	0.142	0.259	0.10	0.144	0.065
Al	0.39	0.058	0.117	0.03	0.027	0.013
Si	0.33	0.043	0.090	0.30	0.220	0.115
Cl	0.59	0.061	0.163	0.19	0.081	0.054
K	0.00	0.000	0.000	0.20	0.075	0.054
Ca	0.65	0.070	0.212	0.40	0.139	0.104
Ti	7.28	0.895	3.220	1.10	0.314	0.280
Fe	4.57	0.850	3.566	154.73	93.970	97.762
		100	100		100	100

The generalized and permanent nature of the adhesion loss observed occurs through a combination of adhesion loss mechanisms. First, the initial adhesion loss occurs as moisture diffuses through the coating and replaces the hydrogen bonds between the coating and the existing thin oxide layer present on the steel surface. Once sufficient moisture collects at the steel-coating interface, Sagüés theorized that cathodic disbondment may proceed by dissolution of the oxide film by hydroxides rather than by alkaline degradation of the coating itself (Sagüés, A.A. 1994). In 1992, Jones noted that cathodic disbondment may also occur at microscopic or smaller flaws in the coating to produce blisters, which do not require a physically obvious defect for initiation (Jones, D. 1992). Figure 7.14 clearly illustrates the effect of corrosion activity on the adhesion of the coating to the substrate.

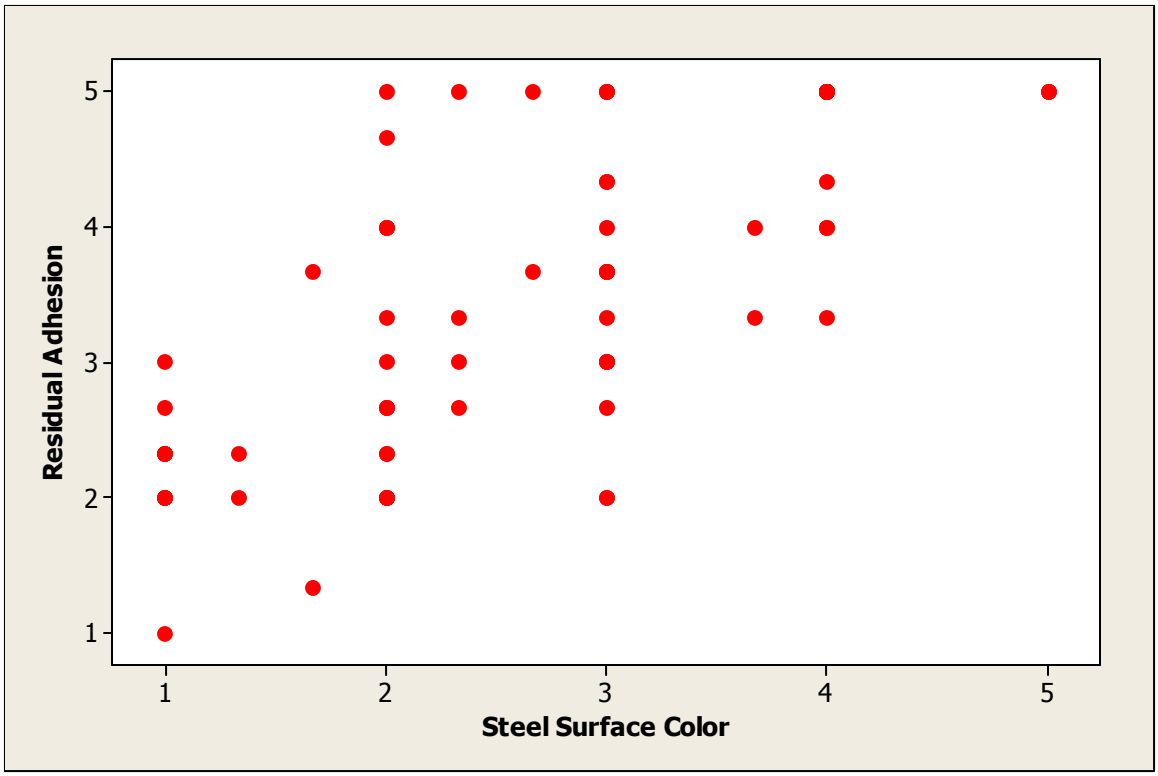

Figure 7.14 Residual Adhesion vs. Steel Surface Color

Additionaly, in 1999 Griffith and Laylor conducted a study of ECR reinforced bridges in Oregon. Just as we have here, they also found extensive adhesion loss. One of the parameters thought to contribute to adhesion loss, in that particular study, was the surface profile of the steel bar. AASHTO A775-97, “Standard Specification for Epoxy Coated Reinforcing Bars”, states: "Average blast profile maximum roughness depth readings of 1.5 to 4.0 mils (0.04 to 0.10 mm), as determined by replica tape measurements using NACE RP-287-87, shall be considered suitable as an anchor pattern." Based on a total of 150 profile measurements, the mean blast profile for longitudinal bars in the tidal zone was 3.00 mils (0.08 mm), with a 95% confidence interval of +/- 0.27 mils (0.007 mm) yet their samples presented considerable adhesion loss (Griffith, A. and Laylor, H.M. 1999). Referencing back to Figure 7.11, the spectra obtained from locations 4 and 5 (Figures 7.15, 7.16 and Table 7.2 below) presented no epoxy residue further supporting the conclusion that the epoxy to rebar adhesion is generally chemical and not mechanical in nature. The carbon signal at both locations is zero.

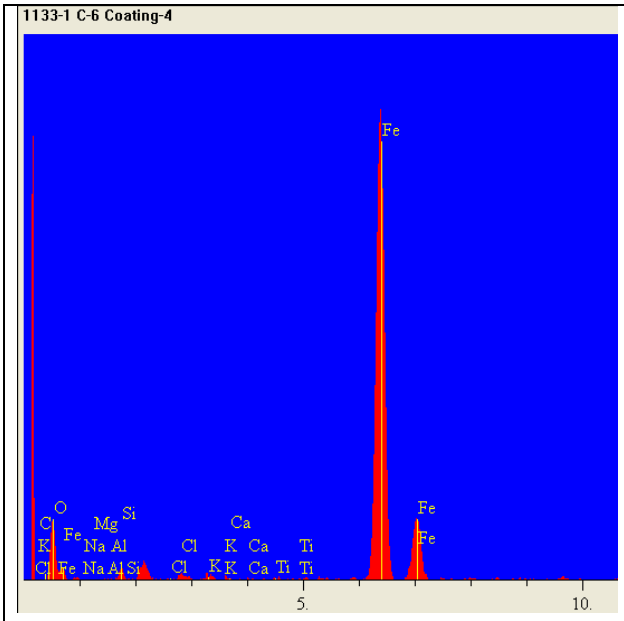

Figure 7.15 Structure 1133-1 C-6 EDS Coating Spectrum

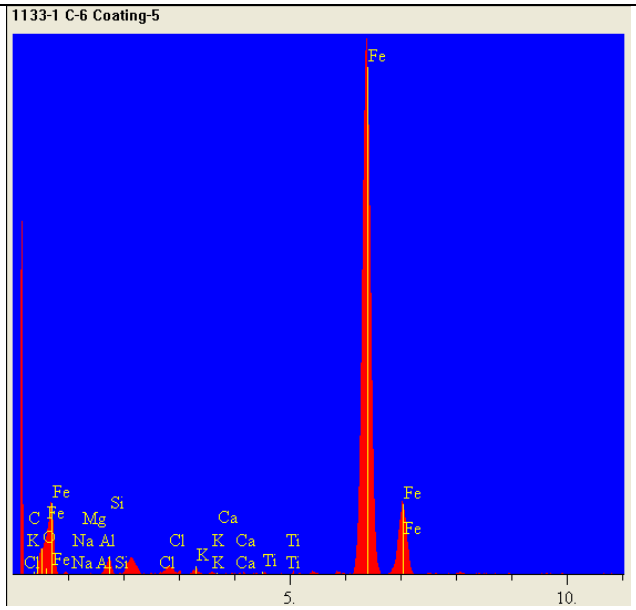

Figure 7.16 Structure 1133-1 C-6 EDS Coating Spectrum

Table 7.2 Structure 1133-1 C-6 EDS Chemical Composition

	Test Location 4			Test Location 5		
Element	Intensity (c/s)	Atomic %	Concentration	Intensity (c/s)	Atomic %	Concentration
C	0.00	0.000	0.000	0.000	0.000	0.000
O	33.38	25.634	9.097	20.40	12.810	4.102
Na	0.28	0.170	0.086	0.52	0.258	0.119
Mg	0.04	0.016	0.008	0.22	0.065	0.032
Al	0.35	0.087	0.052	0.19	0.037	0.020
Si	6.54	1.255	0.782	13.00	2.021	1.136
Cl	0.63	0.071	0.056	0.66	0.060	0.043
K	4.11	0.406	0.352	5.39	0.424	0.332
Ca	1.23	0.116	0.103	0.87	0.065	0.052
Ti	1.57	0.129	0.137	1.73	0.111	0.106
Fe	443.33	72.117	89.327	648.68	84.149	94.058
		100	100		100	100

7.4 Corrosion Activity

The extent of corrosion activity in the extracted ECR samples was determined by measuring the total combined size of visibly corroding sites on the coated bar and

expressing that value as a percentage of the total surface area. The factors believed to influence the bar corrosion were the concrete chloride concentration at bar level, the age of the sample, the epoxy coating curing level, coating thickness, coating color, residual adhesion, the change in T_g from in-situ to fully cured (ΔT_g), and the coating moisture content as previously discussed, plus the number of holidays and damaged areas per length of bar, the coating cracking number and the % cracking and porosity. Similar to coating cracking analysis, these parameters were regressed with the % corroded area as the response as well as individually correlated to determine parameter inter-dependency.

As expected, the % corroded area correlated well with the number of holidays per unit length of bar and the number of damaged areas per unit length of bar. The Pearson correlation values were 0.382 and 0.657. The corresponding P-values were 0.001 and 0.000, respectively. These relationships are presented in Figures 7.17 and 7.18.

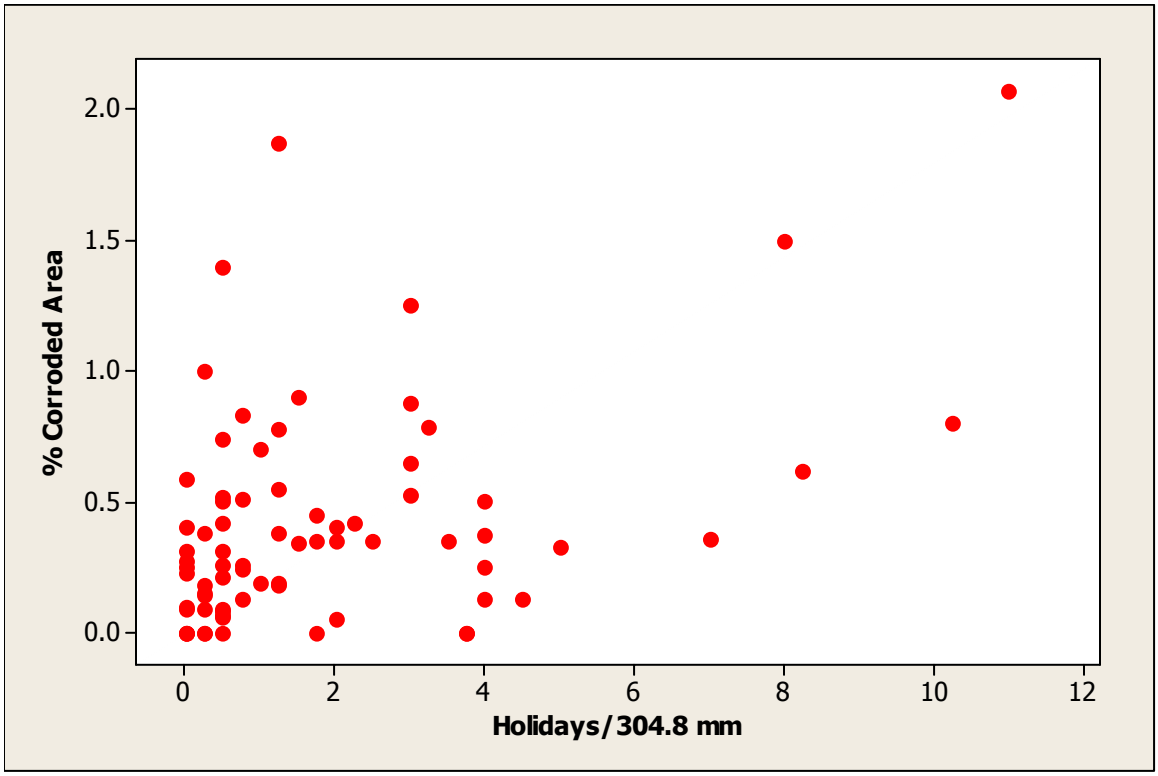

Figure 7.17 % Corroded Area vs. Holidays/304.8 mm

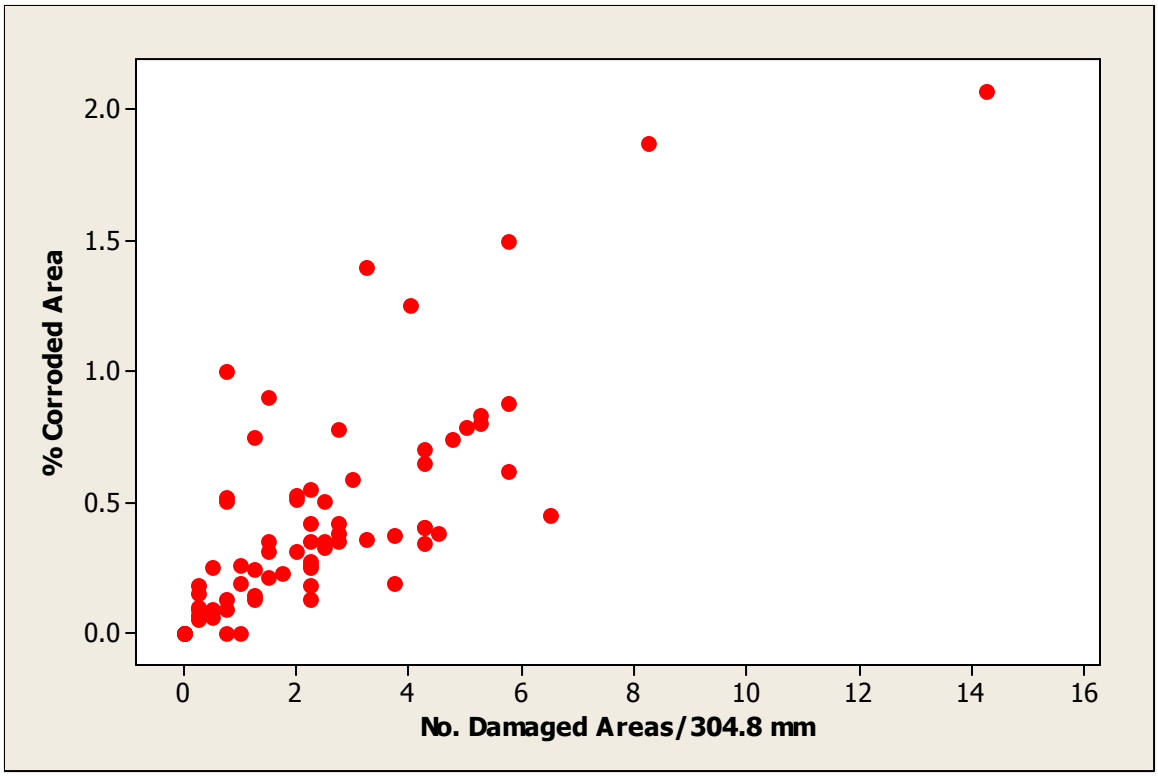

Figure 7.18 % Corroded Area vs. Number of Damaged Areas/304.8 mm

The analysis confirmed the results of numerous previous reports which state that the corrosion severity is directly related to breaches in the coating barrier. More unusual, however, was the fact that the chloride concentration at bar level did not seem to be a corrosion controlling parameter as it is in concrete structures reinforced with uncoated steel. The result may be influenced by the low chloride contents. As presented in the previous section, the chloride concentration in 82% of the tested structure was below commonly accepted corrosion initial levels.

Additionally, the EDAX analysis (Table 7.3) showed only traces or in some cases the complete absence of chlorides on the steel surface, as illustrated by the typical spectra from sample 1007-4 C-3 in Figures 7.20 and 7.21. The referenced spectra were obtained from locations 1 and 4 in Figure 7.19.

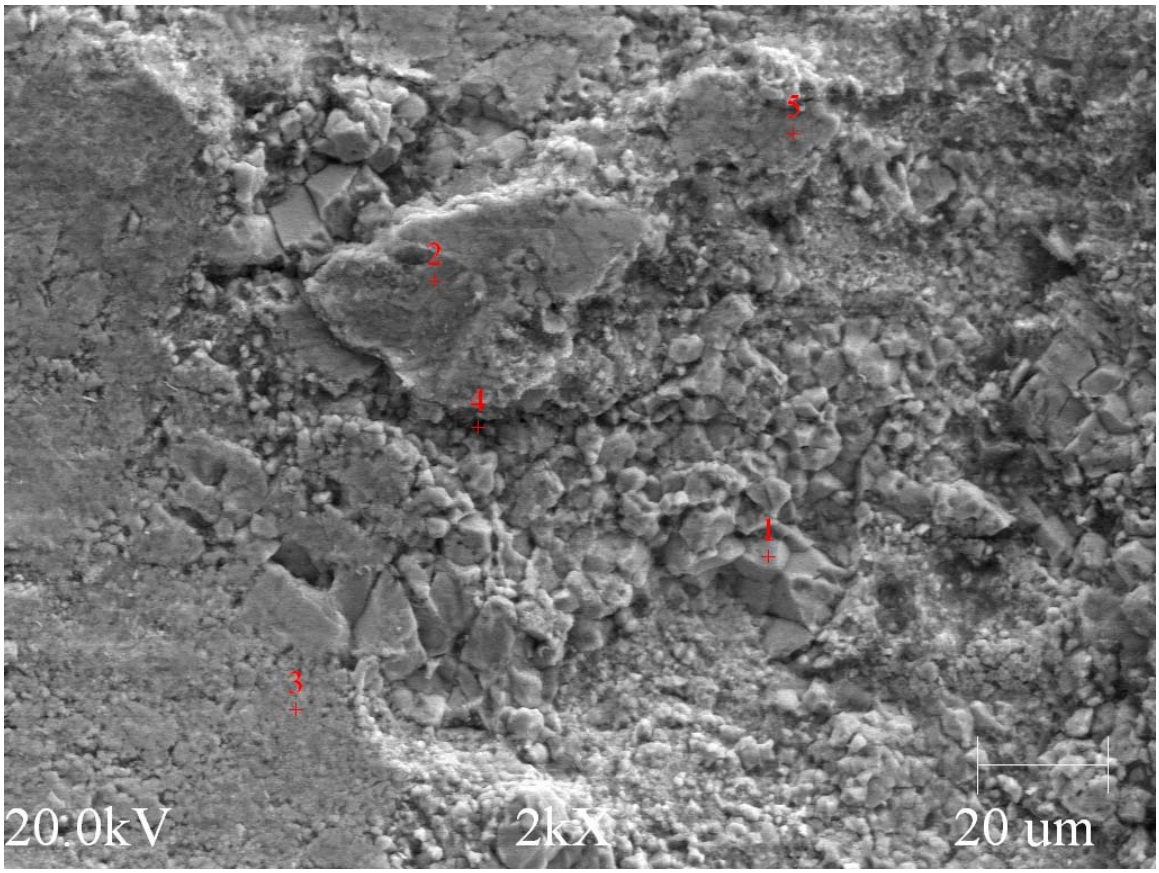

Figure 7.19 Structure 1007-4 C-3 SEM Micrograph

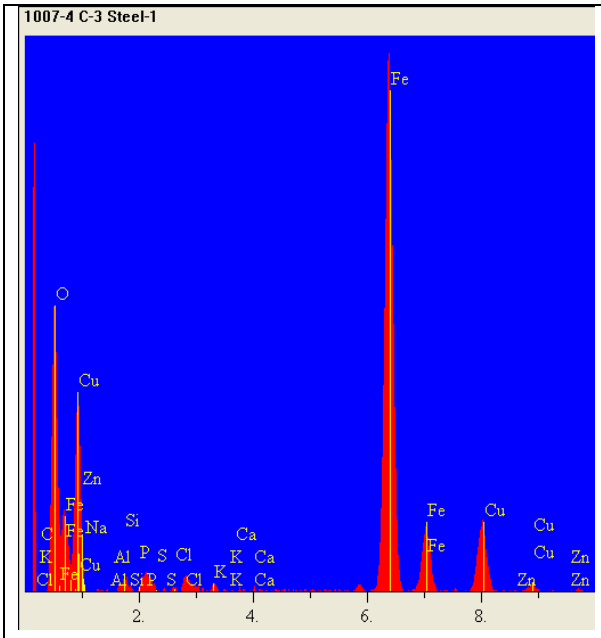

Figure 7.20 Structure 1007-4 C-3 EDS Coating Spectrum

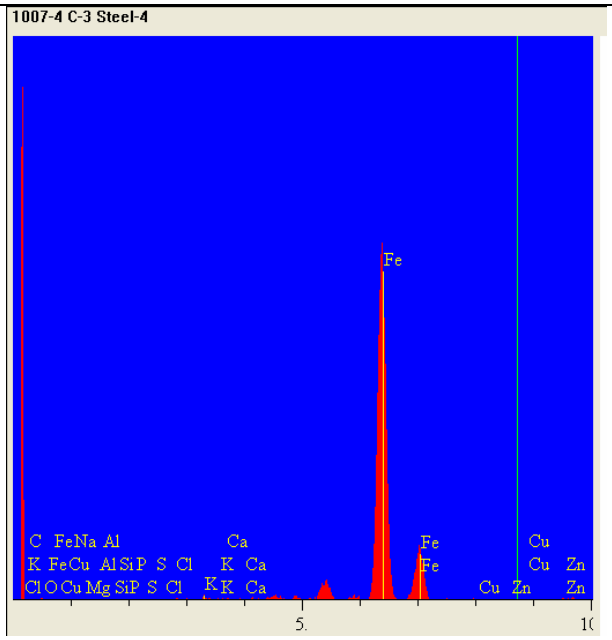

Figure 7.21 Structure 1007-4 C-3 EDS Coating Spectrum

Table 7.3 Structure 1007-4 C-3 EDS Chemical Composition

	Test Location 1			Test Location 4		
Element	Intensity (c/s)	Atomic %	Concentration	Intensity (c/s)	Atomic %	Concentration
C	0.00	0.000	0.000	0.000	0.000	0.000
O	137.48	54.728	25.589	0.41	0.838	0.242
Na	0.00	0.000	0.000	0.03	0.048	0.020
Mg	0.58	0.110	0.078	0.03	0.031	0.014
Al	0.27	0.036	0.028	0.38	0.253	0.123
Si	7.61	0.776	0.637	0.26	0.134	0.068
P	3.88	0.322	0.291	0.26	0.108	0.060
S	2.63	0.182	0.170	0.03	0.009	0.005
Cl	2.35	0.145	0.150	0.02	0.006	0.004
K	4.39	0.241	0.276	1.28	0.321	0.227
Ca	0.60	0.032	0.038	0.54	0.127	0.092
Fe	409.69	35.149	57.363	231.22	97.410	98.316
Cu	8.14	8.197	15.223	0.10	0.498	0.572
Zn	0.50	0.083	0.158	0.27	0.217	0.257
		100	100		100	100

The absence or limited presence of chlorides on the steel surface is also supported by the spectra collected from sample 1133-1 C-3 illustrated in Figures 7.23 and 7.24, while Table 7.3 presents the surface chemical composition at the referenced locations.

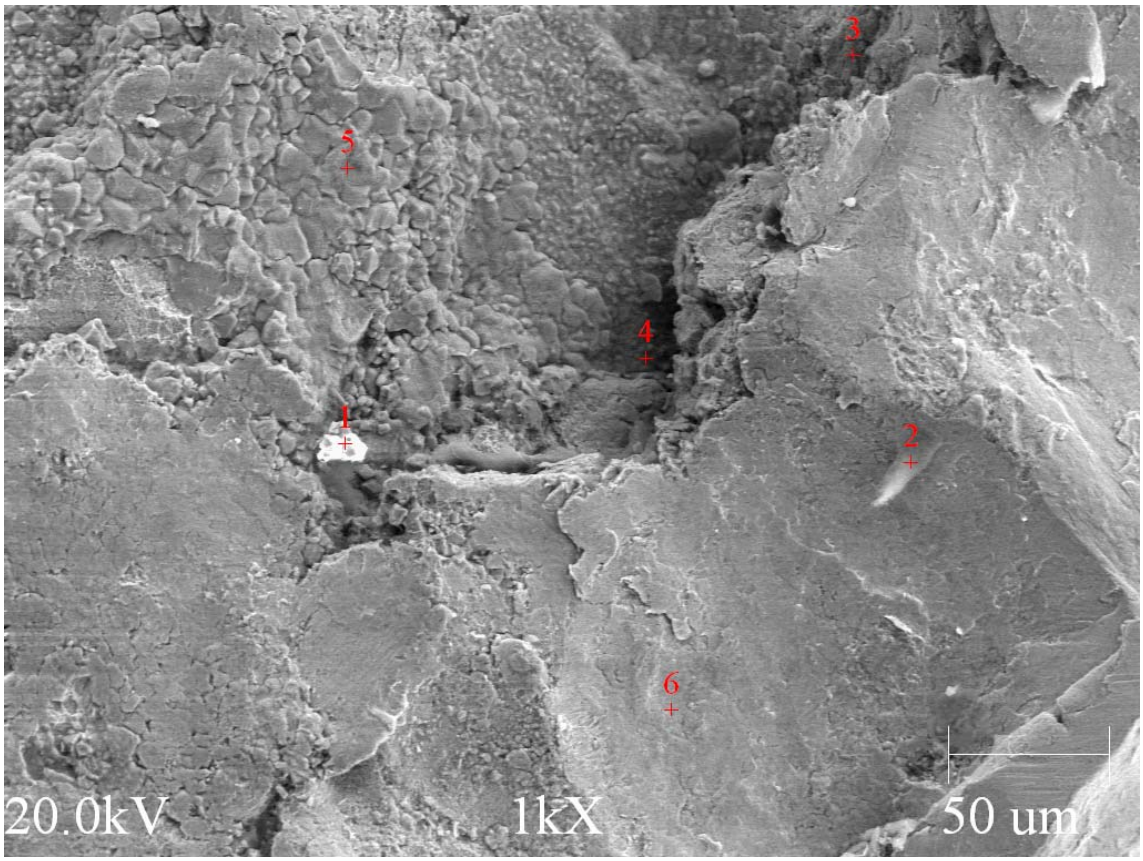

Figure 7.22 Structure 1133-1 C-3 SEM Micrograph

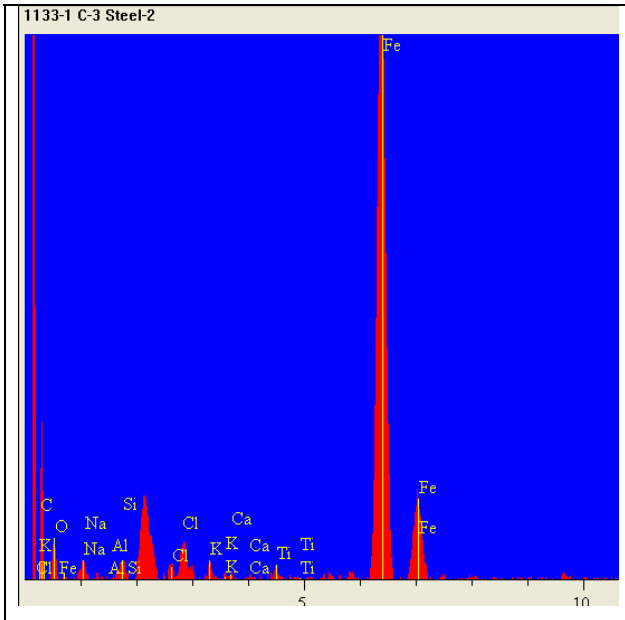

Figure 7.23 Structure 1133-1 C-3 EDS Coating Spectrum

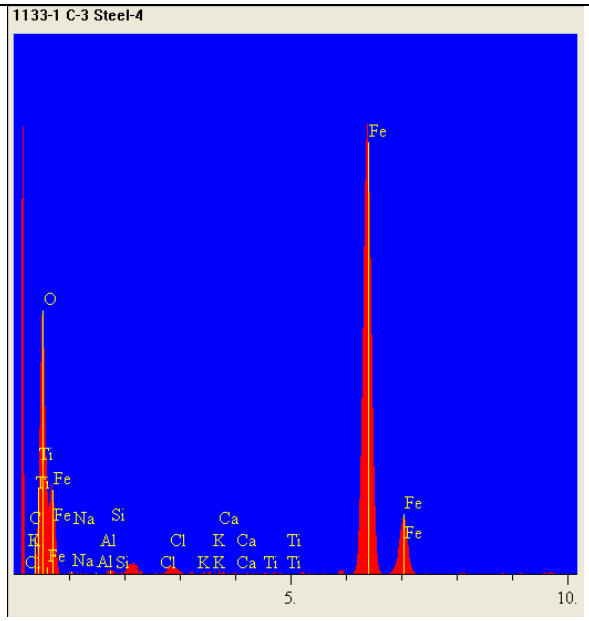

Figure 7.24 Structure 1133-1 C-3 EDS Coating Spectrum

Table 7.4 Structure 1133-1 C-3 EDS Chemical Composition

	Test Location 2			Test Location 4		
Element	Intensity (c/s)	Atomic %	Concentration	Intensity (c/s)	Atomic %	Concentration
C	8.94	53.263	22.641	0.000	0.000	0.000
O	6.76	7.822	4.429	165.81	58.381	28.899
Na	4.07	2.037	1.657	1.28	0.376	0.267
Mg	0.44	0.135	0.116	0.43	0.075	0.056
Al	0.07	0.016	0.015	0.28	0.034	0.028
Si	4.72	0.801	0.796	2.98	0.280	0.244
Cl	3.96	0.420	0.528	0.74	0.043	0.047
K	3.65	0.350	0.484	0.61	0.031	0.038
Ca	0.60	0.032	0.038	1.18	0.059	0.073
Ti	3.02	0.262	0.444	0.88	0.040	0.059
Fe	217.48	34.759	68.699	477.46	40.682	70.290
		100	100		100	100

Based on the regression analysis, at the 95% confidence level, the number of damages/308 mm was the only predictor of corrosion severity with a P-value of 0.000. Decreasing the confidence level to 80% allows for the inclusion of % moisture, ΔT_g and % cracking and porosity as corrosion severity prediction parameters. The P-values were 0.081, 0.093, and 0.171, respectively. Further regression performed using only the parameters with P-values ≤ 0.20 ultimately yielded two parameters as the strongest predictors of corrosion severity: number of damages/304.8 mm and ΔT_g. The P-values were 0.000 and 0.012, respectively.

While the new ECR showed a moderate degree of improvement compared to the extracted ECR with respect to the degree of curing, comparing the number of damaged areas presents a different observation. Statistically, there is a significant difference between the new and the extracted ECR samples, but not as expected. The new samples presented a disproportionally greater number of damages than the extracted samples as illustrated below.

	N	Mean	Standard Deviation	SE Mean
Extracted ECR	226	2.45	2.48	0.16
New ECR	39	10.43	7.37	1.2
Estimate for difference:	-7.97			
95% CI for difference:	(-10.38, -5.56)			
T-Value =	-6.69			
P-Value =	0.000			
DF =	3			

The t-test comparison shows a distinct loss of quality control. Where the extracted samples presented an average of 2.45 damages/304.8 mm, the new ECR samples had a mean of 10.43 damages/304.8 mm. Since it is commonly accepted that corrosion generally initiates at breaches in the coating, the performance of the new bar should be severely impacted. This however, will not become evident for decades.

Similarly, the mean number of holidays/304.8 mm was slightly greater for the new ECR samples at 2.56 holidays/304.8 mm than for the extracted ECR samples at 1.88 holidays/304.8 mm. Statistically, however, the t-test showed that there were no differences between the two sample sets.

One of the limitation of measuring the corrosion activity and severity based only on visible corrosion activity is that it underestimates the actual corrosion activity. (Brown, M.C. 2003). The high oxygen content present on the metal surface presented in Tables 7.3 and 7.4, and the moderate oxygen content presented in Table 7.2, indicate that active corrosion occurs under the coating even in the absence of chlorides.

7.5 Corrosion activity assessment

Finally, further analysis of the ability of commonly accepted non-destructive corrosion investigative techniques to assess the level of corrosion in concrete structures reinforced with ECR was performed. The data supported the assertion that although tests

such as concrete resistivity, half-cell potentials and linear polarization are highly variable, they can in fact provide valuable information regarding corrosion activity.

Concrete resistivity presented weak correlations with two parameters: the chloride concentration at bar level and coating % moisture content. The Pearson correlation values were -0.206 and -0.234, respectively. The corresponding P-values were 0.064 and 0.036. From a theoretical view point, the results are entirely justifiable; an increase in the chloride concentration and moisture results in a decrease in resistivity. Since during resistivity measurements every reasonable precaution was taken to ensure that the bar effects were minimized, the coating moisture content correlation may be explained by the intimate relationship between concrete moisture content and coating moisture content.

Corrosion half-cell potentials presented a negative correlation with the resistivity values. The Pearson correlation value was -0.207 and the P-value 0.067 (Figure 7.25), which is also in agreement with theoretical conditions: higher resistivity results in lower corrosion potentials.

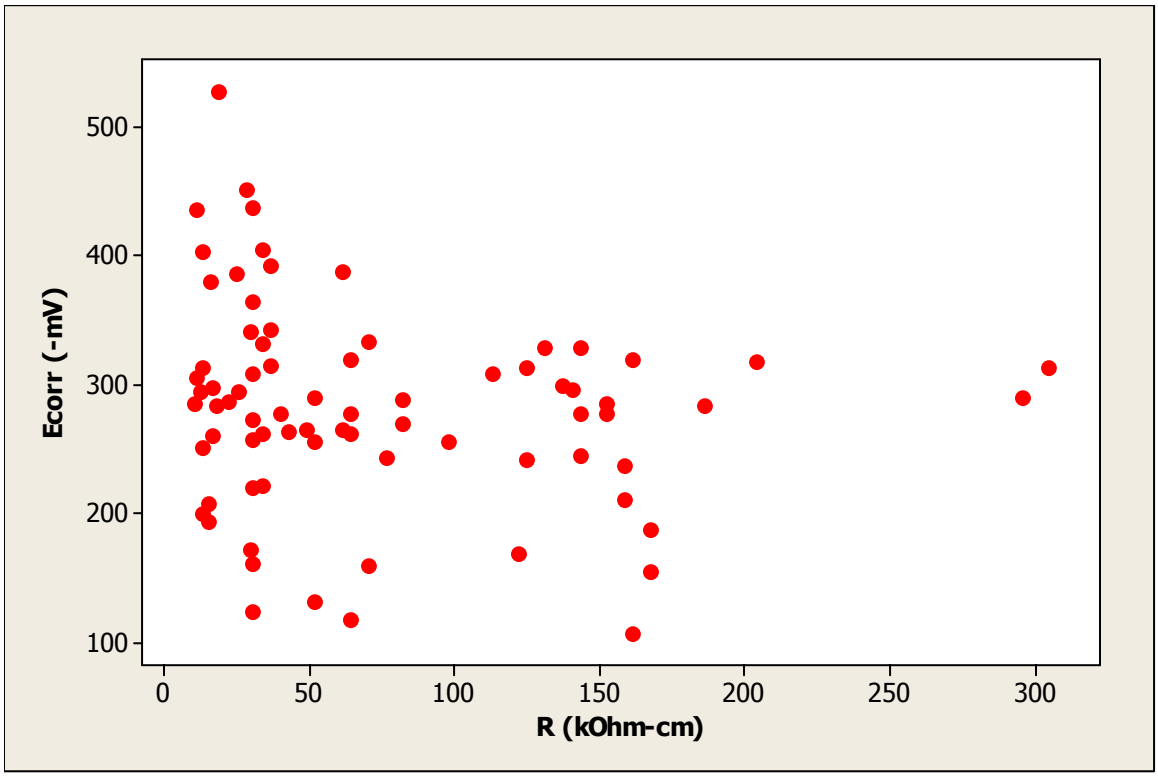

Figure 7.25 Half-cell Potentials vs. Resistivity

Most telling, however, were the linear polarization measurements. At the 95% confidence level, the corrosion current density measurements correlated very well with the chloride concentration at bar level and reasonably well with the coating % moisture content. The Pearson correlation values were 0.408 and 0.268, while the P-values were 0.000 and 0.018, respectively (Figures 7.26 and 7.27). At 90% confidence level, the corrosion current density also correlated with residual adhesion and the number of damaged areas. The Pearson correlation values were 0.196 and 0.200 and the P-values were 0.083 and 0.084.

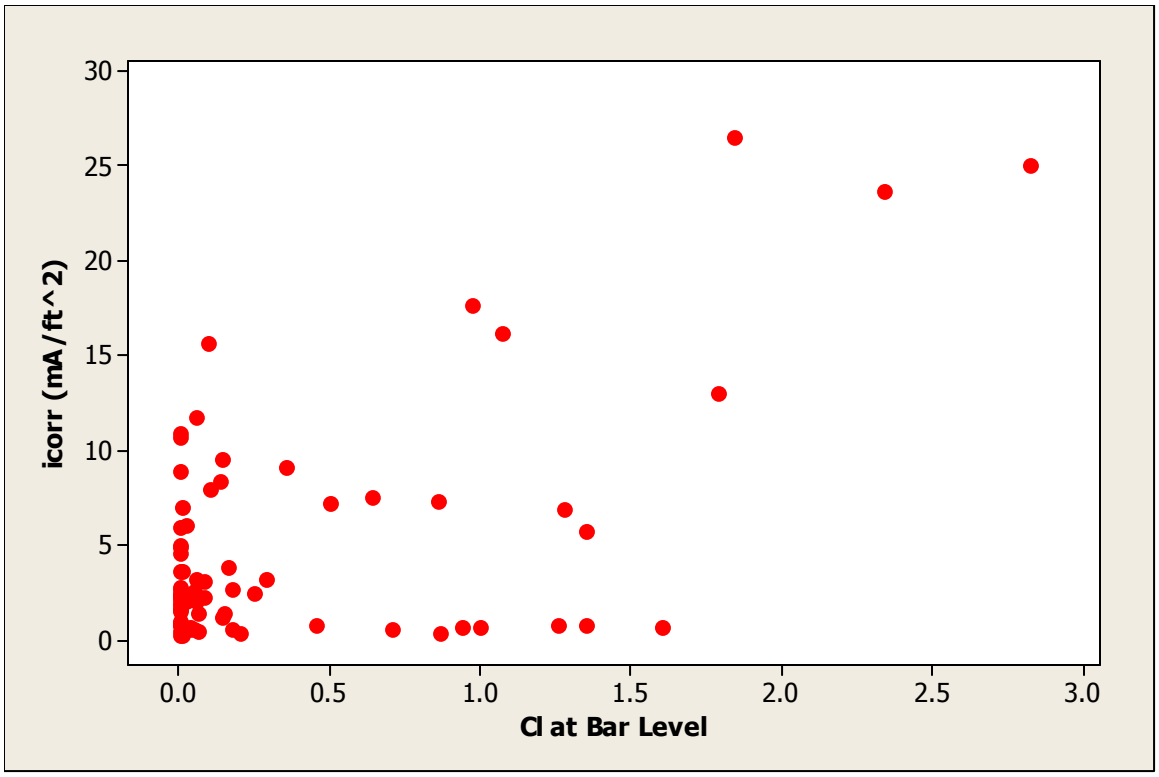

Figure 7.26 Corrosion Current Density vs. Cl^- at Bar Level

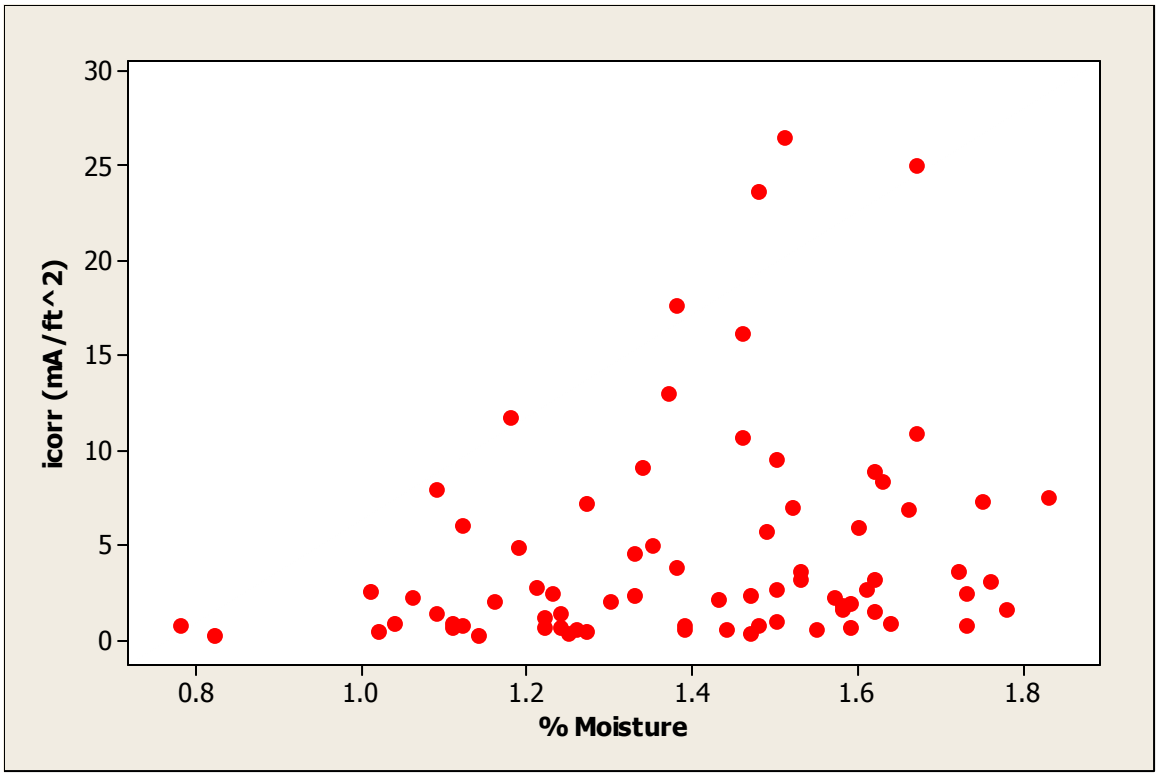

Figure 7.27 Corrosion Current Density vs. % Moisture

While the level of chlorides was zero or close to zero at locations under the coating, corrosion current density measurements seem to indicate that the contribution of chlorides to corrosion activity, particularly at breaches in the coating is relatively significant. The low correlation numbers reflected by the residual adhesion and the number of damaged areas may be a result of large variability inherent to concrete corrosion measurements coupled with the limited accuracy of residual adhesion and visual assessment of the rebar samples.

Until other corrosion protection methods become more prevalent, improving non-destructive corrosion activity assessment methods in ECR reinforced structures is critical. These numbers show that while limited, there is value in performing these measurements concomitant with other commonly available corrosion assessment methods.

To summarize the statistical analysis, the Pearson correlation values and the associated p-values are presented in Table 7.5. The correlations are ordered based on the strength of the relationship.

Table 7.5 Summary of correlation relationships

Correlation Relationship	Pearson Correlation	P-value
Residual adhesion – Color of corrosion products	0.764	0.000
% corroded area – Number of damages/304.4 mm	0.657	0.000
Coating cracking - % coating moisture	0.637	0.001
Residual adhesion – % coating moisture	0.522	0.000
% coating moisture and color of corrosion products	0.442	0.000
Residual adhesion – ΔT_g	0.416	0.000
Linear polarization – % coating moisture	0.408	0.000
% corroded area – Holidays/304.8 mm	0.382	0.001
ΔT_g – Color of corrosion products	0.341	0.002
ΔT_g – Coating thickness	-0.340	0.003
ΔT_g – Holidays/304.8 mm	0.282	0.014
ΔT_g – % coating moisture	0.272	0.014
Linear polarization – Chloride concentration at bar level	0.268	0.018

8.0 CONCLUSIONS

The extracted ECR coating samples presented extensive cracking compared to the new ECR samples in which the coating cracking was limited to only one sample. While no direct correlations with the available parameters existed that could explain the presence of surface cracks, there were a number of correlations that did occur with parameters known to affect the corrosion process. The coating cracking correlated with the level of chlorides at bar level, residual adhesion and percent moisture in the coating. The coating cracking also correlated well with the coating color, indicating that the degradation process affects the pigmentation as well as the coating surface condition. Although the chloride levels, based on bare steel values, may be insufficient to initiate corrosion of the reinforcing steel under the coating, previous research has demonstrated that aged epoxy coatings do indeed develop cracks in the superficial layers in the presence of chlorides (Kotnarowska, D. 1999).

The DSC results showed that both the extracted samples as well as new samples are not fully cured during the manufacturing process. While the curing state of the coating may not have a significant direct influence on adhesion, it does however affect the number of holidays and the moisture absorption of the coating. Less cured coatings having a greater number of holidays as well as higher moisture absorption due to their more porous nature. The coating degree of curing data also showed that the bars are insufficiently and unevenly heated prior to the application of the powder coating.

Additionally, the samples investigated presented significant permanent adhesion loss with little or no epoxy coating residue present on the bar surface. Presently, the absence of coating residue on the bar surface, supported by EDS spectra, seems to indicate that adhesion is primarily chemical in nature and that the contribution of the mechanical dimension of adhesion is minimal at best. Furthermore, the EDS analysis shows that once adhesion is lost, corrosion will proceed unimpeded under the coating even in the absence of chlorides.

The parameters that presented a direct correlation with the observed corrosion activity were the number of holidays and the number of damaged areas per unit length of bar. This indicates that the bare steel exposed to the concrete pore solution at the breaches in the epoxy coating does not passivate as a bare bar under similar exposure conditions allowing it instead to corrode at lower concrete chloride concentration levels than bare bars. Furthermore, the lack of detected chlorides on the surface of the steel bar in the presence of highly elevated oxygen levels demonstrate that the corrosion process continues unimpeded under the coating even in the absence of chlorides.

The results also show a distinct loss of quality control in the handling and possibly storage of new coated bars. The new ECR samples had significantly higher damage density than the samples extracted from concrete, while there was no change in the number of holidays and cure condition.

Finally, the data presented further evidence that while limited, the non-destructive corrosion assessment methods available for bare steel reinforced structures may also be used on ECR reinforced structures. In particular, the corrosion rate measurements correlated reasonably well with the chloride concentrations at bar level. This indicates that while the chlorides may not influence the corrosion activity under the coating, they do influence the corrosion activity at breaches in the coating.

9.0 RECOMMENDATIONS

9.1 Industry Practice

Handling and exposure limits of freshly coated bars have been addressed through the implementation of ASTM standards and specifications. Other parameters, such as fully cured coating, were assumed to be met during the coating process. This study, however, has shown that that is not the case. This condition may be corrected in several ways:

1. Instead of storing the bars outside until needed, the bars should be removed from the bundles in which they are shipped and moved indoors in a heated room at least 24 hours prior to use, thereby equalizing the bar temperature.
2. The bars could also be preheated during or prior to blast cleaning to provide a more uniform bar temperature.
3. Increase the distance between the bar exit from powder chamber to the quenching water spray, increasing the cure time without affecting the manufacturing speed
4. Potentially use radiant heat or an IR oven between the coating chamber and the quenching spray to post cure the coating.

9.2 Future Research

Although shot-blasting the bar surface is of use, particularly with respect to removal of mill-scale and other contaminants, additional rebar surface modification methods need to be investigated to improve the coating adhesion. To this end, electrodeposition of a Zn-Fe alloy has shown promising results not only increasing the wetting properties of the liquefied coating, but also significantly lowering coating permeability (Bajat, J.B. 2003).

In light of the data showing incomplete curing of the coating, the effects of ambient temperature on the embedded ECR rebar need to be investigated. Particularly in areas of the country as well as the world where, seasonally, ambient air temperatures can reach 100°F and more. In such cases, the bridge deck temperatures, and more importantly the temperature of exposed bars waiting to be installed, can increase in temperature close to the glass transition temperature of the coating accelerating the hydrothermal degradation process.

Finally, further study is necessary to determine the extent, scale and the conditions which influence the coating porosity presented in this paper. The effects of the coating structure on the coating corrosion inhibiting ability also need further investigation.

10.0 REFERENCES

Andrande,C. et al (1996). "Corrosion Rate Monitoring in the Laboratory and On-Site." Construction and Building Materials, vol. 10, n. 5, 1996, p. 315 – 328.

Andrande, C. et al (2002). "Standardization to a Reference of 25°C, of Electrical Resistivity for Mortars and Concretes in Saturated or Isolated Conditions." ACI Material Journal, vol. 99, n. 2, March – April 2002, p. 119 – 128.

Apicella, A. et al (1979). **"**Effect of Thermal History on Water Sorption, Elastic Properties and the Glass Transition of Epoxy Resins." Polymer. vol. 20, n. 9, September 1979, Pages 1143-1148

ASHTO LRFD Bridge Design Specifications, Section 5.12.3, 1994.

ASTM (2004). "A 775/A 775M Standard Specification for Epoxy-Coated Steel Reinforcing Bars", ASTM Annual Book of ASTM Standards, vol. 01.04 (Testing and Materials).

ASTM (1991). "C 876-91, Standard Test Method for Half-Cell Potentials of Uncoated Reinforcing Steel in Concrete", ASTM Annual Book of ASTM Standards, vol. 04.02n. (Concrete and Aggregates).

ASTM (2004). "C1152/C1152M-04e1 Standard Test Method for Acid-Soluble Chloride in Mortar and Concrete", ASTM Annual Book of ASTM Standards, vol. 04.02n. (Concrete and Aggregates).

ASTM (2001). "D4060-01 Standard Test Method for Abrasion Resistance of Organic Coatings by the Taber Abraser.", ASTM Annual Book of ASTM Standards, vol. 06.01.

ASTM (2003). "G8-96 Standard Test Methods for Cathodic Disbonding of Pipeline Coatings.", ASTM Annual Book of ASTM Standards, vol. 06.02.

ASTM (2004). "G14-04 Standard Test Method for Impact Resistance of Pipeline Coatings (Falling Weight Test).", ASTM Annual Book of ASTM Standards, vol. 06.02.

ASTM (1998). "G62-87Standard Test Methods for Holiday Detection in Pipeline Coatings." ASTM Annual Book of ASTM Standards, vol. 01.48.

Bajat, J.B., Mišković-Stanković, V.B. and Kaćarević-Popović, Z. (2003). "The influence of steel surface modification by electrodeposited Zn–Fe alloys on the protective behaviour of an epoxy coating." Progress in Organic Coatings, Vol. 47, pp. 49-54.

Bentur, A., Diamond, S. and Berke, N.S. (1997). "Steel Corrosion in Concrete." 1st Edition, Chapman & Hall, New York.

Bentz, Dale P. et al. (1991) "Simulation Studies of the Effects of Mineral Admixtures on the Cement Paste-Aggregate Interfacial Zone." ACI Materials Journal, vol. 88, n. 5, September – October 1991, p. 518 – 529.

Broomfield, John P. (1997). "Corrosion of Steel in Concrete." 1st Edition, Chapman & Hall, New York.

Brown, Michael C. (2003). "Linear Cracking and Chloride Penetration of Concrete Bridge Decks." VTRC Research Proposal, March 2003.

Brown, Michael C. (2002) " Corrosion Protection Service Life of Epoxy Coated Reinforcing Steel in Virginia Bridge Decks." Dissertation in Civil and Environmental Engineering, Virginia Polytechnic Institute and State University.

Bryant, James W. Jr. (2001) "Non-Invasive Permeability Assesment of High-Performance Concrete Bridge Deck Mixtures." Dissertation in Civil and Environmental Engineering, Virginia Polytechnic Institute and State University.

Bungey, J.H. (1989) "Testing of Concrete in Structures." 2nd Edition, Chapman & Hall, New York.

Carey, Francis A. (1996). "Organic Chemistry." 3rd Edition, The McGraw Hill Companies, Inc.

Clear, K.C. (1994). "Effectiveness of epoxy-coated reinforcing steel - Final Report. Canadian Strategic Highway Research Program." Ottawa, ON, pp.128.

Clear, Kenneth C. et. al.(1995). "Performance of Epoxy-Coated Reinforcing Steel in Highway Bridges." National Academy Press, Washington, D.C., 1995.

Clear, Kenneth C. (1989). " Measuring Rate of Corrosion of Steel in Field Concrete Structures." Kenneth C. Clear, Inc. Concrete Materials and Corrosion Specialists, Sterling, Virginia 1989.

Clemeña, Gerardo G. (1992). "Benefits of Measuring Half – Cell Potentials and Rebar Corrosion Rates in Condition Surveys of Concrete Bridge Decks." Virginia Transportation Research Council, Report Number VTRC 92-R16.

Crank J (1975). "The Mathematics of Diffusion." Second Edition, Oxford University Press, Great Britain

De'Nève, B. and Shanahan, M. E. R. (1993). "Water absorption by an epoxy resin and its effect on the mechanical properties and infra-red spectra." Polymer. vol. 34, n. 24, December 1993, Pages 5099-5105.

Dickie, R.A., Hammond, J.S. and J.W. Holubka, J.W. (1981). "Interfacial Chemistry of the Corrosion of Polybutadiene-Coated Steel." Industrial and Engineering Chemistry, Product and Research Development, 20:339 (1981).

Elsener, B et al (1993). "Inspection and Monitoring of Reinforced Concrete Structures – Electrochemical Methods to Detect Corrosion." Insight – non – Destructive Testing and Condition Monitoring, vol. 36, n. 7, July 1994, p. 502 – 506.

Feliu, S. et al (1996). "Techniques to Assess the Corrosion Activity of Steel Reinforced Concrete Structures." ASTM STP 1276.

Fitch MG et al (1995). "Determination of End of Functional Service Life for Concrete Bridge Decks." Transportation Research Record, n. 1490, p. 60 – 66.

Fontana, M.G. and Greene, N.D. (1978). "Corrosion Engineering." McGraw-Hill Company, 1978.

Fontana, Mars Guy (1986). "Corrosion Engineering." McGraw-Hill Company, 1986.

Fulton, F.S. et al (1974). "The Properties of Portland Cements Containing Milled Granulated Blastfurnace Slag", The Portland Cement Institute, Johannesburg, South Africa.

Geenen, F. M. (1991). " Characterization of Organic Coatings With Impedance Measurements." Doctoral Dissertation, Delft University of Technology

Gledhill, R.A., & Kinlock, A.J. (1974). "Environmental Failure of Structural Joints." Journal of Adhesion, Vol. 6, pp. 315-330.

González, S., Gil, M.A., Hernández, J.O., Fox, V. and Souto, R.M. (2001). "Resistance to Corrosion of Galvanized Steel Covered with an Epoxy-Polyamide Primer Coating." Progress in Organic Coatings, v.41, pp. 167–170.

Gowers, K. R. et al (1999). "Measurement of Concrete Resistivity for Assesment of Corrosion Severity of Steel Using Wenner Technique." ACI Materials Journal, vol. 96, n. 5, September – October 1996, p. 536 – 541.

Griffith, A. and Laylor, M.H. (1999). "Epoxy Coating Reinforcement Study." State Research Project #527, Oregon Department of Transportation Research Group.

Hare, C.H. (2000). "Uhlig's Corrosion Handbook." 2nd ed., John Wiley & Sons, Inc., New York, NY, 2000.

Jones, D.A. (1992). "Principles and Prevention of Corrosion." Macmillan Publishing Company, New York, pp. 107-111.

Kessler, R. and Powers, R. (1987). *Corrosion Evaluation of Substructure, Long Key Bridge.* Corrosion Report No. 87-9A. Florida Department of Transportation, Gainesville, 1987.

Kotnarowska, D. (1999). "Influence of ultraviolet radiation and aggressive media on epoxy coating degradation." Progress in Organic Coatings, v.37, pp. 149 – 159.

Kirkpatrick, Trevor J. (2001) "Impact of Specification Changes on Chloride Induced Corrosion Service Life of Virginia Bridge Decks." Master's Thesis in Civil and Environmental Engineering, Virginia Polytechnic Institute and State University.

Kirkpatrick, T.J., Weyers, R.E., Anderson-Cook, C., and Sprinkel, M.M. (2002). "A Model toPredict the Impact of Specification Changes on the Chloride-Induced Service Lifeof Virginia Bridge Decks." VTRC 03-CR4, Virginia Transportation Research Council, Charlottesville, VA, 2002.

Lambert, Paul (1998). "Reinforced Concrete – History, Properties & Durability." Corrosion Prevention Association, Oct. 1998.

Law, D.W. et al (2003). "Evaluation of Corrosion Loss of Steel Reinforcing Bars in Concrete Using Linear Polarization Resistance Measurements." Non-Destructive Testing in Civil Engineering (NDT-CE), Oct 2003, v. 8, n. 10

Leidheiser, H. and W. Funke (1987). "Water disbondement and wet adhesion of organic coatings on metals: A review and interpretation," J. Oil & Colour Chemists' Assoc., 70, No. 5, pp.121-132.

Lewis, D.W. (1985). "Discussion of Admixtures for Concrete." Concrete International: Design and Construction, v. 27, n. 5, May 1985, p. 64 – 65.

Lohtia, R.P. (1995). "Concrete Admixtures Handbook" Noyes Publications, Park Ridge, NJ.

Liu, Y. (1996). "Modeling the Time-to-Corrosion Cracking of the Cover Concrete in Chloride Contaminated Reinforced Concrete Structures." Doctoral Dissertation, Virginia Polytechnic Institute & State University.

Malhotra, V.M. and Carino, N.J. (2004). "Nondestructive Testing of Concrete. Second Edition." CRC Press LLC. West Conshohocken, PA.

Manning, David G. (1995). "Detecting Defects and Deterioration in Highway Structures." National Cooperative Highway Research Program Synthesis of Highway Practice 118.

McMurry, J. and Fay, R.C. (1998). "Chemistry." 2nd Edition, Prentice Hall Inc., Upper Saddle River, New Jersey.

Mehta, P. Kumar (1993). " Concrete Structures, Properties and Materials." Prentice Hall, Englewood Cliffs, NJ.

Montemor, M.F. et al (2000). "Effect of Flyash on Concrete Reinforcement Corrosion Studies by EIS." Cement and Concrete Composites, vol. 22, January 2000, p. 175 – 185.

Munjal, S.K. (1981). "Evaluation of Epoxy-Coated Reinforcing Steel in Bridge Decks." Report No. FHWA-MD-82/03, Maryland State Highway Administration.

Nagi, Mohamad A. and Whiting, David A. (2003). "Electrical Resistivity of Concrete—A LiteratureReview." R&D Serial No. 2457, Portland Cement Association, Skokie, Illinois, USA, 57 pages.

Naish, C. C. et al (1988). " Variability of Potentials Measured on Reinforced Concrete Structures." Materials Performance, vol. 27, n. 4, April 1988, p. 45 – 48.

Nguyen, T. and Martin, J. W. (1996). "Modes and Mechanisms of Degradation of Epoxy-Coated Reinforcing Steel in a Marine Environment." Proceedings of the 1996 7th International Conference on Durability of Building Materials and Components, 7DBMC.

Odian, G. (1981). "Principles of Polymerization." 2nd Edition, John Wiley & Sons, Inc., New York, NY, 1981.

Ostle, B. et al (1995). "Engineering Statistics: The Industrial Experience." Wadsworth, November 1995.

Pianca, F. (1999). "Performance of Epoxy Coated Reinforcement on Ministry Structure – Update", Ontario Ministry of Transportation, October 1999.

Pianca, F. Schell, H. and Cautillo, G. (2005). "The Performance of Epoxy Coated Reinforcement: Experience of the Ontario Ministry of Transportation." International Journal of Materials and Product Technology 2005 - Vol. 23, No.3/4 pp. 286 - 308

Polder, Rob B. et al (2002). "Characterisation of Chloride Transport and Reinforcement Corrosion in Concrete Under Cyclic Wetting and Drying by Electrical Resistivity." Cement and Concrete Composites, vol. 24, 2002, p. 427 – 435.

Poon, S.W. and Tasker, I (1998). "Extending Building Life with Fusion Bonded Epoxy." Asia Engineer, The Journal of the Hong Kong Institution of Engineers, 1998, 17.

Pyc, Wioleta Agata (1998). "Field Performance of Epoxy-Coated Reinforcing Steel in Virginia Bridge Decks." Doctoral Dissertation in Civil and Environmental Engineering, Virginia Polytechnic Institute and State University.

Revie, R.W. (2000). "Uhlig's Corrosion Handbook." 2nd ed., John Wiley & Sons, Inc., New York, NY, 2000.

Romano, D.C. (1988). "Preliminary Investigation of Epoxy-Coated Reinforcing Steel Disbondement: Causes and Effects." Florida Department of Transportation, Materials Office, Gainsville, FL.

Rouw, A.C. (1998). "Model Epoxy Powder Coatings and their Adhesion to Steel." Progress in Organic Coatings, v.34, pp. 181–192.

Sagüés, A.A. and Zayed, A.M., Corrosion of Epoxy Coated Reinforcing Steel in Concrete -- Phase 1. 1989. Gainesville, Florida, Florida Department of Transportation, Materials Office.

Sagüés, A.A. et al (1990). "Marine Environment Corrosion of Epoxy-Coated Reinforcing Steel." Page, C.L., Treadaway, K.W.J., and Bamforth, P.B. Corrosion of Reinforcement in Concrete, 539-550. Applied Elsevier Science Ltd.

Sagüés, A.A. (1991). "Mechanism of Corrosion of Epoxy-Coated Reinforcing Steel in Concrete." Report No. FL/DOT/RMC/0543-3296.

Sagüés, A.A. et al. (1994). "Corrosion of Epoxy-Coated Rebar in Florida Bridges". University of South Florida, College of Engineering.

Sagüés, A.A. et al (1996). "Practical Evaluation of Resistivity of Concrete in Test Cylinders Using a Wenner Array Probe." Cement and Concrete Research, vol. 26, n.12, p. 1779 – 1787.

Seymour, R.B. et al (1990). "Handbook of Organic Coatings: A Comprehensive Guide for the Coatings Industry." New York & London, Elsevier.

Sohanghpurwala, A.A., and K.C. Clear (1990). "Effectiveness of Epoxy Coatings in Minimizing Corrosion of Reinforcing Steel in Concrete." Transportation Research Record, No. 1268, pp. 193-204.

Sohanghpurwala, A.A. et al (1999). "Condition and Performance of Epoxy Coated Rebars in Bridge Decks." Public Roads, November/December 1999.

Smith, J.L. et al (2000). "Materials and Methods for Corrosion Control of Reinforced and Prestressed Concrete Structures in New Construction." FHWA Report Number: FHWA – RD – 00 – 081.

Takewaka, K. et al. (2003). "Simulation Model for Deterioration of Concrete Structures due to Chloride Attack." Journal of Advanced Concrete Technology, v. 1, n. 2, 2003, p. 139-146.

Trethewey, K.R. et al. (1988). "Corrosion for Students of Science and Engineering." Longman Scientific & Technical, p. 228 – 230.

Turner, H.M. (1998). "Conversion Between Network-Level and Project-Level Units of Measure for Use in a Bridge Management System." VTRC Report 99-R4. "Corrosion Protection: Concrete Bridges." http://www.tfhrc.gov/structur/corros/introset.htm. Last accesed Oct 20, 2003.

Tuuti, K. (1980). "Service Life of Structures with Regard to Corrosion of Embedded Steel." International Conference on Performance of Concrete in Marine Environment. St. Andrews-by-the-Sea, Canada, ACI, SP-65, pp. 223 – 236.

Virmani, Y.P., K.C. Clear, and T.J. Pasko, Jr. (1983). "Time-to-Corrosion of Reinforcing Steel in Concrete Slabs, Volume 5: Calcium Nitrate Admixtures or Epoxy-Coated Reinforcing Bars as Corrosion Protection Systems." Report No. FHWA/RD83/012, Interim Report, Washington, DC, Federal Highway Administration.

Virmani, P and Clemena, G. (2001). "Fighting Corrosion in Reinforced Concrete Bridge Decks." The Road Ahead, Virginia Transportation Research Council, Charlottesville, VA, June 2001, pp. 1-7.

Virginia Department of Transportation Road and Bridge Specifications, Section 406, January 1994.

Weed, R.M. (1974). "Recommended Depth of Cover for Bridge Deck Steel." Transportation Research Record, n. 500, p. 32 – 35.

Weyers, RE et al (1993). "Concrete Bridge Protection, Repair, and Rehabilitation Relative to Reinforcement Corrosion: A Methods Application Manual." SHRP-S-360, Strategic Highway Research Program.

Weyers, R.E. (1995). "Protocol for In-service Evaluation of Bridges with Epoxy Coated Reinforcing Steel." NCHRP 10-37B, Final Report, Transportation Research Board, Washington D.C.

Weyers, R.E. and Liu, Y. (1998). "Modeling the Time-to-Corrosion Cracking in Chloride Contaminated Reinforced Concrete Structures." ACI-Materials-Journal, v. 95,

n. 6, 1998, pp 675-681.

Weyers, R.E. et al (2003). "Bridge Deck Cover Depth Specifications." Concrete International, February 2003, v. 25, n. 2, pp. 61 – 64.

Weyers, R.E., Personal Communication with Richard E. Weyers, January, 2004.

Wheeler, M.C. (2003). "Parameters Influencing the Corrosion Protection Service Life of Epoxy Coated Reinforcing Steel in Virginia Bridge Decks." Master's Thesis. Virginia Polytechnic Institute and State University, 2003.

Young, Francis J. et al (1998). "The Science and Technology of Civil Engineering Materials." Prentice Hall, Upper Saddle River, NJ.

Zemajtis, J., R.E. Weyers, M.M. Sprinkel, and W.T. McKeel, Jr. (1996). "Epoxy-Coated Reinforcement - A Historical Performance Review." VTRC 97-IR1, Virginia Transportation Research Council, pp. 4.

Zemajtis, J. (1998). "Modeling the Time to Corrosion Initiation for Concretes with Mineral Admixtures and/or Corrosion Inhibitors in Chloride-Laden Environments." Dissertation in Civil and Environmental Engineering, Virginia Polytechnic Institute and State University.

Zhang, Jieying et al (2000). "Validation of Resistivity Spectra From Reinforced Concrete Corrosion by Kramers – Kronig Transformations." Cement and Concrete Research, vol 31, 2001, p. 603 – 607.

VITA

Andrei Ramniceanu was born in Bucharest, Romania on January 9th, 1976 to Emil-Ioan and Andriana Ramniceanu. In 1991, the family moved from Bucharest to Patchogue located on the southern shore of Long Island, NY. In 1994, he graduated from Patchogue-Medford High School with a Regents diploma.

After moving to Newport News, VA in 1997, and while employed as an engineering technician and structural steel inspector by Professional Service Industries, Inc., Andrei earned an Associate of Science degree in Engineering from Thomas Nelson Community College in 2001. Andrei continued his education, earning Bachelor of Science and Master of Science degrees in Civil and Environmental Engineering from the Virginia Polytechnic Institute and State University in 2003 and 2004, respectively. The title of his Master's thesis is "Correlation of Corrosion Measurements and Bridge Conditions with NBIS Deck Rating." Under a research fellowship from the National Science Foundation, Andrei continued graduate research in corrosion – focusing on the corrosion protection efficacy of fusion bonded epoxy coatings – in his doctoral program. He successfully defended his Doctor of Philosophy dissertation on May 18th, 2007.

Andrei is married to Dr. Kathryn Lois Clasen, who attended James Madison University and the Medical College of Virginia, where she earned a Doctor of Pharmacy degree in 2007.

APPENDICES

Available upon request in digital format.